Iron and manganese removal from borehole water using carbonised orange peels as a biosorbent

By

Bashirah Devajee
211021857

Thesis submitted in fulfilment of the requirement for the degree

Master of Engineering in Civil Engineering

Department of Civil Engineering and Geomatics

Faculty of Engineering and the Built Environment

Cape Peninsula University of Technology

Supervisor: Prof. Veruscha Fester
Co-Supervisor/s: Dr. O Oputu & Dr. B Sone

Cape Town
11 Feb 2025

Declaration

I, **Bashirah Devajee**, declare that **“Iron and manganese removal from borehole water using carbonised orange peels as a biosorbent”** is my original and unaided work and that all the sources that I have used or cited have been indicated and acknowledged by means of complete references. It is being submitted for the Master of Engineering in Civil Engineering Degree at the Cape Peninsula University of Technology. This document has not been submitted for any degree or examination at any other academic institution. Furthermore, it represents my own opinions and not necessarily those of the Cape Peninsula University of Technology.

(Signature)

Signed in Cape Town this ___11th ____day of ____February______2025

Abstract

This study addresses two significant civil engineering challenges: solid waste management and heavy metal water pollution. It proposes using carbonised orange peels, a domestic waste by-product, as a biosorbent for the removal of iron and manganese from borehole water. This approach aims to reduce landfill waste while providing a sustainable method for water treatment.

The orange peels were collected from a local juice shop and the biosorbent was then prepared by drying, grinding, and then carbonising the material at 600°C in an argon atmosphere. Batch experiments were then completed which demonstrated that carbonised orange peels could effectively reduce iron and manganese concentrations. Various experiments were conducted to assess concentration effects (100 ppm diluted to lower concentrations), biosorbent mass (ranging from 0.05 g to 1 g), pH levels (adjusted) and contact time (1 to 90 minutes). Subsequently, column studies were done where water was passed through a packed column containing the biosorbent, with samples collected at different time intervals for analysis. The experimental data was then applied to various adsorption models to assess the performance of the biosorbent. Various characterization techniques were performed such as Scanning Electron Microscopy (SEM), Electron Dispersive Spectroscopy (EDS), Fourier Transform Infrared (FTIR) Spectroscopy and Brunauer Emmet Teller (BET).

The study found experimental biosorption capacities of 11 mg/g for iron (Fe) and 5 mg/g for manganese (Mn). The results showed Fe and Mn removal efficiencies of up to 100% and 75%, respectively. There was a constant percentage removal for iron and the iron concentrations were significantly reduced after treatment while the manganese concentrations varied with initial concentration. The iron performed well in both the model fluid and the borehole water adsorption experiments when compared to manganese. The iron removal was constant even in a binary system. The optimal conditions for maximum biosorption were identified as a biosorbent mass of 0.3 g and a pH of 4. Biosorption was rapid, reaching equilibrium in 40 minutes for manganese. In batch studies, the adsorption of iron and manganese from borehole water by carbonised orange peel followed the Langmuir model. In the kinetic modelling, it was observed that the pseudo second order predicted Q_e as 10 mg/g and the experimental Q_e was calculated as 11.3 mg/g for Fe. For Mn the predicted Q_e is 4.9 mg/g while the experimental Q_e was calculated to be 5.3 mg/g. Therefore, the experimental data was best described by the pseudo second order kinetic model.

Column studies revealed that the breakpoint and saturation point were directly proportional to the column mass while not limited by the flow rate. The highest saturation capacity for COP in column experiments was 1.465 mg/g, achieved under conditions of 11 mg/L manganese inlet concentration, a flow rate of 20 mL/min, and a 0.3 g adsorbent bed. The column biosorption data was best described by the Yoon Nelson model. The biosorbent demonstrated effective performance on borehole water, achieving removal from an initial concentration of 91 mg/L to 0.05 mg/L for iron while the initial concentration for manganese was reduced from 7 mg/L to 2 mg/L. Although, the removal of both iron and manganese was statically significant, only iron was successfully reduced to below the drinking water standards required by the World Health Organisation.

SEM images of the raw orange peels (ROP) and carbonised orange peels (COP) revealed varying degrees of porosity and particle distribution. EDS confirmed the presence of Fe and Mn on the surfaces of both ROP and COP after biosorption. The EDS findings shows that carbonisation of the raw sample can improve biosorption by nearly 3-fold. There were no significant differences in the FTIR spectrum of ROP and COP before and after application for the sorption of Fe and Mn. This indicates that the adsorption of Mn and Fe ions were non-chemical in nature. The BET surface areas of both ROP and COP were found to be very low, which is typical for carbonaceous materials. The surface area of the ROP is seen to increase with carbonisation.

This study concludes that carbonised orange peel is an effective biosorbent for removing iron and manganese from borehole water. This approach not only utilises agricultural waste but also offers a sustainable and eco-friendly solution to water contamination problems. The research advocates for the adoption of this method in water treatment practices, particularly in regions facing similar heavy metal pollution issues.

Acknowledgements

All praises be to Allah the Almighty who is the source of all knowledge and understanding. Peace and blessings upon the greatest teacher of humankind, the Holy prophet Muhammad (Peace Be Upon Him).

I want to show my gratitude to Professor Veruscha Fester for all the guidance and support. I truly feel thankful to her for managing time out of her busy schedule.

I also want to thank my co-supervisor Dr Oputu for his efforts and encouragement during my research as well as his assistance by providing access for sample testing at UCT. I appreciate his time in reviewing my thesis and for providing valuable comments and feedback.

To my other co-supervisor, Dr Sone for his dedication, assistance, and valuable contributions to my research.

I also want to show my appreciation to all the students and staff members at the Cape Peninsula University of Technology for making my stay productive and full of learning. A special thank you to Ms Hannelene Small for her continued support and assistance during this time. Many thanks to Zintle Ntshoko, a former student for her assistance.

Thank you to the Western Cape Government and the Cape Peninsula University of Technology for your financial assistance.

Thank you to everyone who played a part in my research studies, I really appreciate it.

To my parents who always supported me in every way possible, without them I would not be where I am today.

Finally, a special thanks to my husband Mogamad Ashraf Petersen and my children, Nuha and Yaqeen for the support, assistance, and encouragement during my studies.

Dedication

I dedicate this work to my family for their support and sacrifice to my well-being and education. I pray that the Almighty continues to protect and bless my family abundantly.

Table of Contents

Page

List of Figures

Page

List of Tables

Appendices

Glossary – Terms and Concepts

Adsorbent/ Biosorbent	: A material used in the removal of toxic metals from liquid. The terms adsorbent and biosorbent are interchangeable.
Adsorption/ Biosorption	: An interactive process where fluid is collected on the adsorbent surface. The terms adsorption and biosorption are interchangeable.
Biomass	: Organic material derived naturally from animals and plants.
Column	: refers to a reactor that supports a biologically active environment and is a vessel. in which a chemical process is conducted in removing contaminants from a solution.
Equilibrium	: refers to a point in the treatment process where there is no longer a change in time.
Wellfield	: A group of wells or boreholes in an underground reservoir or aquifer.
Aquifer	: A formation of permeable rock able to retain or convey groundwater.
Borehole	: A 15m deep hole in the ground for abstraction of groundwater.
Groundwater	: refers to water located beneath the surface in the saturated zone, below the water
Production borehole	: A deeper borehole is productive if it reaches an anomaly that is favourable for groundwater flow.

List of Abbreviations

WHO	: World Health Organisation
OP	: Orange Peels
ROP	: Raw Orange Peels
FPW	: Fruit Peel Waste
FP	: Fruit Peels
SEM	: Scanning Electron Microscopy
BET	: Brunauer- Emmet-Teller
FTIR	: Fourier Transform Infrared Spectroscopy
COP	: Carbonised Orange Peel
BH	: Borehole
SANS	: South African National Standards

List of Symbols

M : Mass

H : Height in bed column

V : Volume of mass in solution

Q : Adsorption capacity of biosorbent

Q_e : Amount of metal adsorbed at equilibrium per unit weight of adsorbent (mg/g)

Q_t : Amount of metal adsorbed at specified time (mg/g)

Q_m : Maximum biosorbent capacity (mg/g)

V : Volume of mass in solution

Fe : Iron

Mn : Manganese

C_i : Initial Concentration

C_f : Final Concentration

V_i : Initial Volume

V_f : Final Volume

mg/l : milligram per litre

ppm : parts per million

pH : Power of Hydrogen

Chapter 1 Introduction

1.1 Background and Motivation

Two thirds of the earth’s surface consist of water (O’Hehir, 2009). It is the source of life and the most valuable of all natural resources (Mnisi, 2011). However, heavy metal water pollution is a growing environmental problem, especially in developing countries such as South Africa (SA) (Joseph et al., 2019).

According to the SA Water Quality Guidelines (1996) iron consist of five percent of the earth's crust and ranks in the top four elements that exists in abundance. The presence of iron in water is generally an aesthetic issue. However, there have been cases where distribution systems have been affected especially at extremely high concentrations of iron. At this point health effects may become a concern. The presence of manganese in groundwater is almost always related to ferruginous water. It is often found that iron and manganese occur together in groundwater, but the manganese concentrations are typically lower than the iron concentrations (Zhang et al., 2014).

The presence of iron and manganese in groundwater is a serious environmental issue which causes a significant risk to the natural environment (Adekola et al., 2014). Iron and manganese in water cause various issues such as odour, metallic taste, water coloration, corrosion, turbidity, hardness, staining of plumbing fixtures and clogging of pipes. There are numerous ways in which iron and manganese can reach natural and ground waters. Manganese exposure causes harm to the nervous system and there is substantial information available stating the effects of exposure to Mn in water (Mendieta et al., 2011). When iron and manganese in water are exposed to air, they become indissoluble and causes the water to turn a brownish red colour. The challenges caused by iron and manganese are not only aesthetic, but also pose indirect health concerns.

According to the World Health Organization the acceptable aesthetic drinking water limits for iron and manganese are 0.3 and 0.1 mg/L, respectively (Mendieta et al., 2011). Consequently, it becomes essential to remove these heavy metals from wastewater by a suitable treatment technology before circulating it back into the environment (Zhang et al., 2014). Table 1.1 and 1.2 presents the effects for various iron and manganese ranges in water.

Table 1.1 Criteria for the iron range in water (SA Water Quality Guidelines, 1996)

Iron Range (mg/L)	Effects
Water Quality Target Range 0 - 0.1	No taste, other aesthetic or health effects associated with consumption and use.
0.1 – 0.3	Very slight effects on taste and marginal other aesthetic effects. Deposits in plumbing with associated problems may begin to occur. No health effects: the water is generally well tolerated.
0.3 – 1	Adverse aesthetic effects (taste) gradually increase as do possible problems with plumbing. No health effects.
1 - 10	Pronounced aesthetic effects (taste) along with problems with plumbing. Slight health effects expected in young children, and sensitive individuals.
10 - 30	Severe aesthetic effects (taste) and effects on the plumbing (slimy coatings). Slight iron overload possible in some individuals. Chronic health effects in young children and sensitive individuals in the range 10-20 mg/l, and occasional acute effects toward the upper end of this range.
30 - 100	As above. Long term health effects gradually increase.
100 - 300	As above. Chronic health effects. Acute toxicity may begin to appear.
300 - 3000	As above. Chronic and acute health effects. Accidental iron poisoning from water is rare.
3000 – 30 000	As above. Lethal toxicity occurs.

Table 1.2 Criteria for the manganese range in water (SA Water Quality Guidelines, 1996)

Manganese Range (mg/L)	Effects
Water Quality Target Range 0 - 0.05	No health or aesthetic effects; marginal aesthetic problems occasionally found in the 0.02 – 0.05 mg/l range.
0.05 – 0.10	Tolerable range, although slight staining may occur. No health effects.
0.10 – 0.15	Threshold for significant staining and taste problems. No health effects.
0.15 – 1.0	Increasingly severe staining and taste problems. No health effects.
1.0 – 2.0	Very severe staining and taste effects. No health effects.
2.0 – 5.0	Extreme staining, likely to aesthetically unacceptable to a large proportion of users. No health effects.
5 - 14	Unacceptable levels of aesthetic effects. Health effects rare.
14 - 20	Very severe, aesthetically unacceptable staining. Domestic use unlikely due to adverse aesthetic effects. Some chance of manganese toxicity under unusual conditions.
>20	Domestic use unlikely due to extreme aesthetic effects. Chronic toxicity, at high concentrations, possible acute effects.

1.1.1 Conventional methods used for the removal of iron and manganese from water

Khatri et al. (2017) states that biological, membrane technology and nano technology use chemicals in the treatment process, and it is expensive. He further elaborates on eleven conventional methods of which some use chemicals and states that the adsorption method has the potential to be the cheapest option due to green adsorbents. Conventional methods can further be broken down into various other categories such as aeration, ion exchange, electrocoagulation, wetland treatment and adsorption to name a few as indicated in figure 1.1 (Khatri et al., 2017).

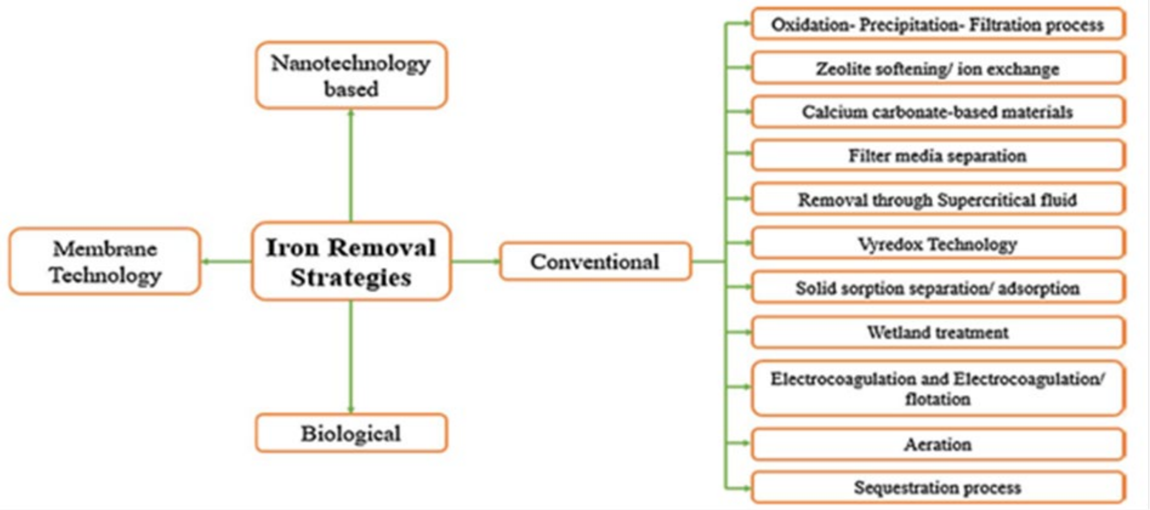

Figure 1.1 Categories of iron removal technologies (Khatri et al., 2017)

The most common methods for heavy metal removal from water consist of membrane filtration, electrocoagulation and activated carbon. These methods are not feasible with respect to developing countries as they do not have access to these costly methods (Joseph et al., 2019).

1.1.2 The reason for selecting biosorption for the removal of iron and manganese in water

In developing countries conventional methods for removing heavy metals from water are not feasible. It is therefore recommended that the planned technologies must be abundant, economical, and environmentally friendly (Park et al., 2010). Biosorption offers the advantages of good efficiency and potentially low cost and promotes a sustainable water management concept (Lim et al., 2013). Park et al. (2013) states that the disadvantages of conventional methods are that they are expensive, removal efficiencies are low and there is a vast amount of chemicals used. Zhang et al. (2014) agrees that conventional methods do have many shortcomings such as large operational costs. Activated carbon has been widely used to remove heavy metals from wastewater, but its high capital and operational costs have led to increased interest in exploring low-cost alternatives. This has driven significant research into using agricultural waste as adsorbents (Zhang et al., 2014). According to Pathak et al. (2015), fruit peel waste (FPW) is abundantly available from the agricultural and food processing industries and holds significant potential in wastewater treatment. Due to its abundance and potentially low cost, FPW is considered a promising candidate for the removal of heavy metals.

1.1.3 The reason for selecting orange peel for the removal of iron and manganese in water

The SA fruit industry produces a large variety of fruit and generates enormous quantities of waste. The portion of the fruit that is typically discarded is called the pomace and this is classified as solid waste. The pomace does not easily degrade (Khan et al., 2015). Reusing this discarded waste will remove them from the environment and circumvent the need for solid-waste handling. Fruit peels (FP) are dumped into municipal landfills, and this then results in disposal issues and pollution (Pathak et al., 2017). Improper disposal or management of biowaste such as fruit peels can contribute significantly to pollution. The harmful effects of biowaste are landfill pollution which causes climate change due to methane emissions, air pollution from the decomposition of the biowaste causing odors, water contamination from the leachate runoff into drinking water sources, soil contamination, public health issues where the public is exposed to pathogens causing diseases and biodiversity loss. Thus, if FP are used as biosorbents it then fulfills a double function where it is used to remove iron from water and simultaneously reduces solid-waste management (Khan et al., 2015). A large variety of fruit that the SA fruit industry produces consist of pineapples, grapes, apples, citrus fruit, pears, and peaches that are produced in the highest quantities (Khan et al., 2015). As can be seen in Table 1.3, citrus fruit is the highest produced fruit crop in South Africa and thus produces the most fruit waste. Pathak et al. (2017) also specifically mentions orange peels in his review paper and found that previous research studies showed excellent removal efficiencies.

Table 1.3 Production and processing data for various fruit crops in South Africa (Khan et al., 2015)

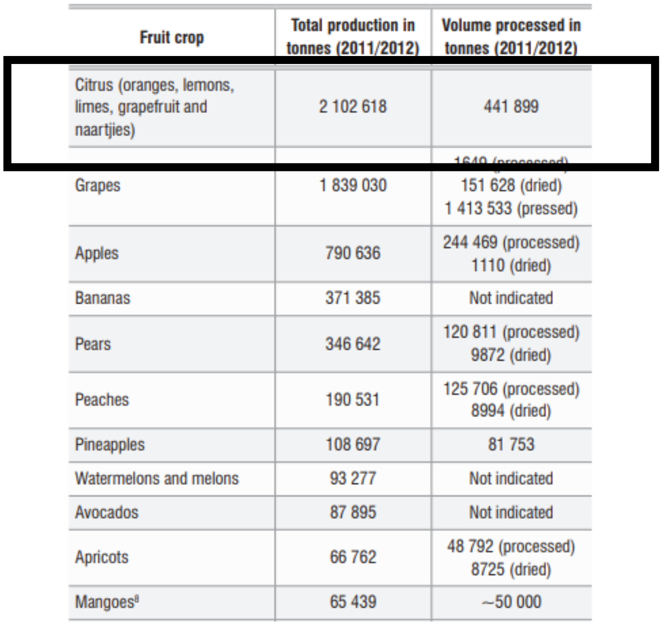

Fruit crop	Total production in tonnes (2011/2012)	Volume processed in tonnes (2011/2012)
Citrus (oranges, lemons, limes, grapefruit and naartjies)	2 102 618	441 899
Grapes	1 839 030	1640 (processed) 151 628 (dried) 1 413 533 (pressed)
Apples	790 636	244 469 (processed) 1110 (dried)
Bananas	371 385	Not indicated
Pears	346 642	120 811 (processed) 9872 (dried)
Peaches	190 531	125 706 (processed) 8994 (dried)
Pineapples	108 697	81 753
Watermelons and melons	93 277	Not indicated
Avocados	87 895	Not indicated
Apricots	66 762	48 792 (processed) 8725 (dried)
Mangoes[8]	65 439	~50 000

In a study done by Nandeshwar et al. (2015) various low-cost adsorbents were compared and although all of them showed potential in their capacity to remove iron, orange peels were the most promising green adsorbent with a 77-90% removal efficiency. Furthermore, many publications such as Khan et al. (2015), Park et al. (2010) and Pathak et al. (2017) indicates that biosorbents can be used as effective materials to remove heavy metals from water. As opposed to the use of traditional wastewater treatment methods, biosorbents should be considered as an alternative method.

Previous adsorption studies in the removal of heavy metals have utilised various biowastes such as banana peels, eggshell powder, coconut shells, and tea waste but only seven studies were found which investigated orange peels in the removal of iron and one study investigated the removal of both iron and manganese in a single system. These studies only investigated adsorption in batch experiments, and most of these studies were also limited by using only synthetic model fluid in experiments as opposed to the treatment application of real-life water sources. They also did not examine binary systems. Therefore, it can be concluded that progress has been made in understanding biosorbents and their applications in batch studies, but gaps remain in the exploration of fixed-bed column studies specifically relating to the use of orange peel wastes as biosorbents for iron and manganese removal. Furthermore, literature studies on real-world applications are scarce and inconsistent. A summary of these literature studies can be seen in Table 1.4

Table 1.4 Summary of previous literature studies utilizing orange peels as a biosorbent for removal of iron and manganese.

Author/s and Year of publication	**Iron/ Manganese**	**Batch/ Column**	**Type of water**	**Single/ Binary**
This study	Iron and Manganese	Batch and Column	Model fluid and Borehole water	Single and Binary
Tadepalli et al., 2016	Iron	Batch	Model fluid	Single
Elsherif, 2017	Iron	Batch	Model fluid	Single
Mamun et al., 2019	Iron	Batch	Model fluid	Single
Adebayo et al.,2016	Iron	Batch	Model fluid	Single
Surovka et al.,2017	Iron and Manganese	Batch	Model fluid	Single
Rashid, 2009	Iron	Batch	Model fluid	Single
Nandeshwar et al., 2015	Iron	Batch	River water	Single

This study will expand on the previous research literature where fruit wastes were successfully used as biosorbents for heavy metal removal from water, with specific reference to a study done by Ntshoko (2020) who investigated the use of pineapple peels in the removal of cobalt. It was found in this study that carbonisation yielded better results as opposed to the chemical treatment. Thus, this research study will specifically focus on the carbonisation treatment of the biosorbent and will test the viability of orange peels as a biosorbent in iron and manganese removal. In previous studies citrus peels showed excellent iron removal efficiencies. This research study will focus on treating existing borehole water samples applied in both batch and column studies and will evaluate the effectiveness of the biosorbent in practical settings. This study will also determine the optimum operating conditions and removal efficiency of the biosorbent and will evaluate the effect of simultaneous removal of iron and manganese from water considering single and binary systems, which few studies have investigated.

1.2 Research problem

Excessive iron and manganese concentrations in drinking water supplies have become a major environmental and health concern, as these metals can lead to toxicity in humans and aquatic life. Despite existing water treatment methods, elevated levels of these metals continue to be detected in several regions, highlighting a need for more effective and sustainable solutions to mitigate heavy metal pollution. The Overstrand Municipality could utilise iron and manganese rich ground water reserves to supplement surface water resources. One of the feasible strategies identified for municipalities in South Africa to augment drinking water supply is water reuse. Thus, an effective treatment method such as adsorption utilising a viable biosorbent is to be tested and validated for further scale-up for use in municipal implementation. Reducing this elevated concentration of Fe and Mn in water samples sourced from different boreholes in a water catchment area in the Overberg region of the Western Cape Province of South Africa, will make this water amenable for human consumption and ensures safe disposal into the environment. Additionally, fruit waste such as citrus peels are dumped into municipal landfills, and this then results in disposal issues and pollution. Conversion of these waste from citrus fruits, specifically orange peels, to adsorbents will be useful for reduction of heavy metal pollution in water from these borehole sites and will simultaneously help reduce the environmental burden of solid waste in landfill sites.

1.3 Research Question

- What operating conditions would optimize adsorption for maximum effectiveness?
- How does the simultaneous removal of iron and manganese affect the adsorption process, considering single and binary systems?
- Which adsorption models best fit the experimental data?

1.4 Objectives and outcomes

The aim of this study is to investigate the use of carbonised orange peel as a biosorbent, to remove iron and manganese from borehole water in batch and column studies, for use in municipal application. The objectives of the study are:

- To prepare and structurally characterize the biosorbent using Scanning Electron Microscope (SEM) and Electron Dispersive spectroscopy (EDS), Fourier Transform Infrared (FTIR) Spectroscopy and Brunauer Emmet Teller (BET) surface area and pore analysis.

- To determine the optimum operating conditions and removal efficiency of the biosorption process, using a model fluid.

- To validate the performance of the fixed bed column with actual borehole water.

- To establish the effect of simultaneous removal of iron and manganese from borehole water considering single and binary systems.

The outcomes for this research study are as follows:

- The functional groups and changes to surface area and morphology will be identified.

- To show the effect of process parameters on the breakthrough curve.
- To show that the chosen biosorbent used is a suitable alternative when subjected to carbonisation for the removal of iron and manganese from borehole water.
- To illustrate that the chosen biosorbent successfully removes both iron and manganese from borehole water.

1.5 Delineation

Due to time and budget constraints this research study will not be exploring certain aspects:

- This study will only be investigating carbonisation as a biosorbent treatment and not chemical or other adsorbent treatment methods.
- The water sample might contain other contaminants and heavy metals but the only metals which will be examined are iron and manganese and the removal thereof.
- Regeneration of the spent sorbent will also not be done.
- A cost analysis will not be conducted in this study but could be addressed in future research.

1.6 Assumptions

Since the borehole water was continually being pumped it was assumed that the conveyance pipelines had not affected the borehole water samples.

1.7 Methodology

In this study, orange peels are applied for the absorptive removal of iron and manganese from borehole water. Adsorption experiments are done in both batch and column mode with the iron and manganese content determined by ICP-OES. Model fluid samples are prepared at various concentrations, masses, contact time and pH and the samples are then tested for iron and manganese ions before and after treatment. The biosorbents are also characterized by Scanning Electron Microscopy (SEM), Electron Dispersive Spectroscopy (EDS), Fourier Transform infrared (FTIR) spectroscopy and Brunauer Emmet Teller N_2 sorption at 77 K. / surface area analysis (BET). The experimental equilibrium data is used to assess the performance of the adsorption process by utilising various batch and fixed bed models and the most effective model is then identified.

1.8 Organisation of dissertation

Chapter 1 Introduction - comprises of the background which describes the research problem and outlines the objectives and outcomes of the research.

Chapter 2 Literature Review and theory - reviews literature on previous studies with regards to biosorption and the utilisation of biosorbents in the removal of heavy metals, particularly iron and manganese. It also includes a review on the literature detailing the process of biosorption specifically with regards to column studies.

Chapter 3 Research methodology - entails the research method and design process that was followed and further discusses materials, experimental procedure and how the results were obtained.

Chapter 4 Structural characterisation of the biosorbent - entails the compilation and discussion of the characterisation done on the orange peels.

Chapter 5 Batch results and findings - entail the presentation and discussion of the batch results. This chapter also draws on the research obtained from previous studies as the results are compared to each other.

Chapter 6 Column results and findings - entail the presentation and discussion of the column results. This chapter also draws on the research obtained from previous studies as the results are compared to each other.

Chapter 7 Conclusion and recommendations - In this chapter, conclusions were drawn from all the findings achieved during the investigation. This will offer a clear indication as to whether the objectives and outcomes were achieved. Recommendations for any future research on the topic are also included in this chapter.

Chapter 2 Literature review and theory

2.1 Introduction

South Africa is a developing country faced with many challenges, even though it is a country rich in natural resources with positive progress in the field of industry and manufacturing (Sayef., 2017). A growing concern in developing countries is rapid industrialisation which causes an increase in environmental pollution especially heavy metal contamination in various water sources. This is particularly problematic in developing countries due to inadequate water treatment technologies and insufficient ability to supply clean water to poor communities (Joseph et al., 2019). In Africa, groundwater is a significant and essential water resource. It is the primary source of enhanced drinking water in several parts of Africa. Heavy metal contaminants in water bodies is a major issue and is the cause of several diseases (Itete et al., 2021).

Iron and manganese are found in surface water as well as in ground water. Continuous consumption of water containing high iron and manganese levels could result in ill health conditions. Additionally, iron and manganese in water results in an unpleasant odour, taste, and reddish colour. Other issues reported are stains on laundry and plumbing fixtures as well as clogging of water pipelines which could be highly problematic if it is a main distribution line (Khatri et al., 2017). Schwarzenbach et al. (2010) recommends that an appropriate set of guidelines, technologies and technical innovations are required to deal with worldwide water pollution. In developing countries rural populations depend on groundwater that is often contaminated. One of the feasible strategies identified for municipalities in South Africa to augment drinking water supply is water reuse. Every city must plan for the utilisation and management of a range of water sources (Muller, 2019). The Overstrand Municipality could utilise iron and manganese rich ground water reserves to supplement surface water resources and it is for this reason solutions such as sustainable water treatment technologies are required.

2.2 Groundwater as an alternative water supply

Groundwater is a valuable water resource and when rainwater seeps into the ground it becomes groundwater and when rainwater seeps into the soil, it creates underground water reservoirs known as aquifers (City of Cape Town, Water Services and the Cape Town Urban Water Cycle, 2018: 4). In South Africa, groundwater is a vital water resource. Awareness and use of groundwater has been growing as well as the need for sustainable management. Enhanced groundwater management schemes are being developed and executed at required levels. These schemes are tailored to local requirements (Braune et al., 2014).

Water is present deep below the ground surface and covers three quarters of the earth's surface. The greatest portion of freshwater on earth is represented by groundwater as can be seen in figure 2.1 (Braune et al., 2014). The recent drought crisis and low rainfall in a warming world has become a concerning issue and has amplified the problem of water scarcity (WWF-SA, 2016). Reliable and safe water resources are a requirement for our economy. The prediction of less rain is expected in the country. The basis of our water supplies are our water resources, and this includes catchments, rivers, wetlands, and aquifers (WWF-SA, 2016).

Continued supply from our water resources is imperative for South Africa's water security. It is crucial that our water resources are preserved, maintained, controlled, restored, and managed. Rivers and lakes are surface water resources used for large urban water supply. Groundwater is a critical resource stored in aquifers, soil, and rock pores, primarily accessed through boreholes. Many rural communities rely on this source for their water supply. Groundwater, along with surface water sources like rivers, wetlands, estuaries, and springs, is replenished by rainfall, highlighting its vital role in sustaining ecosystems and communities (WWF-SA, 2016).

This first step in addressing South Africa’s water security challenges is to understand and unpack groundwater potential. Groundwater sources in South Africa accounts for only 13% of the country’s overall water intake as seen in figure 2.2. The communities that are dependent on groundwater very often have no other sustainable sources. It was highlighted that groundwater resources must play a progressive and strategic role in Africa, especially for rural communities (WWF-SA, 2016). Figure 2.1 indicates that groundwater represents 30.1% of the earth’s freshwater.

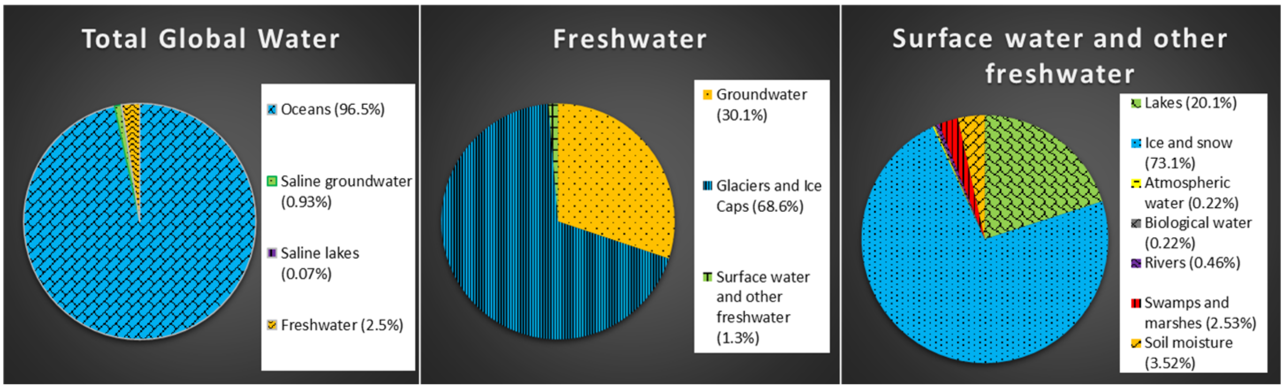

Figure 2.1 Diagram representing the groundwater portion of the earth’s freshwater (Braune et al., 2014)

Dependence on groundwater as a critical water source is increasing at various scales, including small-scale supplies, large-scale systems, and individual boreholes. Groundwater can help mitigate drought impacts due to its substantial storage capacity. Unlike surface water, groundwater is not prone to evaporation losses. During periods of heavy usage, additional stored volumes can be tapped into during droughts, with the aquifer replenished in subsequent non-drought years by reducing water abstraction. This highlights groundwater's vital role in water resource management and resilience (WWF-SA, 2016).

Reddick et al. (2018) states that in 2017, the Western Cape experienced its worst drought which became the main driving force for investment in this sector by various municipalities in the province. The demand for technologies that supported water resilience had increased, and innovative investment prospects launched in four strategic areas, water reuse, monitoring, efficiency, and alternative water supply. The drought put considerable strain on the province's water resources, resulting in potential supply shortages and financial losses. Water restrictions forced citizens to reduce their municipal water consumption. In response, municipalities sought emergency water supplies and re-evaluated their long-term drought resilience plans. Groundwater emerged as a viable alternative water source, with immediate opportunities identified in four key areas (figure 2.3) aimed at enhancing drought resilience and decreasing reliance on conventional surface water sources (Reddick et al., 2018).

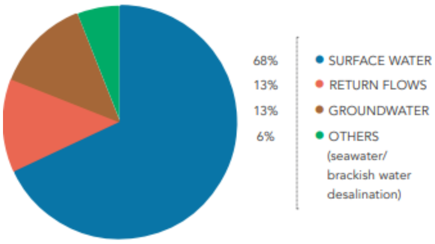

Figure 2.2 Water sources in South Africa (Reddick et al., 2018)

South Africa experiences significant variations in climate and rainfall. Despite being a water-scarce nation, its water consumption exceeds international benchmarks. Currently, the country's water yield is approximately 15 billion m³ per year, with the majority coming from surface water (68%) and return flows that contribute to surface water (13%) as shown in Figure 2.2 (Reddick et al., 2018).

Groundwater development in South Africa holds significant potential, with an estimated national yield of 7-10 billion m³/year, of which only 2-4 billion m³/year is currently utilized. Groundwater can be accessed relatively quickly and cost-effectively compared to other alternative water sources. Several municipalities in the Western Cape are investing in alternative groundwater supplies to mitigate short-term water shortages, recognizing it as a priority option for supply augmentation. Additionally, long-term groundwater projects are being considered, presenting opportunities to reduce reliance on surface water sources, as illustrated in Figure 2.3 (Reddick et al., 2018).

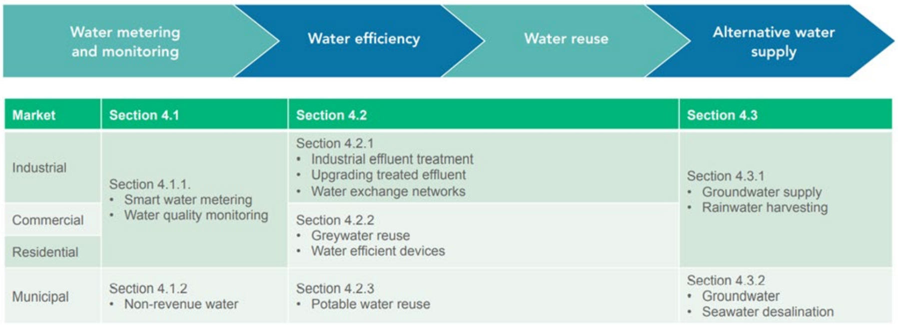

Market	Section 4.1	Section 4.2	Section 4.3
Industrial	Section 4.1.1. • Smart water metering • Water quality monitoring	Section 4.2.1 • Industrial effluent treatment • Upgrading treated effluent • Water exchange networks	Section 4.3.1 • Groundwater supply • Rainwater harvesting
Commercial		Section 4.2.2 • Greywater reuse • Water efficient devices	
Residential			
Municipal	Section 4.1.2 • Non-revenue water	Section 4.2.3 • Potable water reuse	Section 4.3.2 • Groundwater • Seawater desalination

Figure 2.3 Overview of the key opportunity areas (Reddick et al., 2018)

South Africa’s aquifer systems have established their properties through the geological and hydrological history of the area and attributed to the physical and chemical composition of the rock types. A practical aquifer classification and management system was developed to support the regulatory system. It comprises of major, minor, and poor aquifer systems as well as sole source and special aquifers as demonstrated in Table 2.1 (Braune et al.,2014).

Table 2.1 Aquifer systems in South Africa (Braune et al.,2014)

Aquifer System Classification	Coverage of country (%)	General Location
Major Aquifers	18	Primary aquifer systems along the coast; Dolomitic systems in parts of Gauteng, Mpumalanga, the Northern Cape and North-West Province; Rocks of the Table Mountain Group bordering the Cape coast; Parts of the Karoo Supergroup; Cities and towns receiving water from major aquifer systems are Pretoria, Mmabatho, Atlantis, St. Francis Bay and Beaufort West.
Minor Aquifers	67	Minor aquifers occur widely across South Africa with variable borehole yield and water quality. They supply many smaller settlements, e.g. Nylstroom, Williston, Carnarvon and Richmond.
Poor Aquifers	15	Poor aquifers occur mainly in the dry northern and western parts of the country. The generally low borehole yields of poorer quality are, however, still of critical importance to small rural communities.

Growing urbanisation places enormous pressure on our scarce water resource and it is thus important to ensure a sustainable water balance by implementation of various strategies which includes amongst others further utilisation of groundwater (Braune et al.,2014).

2.3 Policies that govern our water

Braune et al. (2014) highlight that South Africa's water resources are governed by the Water Services Act of 1997 and the National Water Act (NWA) of 1998. These laws operate on the principle that all water is part of a single, interconnected cycle and should be managed within a cohesive regulatory framework. The Acts include comprehensive measures for protecting, utilizing, developing, conserving, managing, and controlling the nation’s water resources. Figure 2.4 offers an overview of the legislation governing the sustainable use of groundwater in South Africa (NWRS; DWAF 2013).

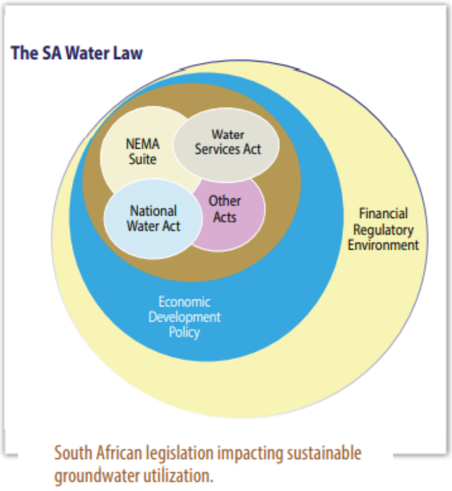

Figure 2.4 Overview of the SA water law (Braune et al.,2014)

2.4 The presence and effects of iron and manganese in water

Pascu et al. (2015) and Ahmad (2012) stated that iron and manganese commonly coexist in deep groundwater where oxygen is scarce, often dissolving in water that flows through organic soil. While their presence can occur naturally, human activities like landfill leaks and industrial discharges also contribute to elevated levels. In anaerobic conditions, iron (Fe^{3+}) and manganese (Mn^{4+}) are reduced to their soluble forms (Fe^{2+} and Mn^{2+}). When this groundwater is pumped to the surface, exposure to air triggers oxidation, converting them to insoluble forms, which can cause issues like precipitation and coloration.

Iron often exists in insoluble forms in groundwater due to geological factors or the use of metallic pumping equipment (Joseph, 2016). Changes in water conditions—such as temperature, pressure, or pH—can facilitate the transition from clear water (containing Fe^{2+}) to red water (containing precipitated ferric hydroxide). The pH significantly influences iron precipitation, and high pH levels accelerate this process.
Manganese, typically found as a stable bivalent ion (Mn^{2+}), also dissolves in groundwater. Upon oxidation, it becomes insoluble and can affect water quality, leading to aesthetic issues such as colour changes and bad odours. Excessive manganese consumption poses health risks, including potential neurological effects (Rudi et al, 2020).

In industrial systems, accumulated iron and manganese can obstruct pipelines, reduce water pressure, and increase operational costs, as well as promote bacterial growth that causes further aesthetic issues. The World Health Organization recommends aesthetic limits of 0.3 mg/L for iron and 0.1 mg/L for manganese, with chronic exposure limits of 2 mg/L and 0.4 mg/L, respectively. When concentrations exceed these standards, treatment is necessary to ensure safe drinking water (Mendieta et al., 2011).
Overall, the presence of iron and manganese in groundwater poses challenges for municipalities in delivering safe and aesthetically pleasing water to consumers, often prompting treatment driven by aesthetic rather than health concerns (Tobiason et al., 2016).

2.5 Forms of iron and manganese in water

Iron in water exists in various forms, primarily classified as soluble ferrous iron (Fe^{2+}) and insoluble ferric iron (Fe^{3+}) (Khatri et al., 2017). While pure iron is silvery, it typically appears as greyish-black or brown due to oxidation (Ramachandra, 2005). The presence of iron in natural water can result from domestic or industrial waste disposal or geological processes. In groundwater, iron is generally found in its bivalent, soluble form (Fe^{2+}), which can easily oxidize to ferric iron (Fe^{3+}) upon exposure to air (Oram, 2012).
In borehole water, iron is typically found in three forms:

1. **Bacterial Iron**: Identified by slime, associated with microbial activity.
2. **Ferric Iron (Red Water Iron)**: Formed when oxygen oxidizes ferrous iron; it appears as red-colored deposits.
3. **Ferrous Iron (Clear Water Iron)**: Found in anoxic conditions, commonly in deeper groundwater, and forms as soluble ferrous bicarbonate (Fe^{2+}).

Manganese, a greyish-white metal, is also present in various oxidation states, primarily as manganous ion (Mn^{2+}). While manganese can be neurotoxic at high concentrations, its effects are often more aesthetic than toxic in typical water supplies (Joseph, 2016). Upon oxidation, manganese converts to manganic ion (Mn^{4+}), leading to precipitation and the formation of black hydrated oxides.
Overall, both iron and manganese pose challenges in water quality management, affecting aesthetic and operational aspects of water systems (WHO,1996).

2.6 Iron and manganese removal methods

Iron removal methods can be classified into four main branches which consist of conventional methods, biological methods, membrane technology-based methods and nanotechnology-based methods. Conventional methods can further be broken down into various other categories such as aeration, ion exchange, electrocoagulation, wetland treatment and adsorption to name a few (Khatri et al., 2017). The most common methods for heavy metal removal from water, consist of activated carbon, membrane filtration, electrocoagulation, and adsorption. These methods are not feasible with respect to developing countries. In developing countries, anticipated methods should be easy to acquire, be able to be constructed by semi-skilled local workers and should have minimal operating and maintenance costs. Therefore, it is important to explore the use of potentially low-cost and locally available materials (Joseph et al., 2019). The modification of the current adsorption method should be explored by utilising biosorbents that are abundant and cheap alternatives.

Manganese and iron present different challenges and there are various types of treatment technologies available that are effective in the removal of iron and manganese from water. However, it is worth noting that not all methods are uniformly effective under several conditions (Pascu et al., 2015). Table 2.2 presents a summary of the various available removal or treatment technologies.

Table 2.2 Methods for heavy metal removal (Emenike, 2016)

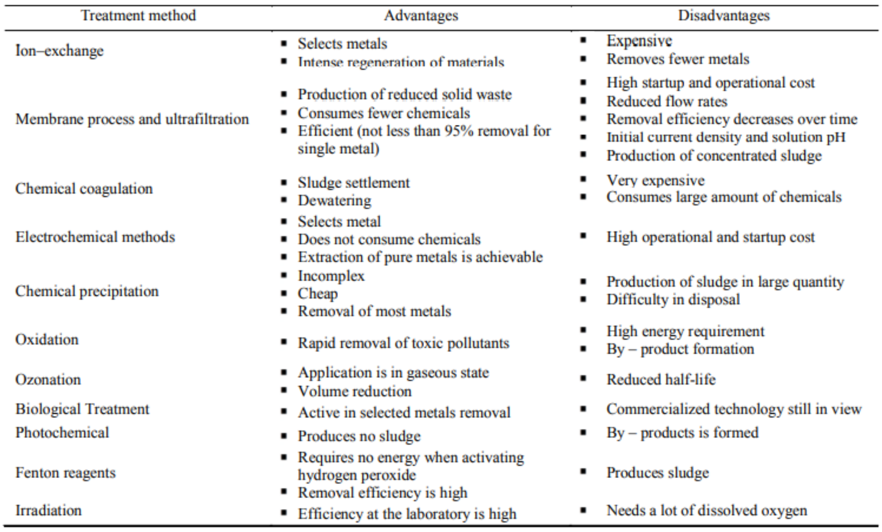

Treatment method	Advantages	Disadvantages
Ion–exchange	▪ Selects metals ▪ Intense regeneration of materials	▪ Expensive ▪ Removes fewer metals
Membrane process and ultrafiltration	▪ Production of reduced solid waste ▪ Consumes fewer chemicals ▪ Efficient (not less than 95% removal for single metal)	▪ High startup and operational cost ▪ Reduced flow rates ▪ Removal efficiency decreases over time ▪ Initial current density and solution pH ▪ Production of concentrated sludge
Chemical coagulation	▪ Sludge settlement ▪ Dewatering	▪ Very expensive ▪ Consumes large amount of chemicals
Electrochemical methods	▪ Selects metal ▪ Does not consume chemicals ▪ Extraction of pure metals is achievable	▪ High operational and startup cost
Chemical precipitation	▪ Incomplex ▪ Cheap ▪ Removal of most metals	▪ Production of sludge in large quantity ▪ Difficulty in disposal
Oxidation	▪ Rapid removal of toxic pollutants	▪ High energy requirement ▪ By – product formation
Ozonation	▪ Application is in gaseous state ▪ Volume reduction	▪ Reduced half-life
Biological Treatment	▪ Active in selected metals removal	▪ Commercialized technology still in view
Photochemical	▪ Produces no sludge	▪ By – products is formed
Fenton reagents	▪ Requires no energy when activating hydrogen peroxide ▪ Removal efficiency is high	▪ Produces sludge
Irradiation	▪ Efficiency at the laboratory is high	▪ Needs a lot of dissolved oxygen

2.7 Chemistry of iron and manganese

2.7.1 Chemistry of iron

Ahmad (2012) says that iron in water can be present in either soluble (Fe^{2+}) or insoluble form (Fe^{3+}).

The process of oxidizing Fe^{2+} to Fe^{3+} is illustrated in Figure 2.5 and the process can also be presented as per equation 2. 1.

Figure 2.5 The oxidation of ferrous iron to ferric iron occurs because of exposure to oxygen (Ahmad, 20

$Fe^{+2} = Fe^{+3} + e^{-}$ Equation 2.1

In environments with high dissolved oxygen concentrations, the ferric ion (Fe^{3+}) can react with hydroxyl groups, leading to the formation of solid precipitates as shown in equation 2.2.

$Fe^{+3} + 3OH^{-} = Fe\ (OH)_3$ Equation 2.2

The entire sequence of oxidation-reduction reactions can be expressed as shown in equation 2.3.

$Fe^{+2} + 3H_2O = Fe\ (OH)_3 + 3H^{+} + e^{-}$ Equation 2.3

Ahmad (2012) states that the stability of iron is influenced by both pH and the redox potential (pE), which represents the electron activity. A high pE value indicates oxidizing conditions where iron becomes insoluble, while low pE values suggest reducing conditions where iron remains soluble, as illustrated in the Eh-pH stability chart (Figure 2.6).

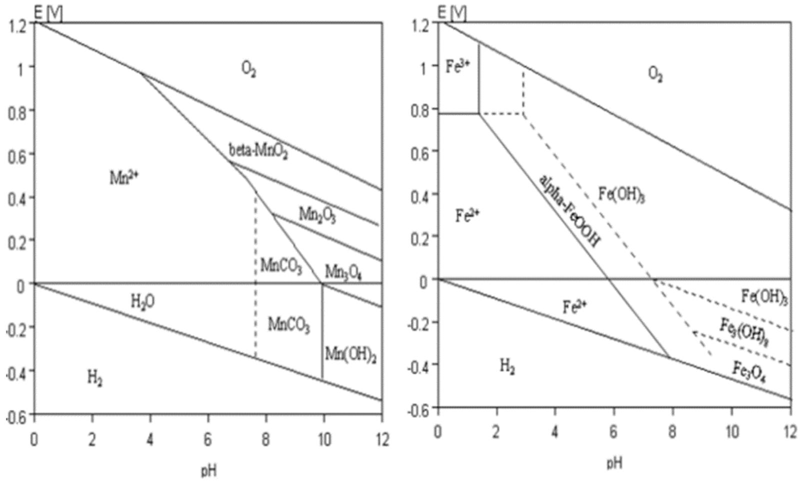

Figure 2.6 Eh-pH stability chart for iron and manganese (Ahmad, 2012)

2.7.2 Chemistry of manganese

Ahmad (2012) also states that manganese exists in soluble (Mn^{2+}) or stable (Mn^{4+}) form in water.

Equation 2.4 below illustrates how one form of manganese is transformed into other (Ahmad, 2012).

$$Mn^{2+} + 2H_2O = MnO_2 + 4H^+ + 2e^- \quad \text{Equation 2.4}$$

2.8 Adsorption mechanism

Adsorption is a process where a fluid is collected on the adsorbent surface. This then forms a molecular film called the adsorbate and it may be solid or liquid form as shown in Figure 2.7. The adsorbate is the substance that is adsorbed and the surface on which it is adsorbed is called adsorbent. In wastewater treatment, adsorption is one of the most used methods as it is effective in the treatment of heavy metals (Khatri et al., 2017). Biosorption is defined as the ability of biological material to accumulate or remove substances such as heavy metals from aqueous solutions. However, the terms adsorption and biosorption are interchangeable.

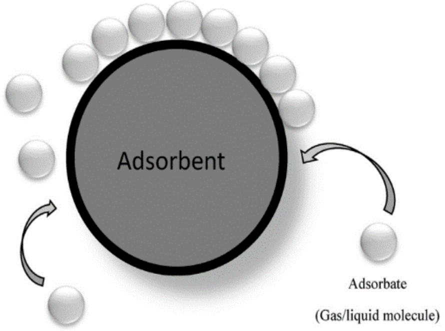

Figure 2.7 Adsorption process relating to the interaction between the adsorbent and adsorbate (Rudi et al., 2020)

Rudi et al., (2020) states that adsorption is an interactive process where a liquid component adheres to the surface of a solid adsorbent through physical or chemical interactions, influenced by intermolecular forces. This segregation process allows for the isolation of metal ions and can be conducted using either batch or continuous methods.

There are two main types of adsorption processes:

1. **Physical Adsorption**: Involves weak intermolecular forces between the adsorbent and adsorbate. This type can result in multilayer adsorption, offering high adsorption capacity. It is typically reversible.
2. **Chemical Adsorption**: Involves stronger interactions through chemical bonding or electron transfer, resulting in a permanent reaction known as activated adsorption. This process is generally irreversible and limited to monolayer adsorption, making regeneration of the adsorbent more challenging.

Overall, the choice between physical and chemical adsorption depends on the specific application and desired outcomes in metal ion removal or other separation processes (Rudi et al., 2020). Figure 2.8 illustrates the processes involved in both physical and chemical adsorption between the adsorbent and the adsorbate.

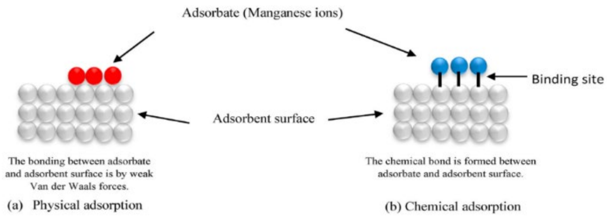

Figure 2.8 The mechanism of (a) physical and (b) chemical adsorption (Rudi et al., 2020)

During the adsorption process, all available active sites are filled through either physical or chemical adsorption (Rudi et al., 2020). Figure 2.9 shows the steps in the adsorption process.

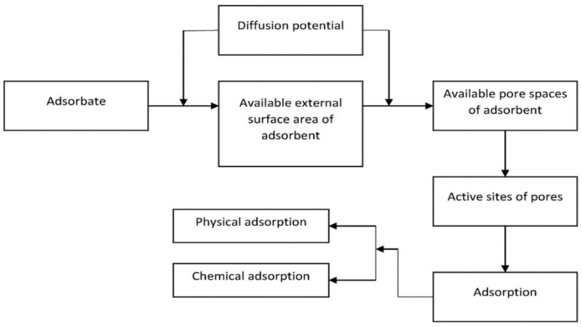

Figure 2.9 Steps involved in the adsorption process (Rudi et al., 2020)

Pathak et al (2015) presents a detailed diagram of the overall FPW adsorption process as per Figure 2.10 which includes pre-treatment, characterisation, adsorption, and regeneration amongst others.

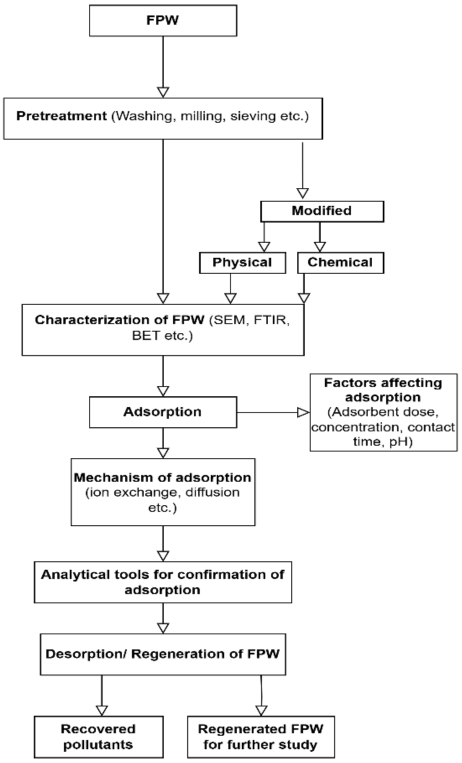

Figure 2.10 Overall adsorption process using FPW (Pathak et al., 2015)

Figure 2.11 also illustrates the adsorption-oxidation mechanism of adsorptive Fe removal where Fe^{2+} is adsorbed on the surface of the adsorbent. Once oxygen is introduced the Fe^{2+} is oxidized and forms a new surface for adsorption (Ahmad, 2012).

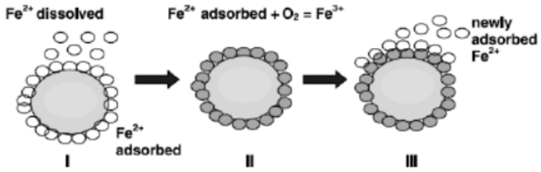

Figure 2.11 Adsorption-oxidation mechanism (Ahmad, 2012)

2.9 Fundamental of biosorption

According to Maksoud et al. (2019) the implementation of biosorption is pragmatic and contributes to sustainable development as it is seen as an environmentally friendly, profitable, and effective water treatment method. Biosorption has demonstrated a reduction of contaminant levels in drinking water, to the standards as set out by the WHO. This basic biosorption process conforms with the principles of green chemistry and can be defined as the uptake, built on the usage of non-living biomasses for the removal of biowaste. This method contributes to waste minimization, which can improve or remedy many environmental issues. Additional favourable attributes of biosorption includes flexibility, readily available materials, low energy conditions, potentially low operating and manufacturing cost, ease of operation and high efficiency.

Kratochvil et al. (1998) says biosorption of heavy metals seems to be incredibly cost-efficient. Bed sorption column experiments is efficient for the purpose of lab scale studies. It is seen that biosorbents are easily regenerated which means it is capable of being reused in several sorption cycles. The concept of biosorption as a successful method has been gradually developing over the years. Compared to other conventional methods this method is seen as a creditable or worthwhile option in wastewater treatment.

Sorption is defined as an occurrence relating to physical chemistry where the sorbate concentrates on the surface of another sorbent. Biosorption happens when the sorbate is captured from the aqueous solution using a biological pattern. Absorption occurs when one material is integrated in one state and then into another material in another state. On the other hand, adsorption occurs when the sorbate physically bonds with the surface of a sorbent (Maksoud et al.,2019).

2.10 Selection of biosorbent

The main aspects to consider when selecting and preparing a biosorbent is its suitability, cost efficiency as well as its source. A biomass classified as waste is more favourable as opposed to non-waste alternatives. A few positive attributes noted are the fact that the need for growth is not required and the ability to reuse and recover the biosorbent. Additional favourable characteristics of a selected biosorbent includes Eco friendliness, availability, feasibility, high removal efficiency under variable parameters and also ability for regeneration of the spent sorbent. It is also desirable that the chosen material is easily adaptable to various designs (Maksoud et al.,2019).

2.11 Agricultural/ fruit peel waste

Agricultural waste is defined as organic by-products disposed of during the process of production. This broad term can further be broken down and comprises of agricultural waste, plant waste, rural waste, crop stalks, livestock, poultry, and animal manure. There are many benefits of using agricultural waste as biosorbents such as huge quantities, extensive supply range, environmental friendliness, biodegradability, and reproducibility. The use of agricultural waste as biosorbents in the treatment of various water pollutants such as heavy metals has been proved to be a favourable method as demonstrated by numerous studies over the years. This is due to its high porosity, loose surface, chemical and mechanical stability, and the fact that these wastes are considered as inexpensive, natural, and effective. There are many advantages associated with agriculture waste biosorbents and it is therefore seen as effective, efficient, sustainable, and suitable alternatives, as opposed to the expensive commercial adsorbents widely used in water treatment such as activated carbon. Agricultural waste is used in fertilizer, energy, and wastewater treatment and these are among the most important applications (Maksoud et al.,2019). The portion of the fruit that is typically discarded is called the pomace, the pomace does not easily degrade (Khan et al., 2015). Reusing this discarded waste will remove them from the environment. FPW are dumped into municipal landfills, and this then results in disposal issues and pollution (Pathak et al., 2017). Thus, if FP are used as biosorbents it then fulfills a double function where it is used to remove iron from water and simultaneously reduces solid-waste management (Khan et al., 2015). Fruit peel waste (FPW) has shown significant potential for removing a range of contaminants from water, including the effective elimination of heavy metals from aqueous solutions (Pathak et al., 2015).

2.11.1 Waste materials previously used as biosorbents

Joseph et al. (2019) reviews the following materials:

- Agricultural waste from nuts such as peanuts and pistachio cashew
- Fruit and vegetable waste such as banana, lemon, orange peels and corn
- Naturally occurring soil such as seaweeds
- Other waste materials such as tea waste, and industrial by-products

2.12 Citrus waste and waste management

According to Mahato et al. (2020) citrus is one of the most widely cultivated fruit crops globally, but about half of the fruit produced in the food processing industry ends up as waste, contributing to pollution. This discarded biomass, which includes peels, seeds, and inedible parts, could be repurposed as a biosorbent for removing toxic metals from wastewater, rather than being sent to waste disposal facilities. Traditional waste disposal methods incur significant transportation costs and require suitable disposal sites.

Mahato et al. (2021) illustrates the conventional methods of citrus waste removal from food processing industries and highlight their negative environmental impacts in Figure 2.12. This approach emphasizes the potential for transforming waste into a valuable resource, promoting both sustainability and pollution reduction.

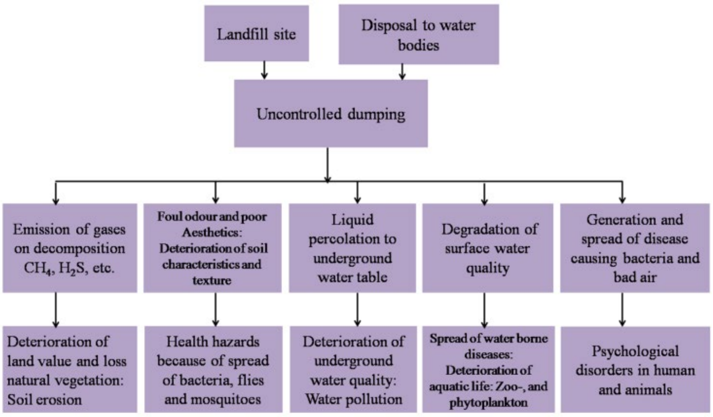

Figure 2.12 Traditional methods of waste disposal from citrus processing plants and its environmental effects (Mahato et al., 2021)

Previous studies have highlighted the use of various potentially low-cost agricultural wastes, such as rice husk, tea waste, banana peel, and orange peel, as adsorbents for removing heavy metals from wastewater. However, the removal efficiency of these adsorbents is often limited. To improve their effectiveness, biosorbents can be modified. Among them, citrus peels have been identified as a potentially cost-effective and affordable option. By transforming this waste material into a valuable product, it can serve as a potentially low-cost adsorbent for heavy metal removal, simultaneously addressing environmental pollution concerns (Mahato et al., 2021). Figure 2.13 illustrates the environmental impact of heavy metal pollution.

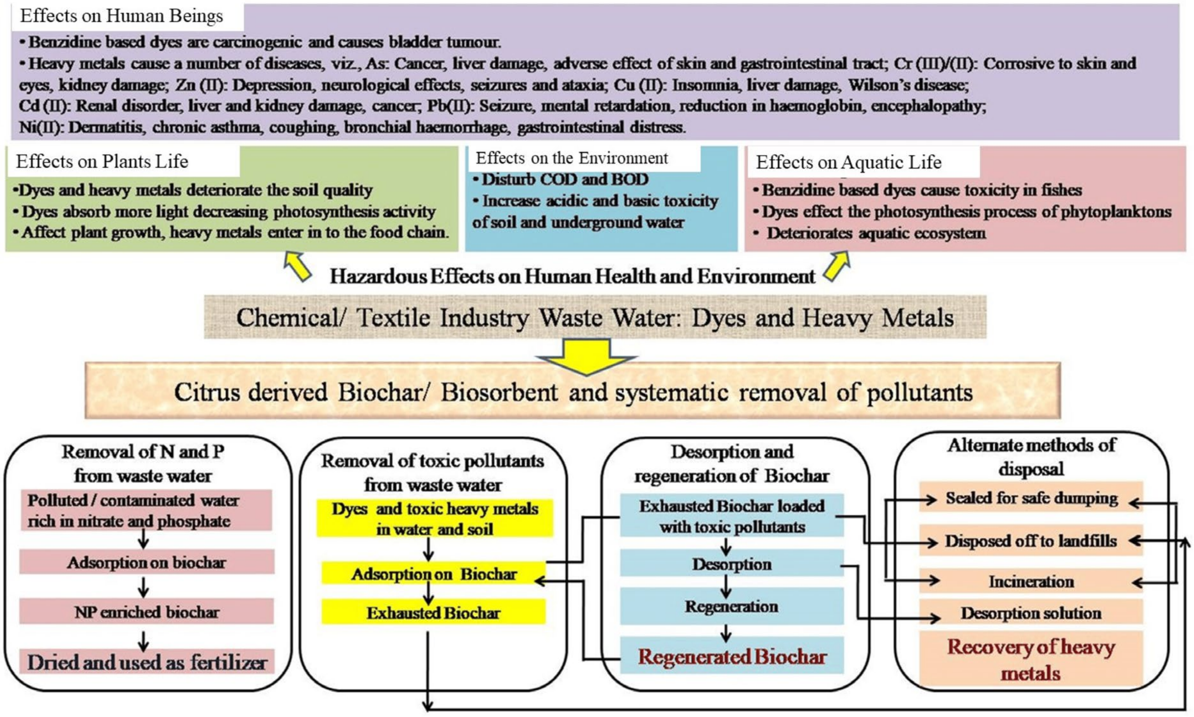

Figure 2.13 The harmful impacts of dyes and heavy metals in wastewater from chemical and textile industries on human health and the environment, and the potential use of citrus waste as biosorbents for remediation (Mahato et al., 2021).

2.13 Physical properties point of zero charge and surface pH of orange peels

2.13.1 Physical properties

Pathak et al. (2017) assessed the physical properties of various fruit peels (FP) as can be seen in Table 2.3. The physical properties included the bulk density, water absorption capacity and porosity amongst others. This work showed that citrus peels (CP) had the highest water adsorption capacity but the lowest bulk density when compared to other FP's. However, orange peels (OP) had the lowest porosity but the highest bulk density. Pathak et al. (2017) established that the variations in bulk densities of the various peels were largely due to differences in particle shape and size and the high water absorption capacity of FP was attributed to the high fibre content of peels due to hydrophilic groups.

Table 2.3 Physical properties of FP (Pathak et al., 2017)

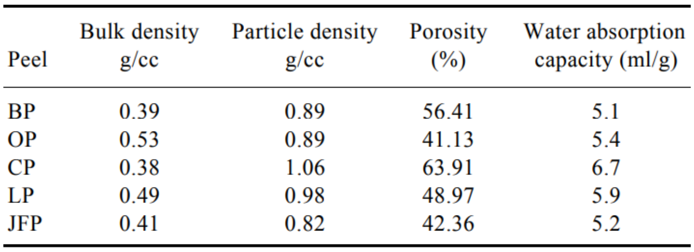

Peel	Bulk density g/cc	Particle density g/cc	Porosity (%)	Water absorption capacity (ml/g)
BP	0.39	0.89	56.41	5.1
OP	0.53	0.89	41.13	5.4
CP	0.38	1.06	63.91	6.7
LP	0.49	0.98	48.97	5.9
JFP	0.41	0.82	42.36	5.2

2.13.2 Point of zero charge and surface pH

Pathak et al. (2017) highlight the importance of the point of zero charge (pHpzc) in adsorption studies, as it indicates the ionization characteristics and interactions between the adsorbent and adsorbate. In batch studies conducted to determine the pHpzc of various fruit peels (FPs), it was found that the pH at which the surface of the fruit peels is neutral is referred to as pHpzc as seen in Table 2.4.

Cation adsorption is favoured when the pH is greater than the pHpzc, while anion adsorption is favoured when the pH is lower. The study revealed that the pHpzc and surface pH values of orange peels (OP) and citrus peels (CP) are in the range of 3–4, indicating a predominance of acidic functional groups over basic ones on their surfaces. Consequently, this suggests that these peels are suitable for the adsorption of cations (Pathak et al., 2017).

Table 2.4 Point of zero charge and surface pH of some FP (Pathak et al., 2017)

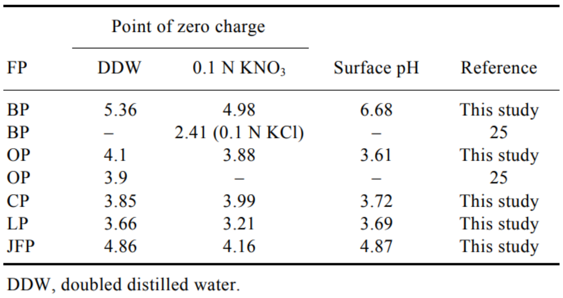

	Point of zero charge			
FP	DDW	0.1 N KNO_3	Surface pH	Reference
BP	5.36	4.98	6.68	This study
BP	–	2.41 (0.1 N KCl)	–	25
OP	4.1	3.88	3.61	This study
OP	3.9	–	–	25
CP	3.85	3.99	3.72	This study
LP	3.66	3.21	3.69	This study
JFP	4.86	4.16	4.87	This study

DDW, doubled distilled water.

Pathak et al. (2017) concludes that fruit peels (FP) possess surface properties characterized by a higher number of acidic sites and various functional groups, along with rough and porous surfaces. These features enable effective removal of heavy metals from liquids using fruit peels. However, the study notes that modified fruit peel waste (FPW) exhibits superior adsorption performance compared to raw or unmodified samples, indicating that treatment or modification enhances its efficacy as a biosorbent.

2.14 Biosorbents used for the removal of iron and manganese

In recent years, there have been quite a few research studies conducted on the removal of iron from water. Below are a few examples:

Nandeshwar et al. (2015) evaluated orange peels, sawdust, coconut shells and C.procera leaves. They found that these adsorbents have the potential to remove iron and their iron removal efficiency further increases after activation. The most promising green adsorbent was found to be orange peels with a 77 to 90% removal efficiency. Ashour et al. (2017) explored untreated natural eggshell and treated eggshell. They found that the treated eggshell shows better results than the untreated one. Beenakumari (2009) did an investigation into coconut shells and has found it to be a good adsorbent to remove the iron in drinking water. They also recommended that further studies could focus on increasing the shaking time of the system. Shokoohi et al. (2009) examined dried biomass of activated sludge (DAS) and they found that it was able to remove iron from water.

Abdel-Ghani et al. (2009) researched Typha domingensis leaf powder and they found that it was successful in the removal of Al (Aluminium), Fe (Iron), Zn (Zinc) and Pb (Lead). They recommend future studies could include more parameters to assess the possibility of the use of biomass for technological applications. Nabanita et al. (2012) explored heartwood charcoal of Areca catechu (HCAC) and they found it to be an efficient adsorbent for iron removal from the collected groundwater. HCAC could remove up to 98% of total iron under optimum conditions. They recommend that further studies could examine the design of a pilot plant.

Pinto et al. (2010) investigated chitin, a material sourced from crab and shrimp shells, and its effectiveness as a biosorbent for metal removal. The study focused on two products derived from crab shells: Chitorem SC-20 and Chitorem SC-80. The findings revealed that SC-20 effectively removed iron, lead, and zinc completely, while it only partially removed cadmium, cobalt, copper, and manganese. SC-80 demonstrated partial removal of cobalt, manganese, lead, and cadmium, but this was contingent upon the absence of precipitation. A critical factor influencing metal removal was identified as pH, which also affected the adsorption rate. Poor metal removal was observed under acidic conditions, whereas effective removal occurred at alkaline and neutral pH levels.

Hemamalini et al. (2018) explored agricultural waste such as sugarcane bagasse, rice husk and medicinal plants. They found that the removal efficiency of rice husk ash, sugarcane bagasse, tulsi powder and vettiver were found to be 91.02%, 94.90%, 75.52% and 74.84% respectively. Many of above articles only researched lab scale studies and no real-life applications or real-life samples were implemented.

There have also been research studies conducted on the removal of manganese from water. Below are a few examples:

Rudi et al. (2020) reviewed various studies on the use of agricultural waste as adsorbents for manganese removal from water, noting that these materials demonstrated excellent performance. Specifically, orange peels, tangerine peels, and banana peels achieved manganese removal efficiencies of 96%, 92%, and 97.4%, respectively. Similarly, Muthuraman (2017) explored the use of natural adsorbents, including

Moringa oleifera leaves, Borassus flabellifer, and Mangifera indica, and reported high removal efficiencies of 99%, 96%, and 93% for manganese. These findings highlight the effectiveness of both agricultural waste and natural adsorbents in reducing manganese levels in water.

2.15 Biosorbents used for the removal of other heavy metals

Ahmad et al. (2015) reviewed chemically oxidised pineapple peels as a biosorbent for the removal of Cd (Cadmium) and Pb (Lead) and found that the biosorption capacity for the pristine pineapple peel did not perform as well as the oxidised pineapple peel. He found that the pineapple fruit peel waste was economical and an effective biosorbent and thus he agrees that it is a promising alternative. Feng et al. (2010) compared modified (OPAA) and unmodified orange peels (OP) as a biosorbent for the removal of Pb (Lead), Cd (Cadmium) and Ni (Nickel) and found that the use of OP as a biosorbent produced great potential due to its high content of pectin, lignin, hemicellulose and cellulose. They found that OPAA is more effective than OP for the biosorption of Pb, Cd and Ni. If the biosorbent is regenerated and reused this will ensure that the biosorption process is more economical. OPAA has proved to be an effective alternative due to its potentially low costs, natural and abundant availability as well as high biosorption capacity.

2.16 The potential for fruit peel waste as a biosorbent versus other removal methods

Khan et al. (2015) emphasizes the need for focused efforts on renewable resources and the development of technologies to convert these resources into valuable products. This shift is essential for advancing a bio-based economy, promoting sustainability through a technology-driven model for economic growth.
In South Africa, citrus fruits and pineapples are among the most produced fruits, primarily in the Western and Eastern Cape Provinces. The fruit industry generates significant amounts of waste, including skins, seeds, and fibres, which are often discarded. However, South Africa possesses substantial resources in the form of fruit waste, presenting a promising opportunity for their utilization, particularly in wastewater treatment. This approach could enhance sustainability while addressing waste management challenges.

Pathak et al. (2017) says after consumption of fruits a peel is left behind which is an irritant to the environment and is seen as solid waste. This waste can be used in various applications such as low-cost biosorbents etc. The world’s leading produced fruit is Citrus Fruit peels (FP) dumped into municipal landfills which causes disposal issues and pollution. It is for this reason the reuse of FP will be ideal. This will improve the solid waste management process. Maksoud et al. (2019) states that biosorbents are naturally occurring in large quantities and they have potentially low costs and the ability to be redeveloped. These are the reasons why biosorbents are seen to have an advantage over other adsorbents. The use of waste material encourages ideologies such as recycling, regeneration, and the circular economy. Joseph et al. (2019) concurs and adds that considerable research has been conducted on the use of low-cost adsorbents for heavy metal removal from water. Researchers have found that these materials are highly effective in eliminating heavy metals, with agricultural waste proving to be the most efficient at this task.

Babel et al. (2002) also agree and say the use of low-cost adsorbents may add to the concept of sustainable development and says undeniably low-cost adsorbents offer many favourable advantages. Renge et al. (2012) says that the industry demands ground-breaking technologies which are inexpensive, energy efficient and low maintenance. The adsorption method is technically easy to implement and economically viable. It is apparent that low-cost adsorbents have demonstrated excellent removal capabilities. Many researchers commonly utilise the adsorption process for the removal of heavy metals. There is a need for an economical and safe method for the removal of heavy metals from water and this has encouraged research interest on cost effective alternatives.

Ramachandra et al. (2005) says in spite of the amount of available laboratory data, there is a need to examine feasible non-conventional low-cost adsorbents to meet the expanding demand due to the considerable number of dyes and heavy metals in the environment. Fu et al. (2010) recommends that although membrane technology can remove heavy metals with high efficiency, there are still many limitations related to this technology such high costs and complexity to name a few. Biosorption of heavy metals is therefore still seen as an extremely more attractive alternative. Even though both options are able to successfully remove heavy metals it should be noted that the selection of the most appropriate option depends on various factors amongst others such as operation expenses, dependability and environmental influence.

Lim et al. (2013) states that traditional, expensive chemical methods for removing heavy metals require longer contact times. In contrast, low-cost adsorbents can replace these high-cost methods while delivering better results. As such, low-cost adsorbents are recommended as a viable option for sustainable development. However, Khatri et al. (2019) acknowledges that biosorption is an effective and cost-efficient method for iron removal but suggest that nanotechnology offers superior efficiency. They propose that using naturally available nanomaterials could reduce the production costs of nanomaterials. Furthermore, they recommend that future research on iron removal should explore newer technologies such as membrane and nanotechnology. They also suggest a combination of these methods with conventional methods to enhance effectiveness.

Recent studies have shown that while combining membrane and nanotechnology offers promising potential for remediating various contaminants, the recovery of these nanomaterials becomes challenging, and they may also exhibit a certain level of toxicity. Amin et al. (2014) agrees that the use of nanomaterials in wastewater treatment holds great promise for both current and future research. Jun et al. (2018) highlights that various membrane types have strong potential for effectively removing contaminants, with the successful integration of materials into membrane structures slightly enhancing their performance. Despite the potential of nanomaterials as a viable alternative in the industry, several challenges remain.

Joseph et al. (2019) states that biosorbents are low-cost, cost-effective materials that can be effectively used to remove heavy metals from water. These materials are readily available in large quantities, and their implementation in water treatment systems requires minimal expertise, making them ideal for use in developing countries. The authors suggest that further research should be conducted in various developing nations to identify and explore other low-cost adsorbents. Special attention should be given to abundant waste materials, as their use could reduce waste disposal, enhance water quality, and contribute to environmental sustainability.

It is clear from the above that certain authors agree that low-cost biosorbents is the way forward especially in a developing country such as South Africa and the fact that it promotes recycling and a circular economy. However, others recommend that newer technologies such as nano technology should be explored instead, but these technologies are expensive and there are still many unknowns with regards to its application. Additionally, these technologies would not necessarily work in a developing country even in the near future.

2.17 Adsorbent treatment or modifications

Adsorbents can be used in their natural form or modified to enhance their adsorption capacity. Agricultural wastes typically exhibit low adsorption capacity when used unmodified, so physical or chemical modifications are often necessary. Physical modifications may include processes like heating, freezing, and drying, while chemical treatments involve washing with detergents or treating with acids. These chemical processes help remove surface impurities and create reactive functional groups on the adsorbent's surface (Rudi et al., 2020).

Citrus waste biosorbents can be developed through various methods, including:

- Mechanical Grinding
- Physicochemical Treatment
- Thermochemical Treatment
- Biochemical Methods Using Enzymes

Figures 2.14 and 2.15 illustrate the different modification processes for citrus peel wastes, highlighting the diverse approaches to enhancing their effectiveness as adsorbents (Mahato et al., 2021).

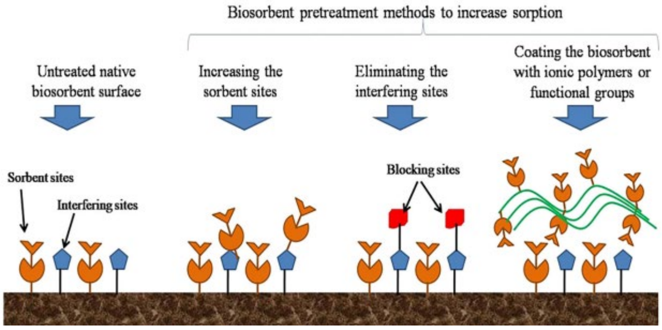

Figure 2.14 Citrus waste derived biosorbent surface (Mahato et al., 2021)

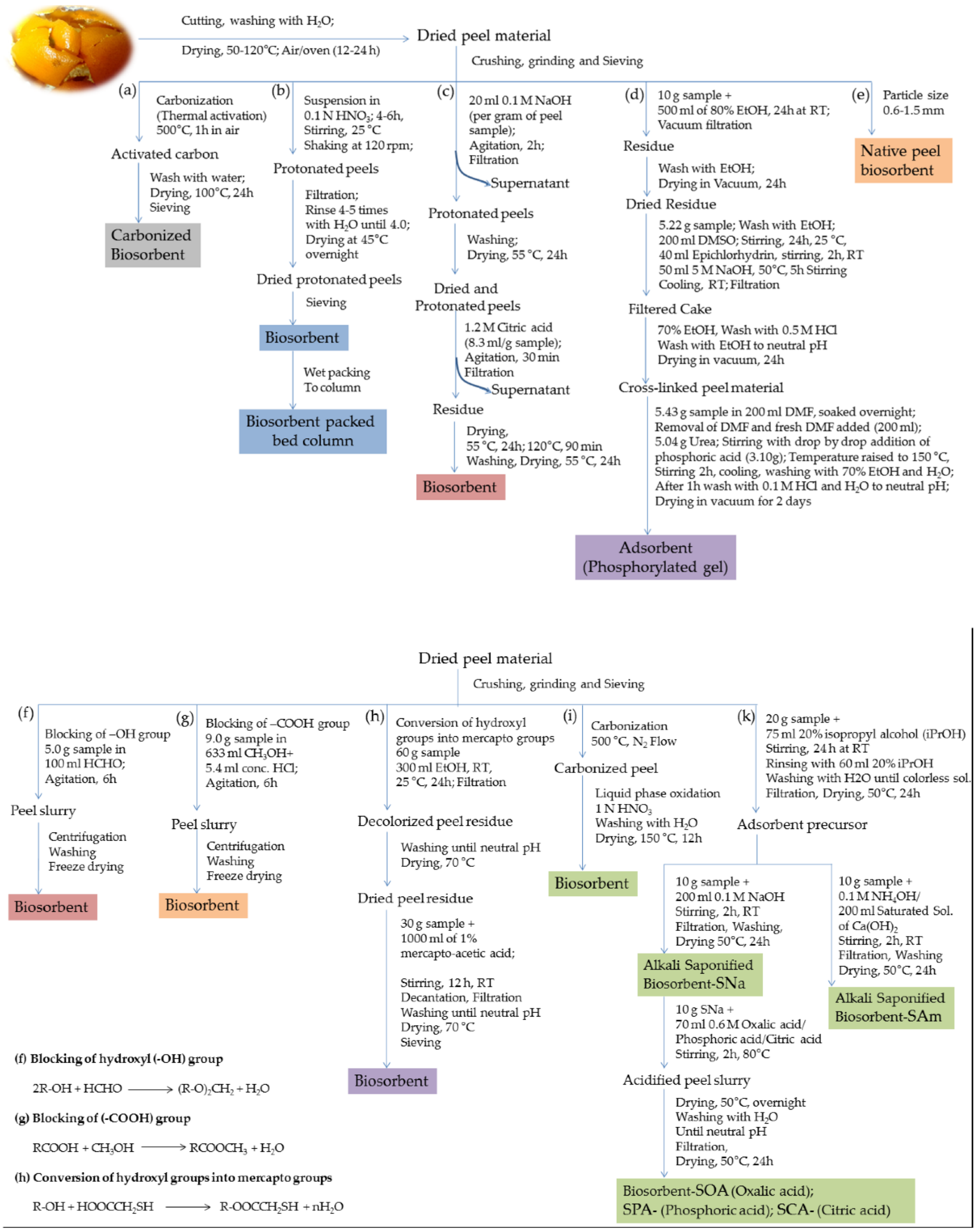

Figure 2.15 Various techniques for pre-treating precursor materials in the preparation of biosorbents from citrus waste (Mahato et al.,2021)

The carbonization process involves heating dried citrus peels to high temperatures in an inert atmosphere, such as nitrogen, to prevent excessive oxidation (Mahato et al., 2021). Studies on activated carbon derived from citrus peel waste have demonstrated its effectiveness in adsorption applications. The carbonized citrus peel achieved a maximum adsorption capacity of 125 mg/g. This process, along with other modification methods, is illustrated in Figure 2.15.

Pathak et al. (2015) emphasize the necessity of treating or modifying fruit peel waste (FPW) before its use. Various physical, chemical, and other modification methods have been researched, as summarized in Figure 2.16. The findings indicate that while physical modifications are generally simple and cost-effective, they tend to be less effective compared to chemical treatments in enhancing adsorption capacity.

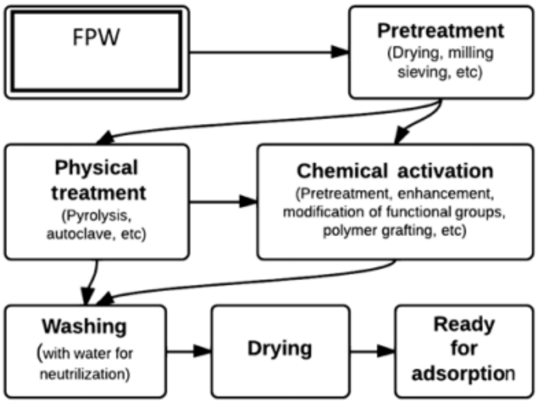

Figure 2.16 A flowchart illustrating the processing of various types of raw FPW (Pathak et al., 2015)

2.18 Factors affecting biosorption

As stated by Mimouni (2018), the biosorption process and its efficiency are influenced by several factors, which are generally consistent across the uptake of different metal ions. For the removal of Fe and Mn, key factors include initial concentration, temperature, pH, biosorbent dosage, particle size, and modifications to the biosorbent.

2.18.1 pH

Emenike et al. (2016) highlight the significant influence of pH on metal adsorption, noting that adsorption generally increases with rising pH until a certain point, after which further increases in pH can lead to decreased adsorption.

The 'p' in pH represents "power," while 'H' denotes hydrogen ion concentration. The pH scale ranges from 0 to 14 (Figure 2.7), where values below 7 indicate acidity, values above 7 indicate basicity, and a pH of 7 is considered neutral (O’Hehir, 2009). Additionally, reactions involving waters containing ferrous ions typically occur at lower pH levels (Joseph, 2016). This relationship underscores the importance of pH management in processes aimed at optimizing metal removal from water.

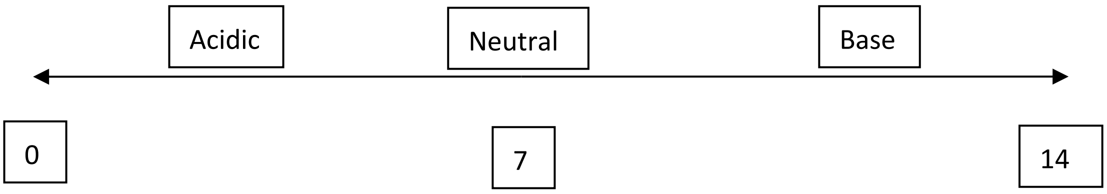

Figure 2.17 pH Scale (O’Hehir, 2009)

2.18.2 Concentration

Previous studies examining the effect of concentration on metal adsorption using agricultural adsorbents found that with an increase in concentration there is an increase in adsorption (Emenike et al., 2016).

2.18.3 Temperature

Several studies have examined the impact of temperature on metal adsorption, revealing that temperature influences both the solubility of metals and the rate of diffusion. Depending on the nature of the adsorption process, temperature can affect it in either an endothermic or exothermic manner (Emenike et al., 2016).

2.18.4 Biosorbent dosage

The adsorbent dosage is a vital factor in the determination of a biosorbent capacity for a given initial ion concentration (Elsherif, 2017).

2.18.5 Particle size effect

The metal adsorption capacity of an adsorbent is influenced by its total available surface area, which depends on the particle size. Smaller particle sizes lead to a larger surface area, thereby enhancing the adsorption capacity (Emenike et al., 2016).

2.19 Advantages and disadvantages of biosorption

Table 2.5 summarises the advantages and disadvantages of the biosorption technology.

Table 2.5 Summary of the advantages and disadvantages of biosorption (Mimouni, 2018)

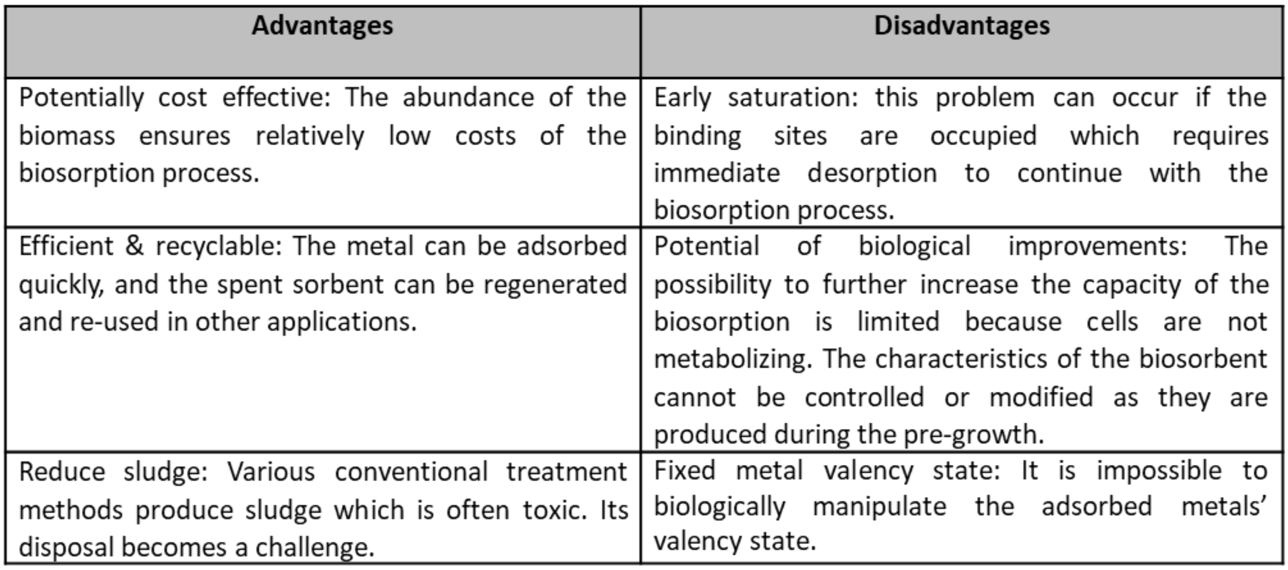

Advantages	Disadvantages
Potentially cost effective: The abundance of the biomass ensures relatively low costs of the biosorption process.	Early saturation: this problem can occur if the binding sites are occupied which requires immediate desorption to continue with the biosorption process.
Efficient & recyclable: The metal can be adsorbed quickly, and the spent sorbent can be regenerated and re-used in other applications.	Potential of biological improvements: The possibility to further increase the capacity of the biosorption is limited because cells are not metabolizing. The characteristics of the biosorbent cannot be controlled or modified as they are produced during the pre-growth.
Reduce sludge: Various conventional treatment methods produce sludge which is often toxic. Its disposal becomes a challenge.	Fixed metal valency state: It is impossible to biologically manipulate the adsorbed metals' valency state.

2.20 Characterisation

There were various characterisation techniques utilised to assess the characteristics of adsorbents where SEM & EDS, FTIR and BET were the most commonly found in the literature reviewed on adsorption.

2.20.1 Scanning Electron Microscope (SEM) & Electron Dispersive Spectroscopy (EDS)

Scanning Electron Microscopy (SEM) is a valuable tool for defining the characteristics and identifying the surface morphology of biosorbents. Pathak et al. (2017) conducted characterization experiments on various fruit peel wastes, including orange peels (OP) and citrus peels (CP). The microscopic observations revealed that the surface of fruit peels (FP) was generally uneven and rough, featuring some fibrous material as can be seen from Figure 2.18. The particle shapes and sizes varied significantly, ranging from spherical forms to elongated flakes. Specifically, while the surface of OP was rough and contained distributed fibers, it had fewer pores compared to banana peels (BP). In contrast, CP exhibited an irregular surface with negligible, tiny pores, highlighting the structural differences among the various fruit peels studied.

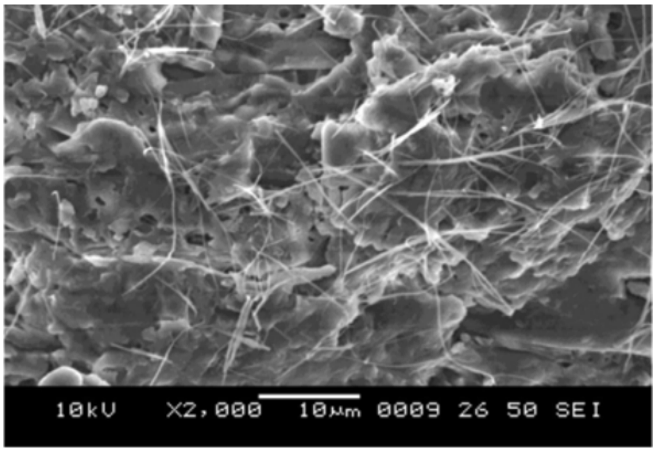

Figure 2.18 SEM image of OP (Pathak et al., 2017)

Adebayo et al. (2016) employed scanning electron microscopy (SEM) to examine activated carbon produced from orange peels (AOP) and acid-modified orange peels (MOP). The study revealed that both types of peels displayed a heterogeneous and microporous structure, characterized by rough surfaces with crater-like pores. The particles were irregularly shaped with a microrough texture. Notably, the morphology of the carbonized orange peels indicated a highly porous surface compared to that of the acid-treated peels. This increased porosity in the carbonized peels resulted from the destruction of the material by heat, leading to the formation of very small particles with a larger surface area. However, the overall porosity of the carbonized peels was found to be less than that of the acid-treated peels, indicating differences in structural characteristics between the two modification methods.

In a study done by Hamidon et al. (2019) he also used SEM to examine the citrus peel characteristics and found that the peel particles before adsorption were rough with a porous honeycomb-like structure. This was beneficial for adsorption of metals. Figure 2.19 shows the morphology of the peels before and after adsorption. It is seen from the figure presented that the peel's particle pores were diverse. However, a significant change in the peels structure was observed after the adsorption process. The surface of the peel particles also became smoother. It was concluded that this was the case because the peels and the metal was bound in the water. It was also apparent that the empty spaces of the surface of the peels decreased after adsorption.

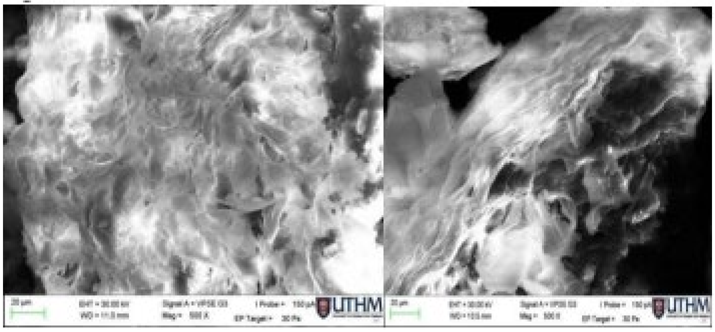

Figure 2.19 SEM micrographs of CP before and after biosorption (Hamidon et al., 2019)

According to Pathak et al. (2017), orange peel (OP) is a significant by-product of oranges, which are the most widely produced fruit globally. OP contains various components, including pectin, hemicellulose, cellulose, chlorophyll pigments, lignin, and other low molecular weight compounds. It has been reported that OP possesses antioxidant, germicidal, and anticarcinogenic properties, potentially offering health benefits for conditions such as colon and breast cancer, muscle pain, skin inflammation, stomach issues, and ringworm. Additionally, citrus peel (CP) is a valuable source of essential oils, which are used in pharmaceuticals, cosmetics, and to enhance the shelf life of certain food products. Table 2.6 and 2.7 provides an analysis and composition of various FP.

Table 2.6 Analysis of various FP (Pathak et al., 2017)

	Proximate analysis				Ultimate analysis				
FP	Moisture (%)	Ash (%)	Volatile matter (%)	Fixed carbon (%)	N (%)	C (%)	H (%)	S (%)	O (%) (by difference)
BP	9.80	5.01	85.26	0.07	1.30	40.24	6.14	0.098	52.22
OP	7.91	5.25	86.70	0.14	1.15	38.91	6.19	0.11	53.64
CP	7.58	4.32	86.54	1.56	0.64	38.51	6.20	0.10	54.55
LP	6.10	5.40	87.16	1.34	1.27	40.33	5.96	0.19	52.25
JFP	6.48	6.32	86.28	0.92	0.90	40.04	5.86	0.12	53.08

Table 2.7 Composition of FP (Pathak et al., 2017)

Value (% dry basis)					
Parameters	BP[72]	OP (ref. 61)	CP (ref. 48)	LP (ref. 48)	JFP
Cellulose	12.17 ± 0.21	9.21	20.8	23.1	nd
Hemicellulose	10.19 ± 0.12	10.50	17.2	8.09	nd
Acid-detergent lignin (ADL)	2.88 ± 0.05	0.84	8.9	7.6	nd
Total sugars (sucrose + glucose + fructose)	29.83 ± 0.29	16.90	21.6	6.5	nd
Protein	5.13 ± 0.14	6.50	n.d.	7.0	nd
Pectin	15.9 ± 0.26	42.50	14.2	13.0	nd
Ash	9.81 ± 0.42	3.50	3.0	2.5	nd

Polyphenolics, fat and other extractives make up for the remainder of the composition. *nd, not done.

2.20.2 Fourier transforms infra-red spectrometer (FTIR)

The Fourier Transform Infrared Spectrometer (FTIR) is used to identify and quantify the various functional groups present on the surface of the adsorbent. According to Li et al. (2008), the functional groups identified in the FTIR spectrum are influenced by the adsorbate ions. The position and intensity of each band in the spectrum correspond to specific functional groups on the adsorbent as described in Table 2.8.

Table 2.8 A simplified correlation chart (Pavia et al., 2001)

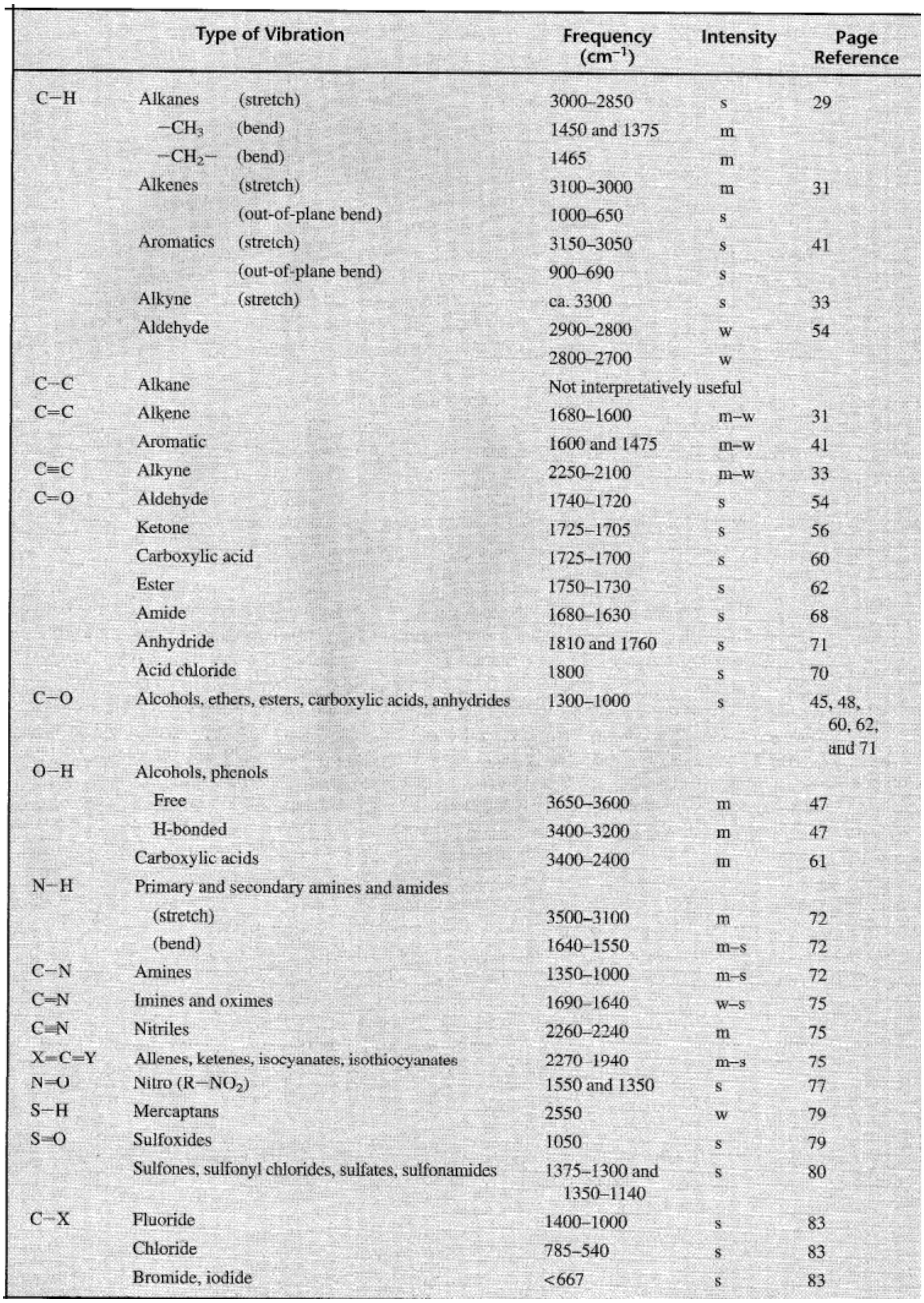

Type of Vibration		Frequency (cm^{-1})	Intensity	Page Reference
C−H	Alkanes (stretch)	3000–2850	s	29
	$-CH_3$ (bend)	1450 and 1375	m	
	$-CH_2-$ (bend)	1465	m	
	Alkenes (stretch)	3100–3000	m	31
	(out-of-plane bend)	1000–650	s	
	Aromatics (stretch)	3150–3050	s	41
	(out-of-plane bend)	900–690	s	
	Alkyne (stretch)	ca. 3300	s	33
	Aldehyde	2900–2800	w	54
		2800–2700	w	
C−C	Alkane	Not interpretatively useful		
C=C	Alkene	1680–1600	m–w	31
	Aromatic	1600 and 1475	m–w	41
C≡C	Alkyne	2250–2100	m–w	33
C=O	Aldehyde	1740–1720	s	54
	Ketone	1725–1705	s	56
	Carboxylic acid	1725–1700	s	60
	Ester	1750–1730	s	62
	Amide	1680–1630	s	68
	Anhydride	1810 and 1760	s	71
	Acid chloride	1800	s	70
C−O	Alcohols, ethers, esters, carboxylic acids, anhydrides	1300–1000	s	45, 48, 60, 62, and 71
O−H	Alcohols, phenols			
	Free	3650–3600	m	47
	H-bonded	3400–3200	m	47
	Carboxylic acids	3400–2400	m	61
N−H	Primary and secondary amines and amides			
	(stretch)	3500–3100	m	72
	(bend)	1640–1550	m–s	72
C−N	Amines	1350–1000	m–s	72
C=N	Imines and oximes	1690–1640	w–s	75
C≡N	Nitriles	2260–2240	m	75
X=C=Y	Allenes, ketenes, isocyanates, isothiocyanates	2270–1940	m–s	75
N=O	Nitro ($R-NO_2$)	1550 and 1350	s	77
S−H	Mercaptans	2550	w	79
S=O	Sulfoxides	1050	s	79
	Sulfones, sulfonyl chlorides, sulfates, sulfonamides	1375–1300 and 1350–1140	s	80
C−X	Fluoride	1400–1000	s	83
	Chloride	785–540	s	83
	Bromide, iodide	<667	s	83

Bands in the 3400–3700 cm^{-1} range indicate the presence of free O-H hydrogen bonds. The region between 2900–3400 cm^{-1} corresponds to stretching vibrations of hydroxyl and aliphatic groups. Bands within the 2870–2900 cm^{-1} range suggest the presence of alkyl groups, specifically C-H stretching. Bands around 1745 cm^{-1} and 1642 cm^{-1} indicate the presence of C=O functional groups, which are associated with the antisymmetric stretching of aldehydes, ketones, and ester groups (Ahmad et al., 2016).

Pathak et al. (2017) analyzed the FTIR spectra of various fruit peel wastes (FP) to identify the functional groups present on their surfaces. The results, summarized in Table 2.9 and Figure 2.20, highlighted the presence of several functional groups, including carboxylic acids, alcohols, alkanes, phenols, alkyl halides, amines, amino acids, and aromatic compounds. Focusing on the orange peel (OP) spectrum, intense bands were noted at 3352, 2919, 1739, 1691, 1603, 1531, 1398, 1051.75, and 636.94 cm^{-1}, indicating the presence of various functional groups such as alcohol, phenol, carboxylic acids, amines, amides, ketones, esters, ethers, and amino acids. Similarly, the citrus peel (CP) exhibited strong peaks at 3351, 2917, 1741, 1683, 1604, 1533, 1400, 1054, and 609 cm^{-1}, confirming the same functional groups. The presence of carboxylic acids makes fruit peels suitable for metal adsorption, with pectin, cellulose, or lignin typically being the sources of these acids. Additionally, hydroxyl groups in FP are crucial for adsorption. Importantly, the FTIR spectra did not show peaks in the 2220 to 2260 cm^{-1} range, which would indicate cyanide groups, confirming that no toxic substances were present in the fruit peels analyzed.

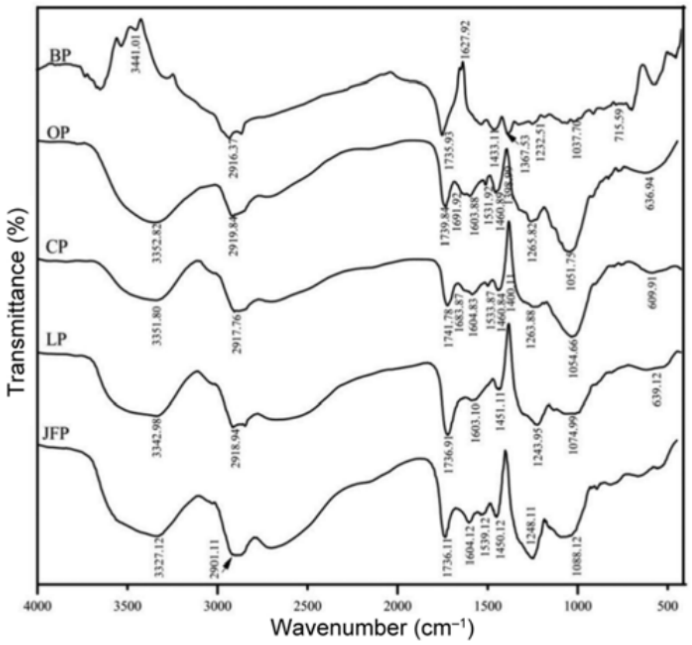

Figure 2.20 FTIR of FP (Pathak et al., 2017)

Table 2.9 FTIR peaks for FP (Pathak et al., 2017)

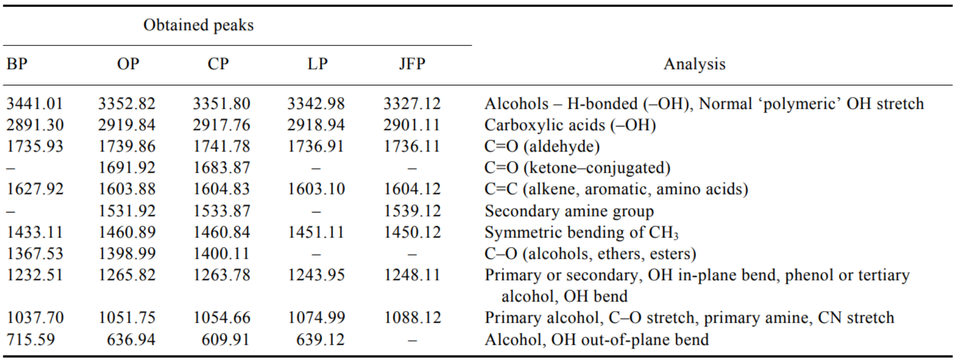

Obtained peaks					
BP	OP	CP	LP	JFP	Analysis
3441.01	3352.82	3351.80	3342.98	3327.12	Alcohols – H-bonded (–OH), Normal ‘polymeric’ OH stretch
2891.30	2919.84	2917.76	2918.94	2901.11	Carboxylic acids (–OH)
1735.93	1739.86	1741.78	1736.91	1736.11	C=O (aldehyde)
–	1691.92	1683.87	–	–	C=O (ketone–conjugated)
1627.92	1603.88	1604.83	1603.10	1604.12	C=C (alkene, aromatic, amino acids)
–	1531.92	1533.87	–	1539.12	Secondary amine group
1433.11	1460.89	1460.84	1451.11	1450.12	Symmetric bending of CH_3
1367.53	1398.99	1400.11	–	–	C–O (alcohols, ethers, esters)
1232.51	1265.82	1263.78	1243.95	1248.11	Primary or secondary, OH in-plane bend, phenol or tertiary alcohol, OH bend
1037.70	1051.75	1054.66	1074.99	1088.12	Primary alcohol, C–O stretch, primary amine, CN stretch
715.59	636.94	609.91	639.12	–	Alcohol, OH out-of-plane bend

According to Hamidon et al. (2019), the FTIR spectrum of Citrus Peels (CP), as illustrated in Figure 2.21, reveals several key peaks. The intense peak at 3276 cm^{-1} corresponds to the hydroxyl (OH) group, indicating the presence of alcohols. The small peak at 2922 cm^{-1} represents C-H stretching vibrations, while the weak peak at 1415 cm^{-1} also indicates C-H group vibrations. Two notable peaks at 1604 cm^{-1} and 1016 cm^{-1} are attributed to the stretching vibrations of C=O and C=C, which are characteristic of aromatic groups. Additionally, the wide peak at 1234 cm^{-1} may result from C-O-C stretching vibrations or C-C vibrations. Overall, these peaks highlight the diverse functional groups present in citrus peels, contributing to their potential as biosorbents.

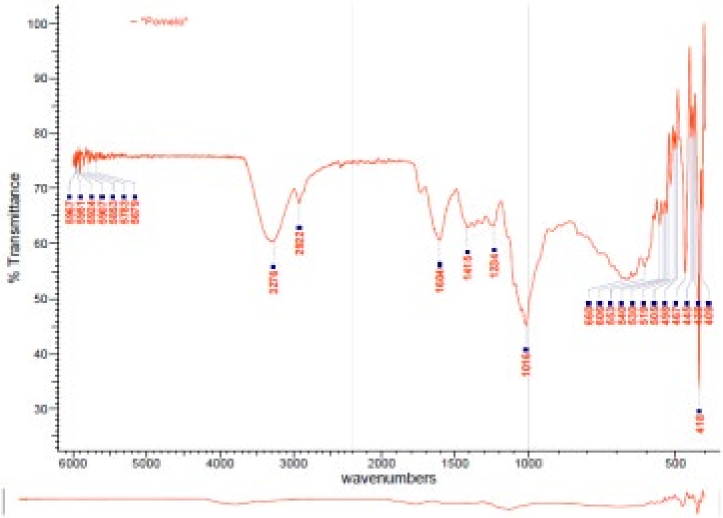

Figure 2.21 FTIR spectra of the CP (Hamidon et al., 2019)

Feng et al. (2010) investigated chemically modified orange peels (OPAA) as an adsorbent for removing lead, cadmium, and nickel ions. FTIR analysis was performed to identify functional groups in the modified peels. As shown in Figure 2.22, a strong absorption peak at 3440 cm^{-1} corresponded to O–H stretching vibrations linked to cellulose, pectin, absorbed water, and lignin. The peak at 2921 cm^{-1} was associated with C–H stretching vibrations from methyl, methylene, and methoxy groups. A peak at 1732 cm^{-1} represented C=O stretching vibrations from non-ionic carboxyl groups, likely from carboxylic acids or their esters. Bands in the 1300–1000 cm^{-1} range were attributed to C–O stretching vibrations in carboxylic acids and alcohols, indicating a high concentration of carboxyl and hydroxyl groups. Upon comparing the FTIR spectra of metal-adsorbed OPAA, the peaks at 3440, 1732, 1575, 1455, and 1060 cm^{-1} shifted to 3408, 1717, 1545, 1449, and 1045 cm^{-1}, respectively, reflecting the biosorption of metal ions. These shifts highlight the significant role of acidic groups in the adsorption process.

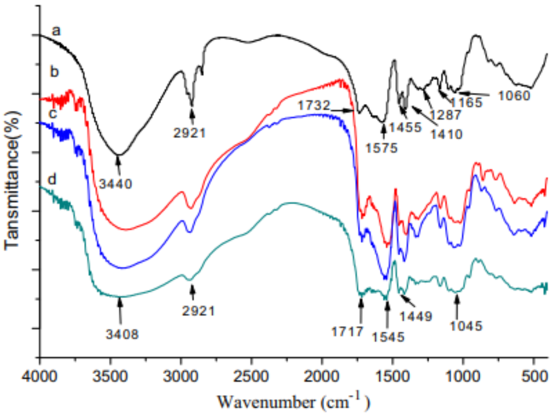

Figure 2.22 FTIR spectrum of (a) OPAA (b) OPAA-Pb (c) OPAA-Cd (d) and OPAA-Ni (Feng et al., 2010)

Adebayo et al. (2016) examined the adsorptive capacity of Modified Orange Peels (MOP) and Activated Orange Peels (AOP). Their FTIR analysis, as shown in Figure 2.23, identified several significant functional groups in both types of orange peel. The spectrum displayed bands at 3356 cm^{-1} and 3369 cm^{-1}, attributed to O-H vibrations in hydroxyl groups. These hydrogen-bonded OH groups typically appear in the 3200–3650 cm^{-1} range, characteristic of alcohols and phenols. Additionally, bands around 2930 cm^{-1} and 2850 cm^{-1} corresponded to C-H vibrations, indicating the presence of alkane functional groups. Overall, the findings suggest that orange peels contain a diverse array of functional groups, including carboxyl, phenolic hydroxyl, carbonyl, and lactone groups, which contribute to their effectiveness in metal removal.

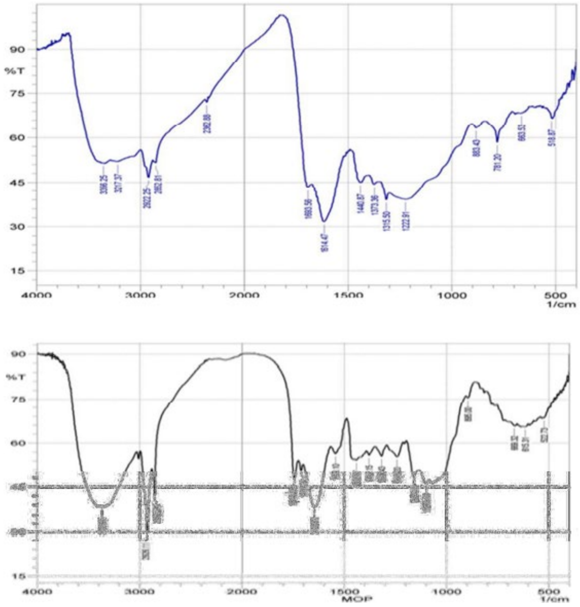

Figure 2.23 FTIR spectra for MOP and AOP (Adebayo et al., 2016)

Mahato et al. (2021) emphasizes that carboxyl and hydroxyl functional groups on the adsorbent surface play a pivotal role in the adsorption process. Furthermore, other functional groups, such as amide, sulfonate, phosphate, and amino groups, also contribute significantly to the adsorption mechanism.

2.20.3 Brunauer Emmet Teller (BET)

Khalfaoui (2003) states that the Brunauer-Emmett-Teller (BET) method is used to assess the surface morphology of materials, specifically their pore area, volume, and size distribution. Traditionally, BET is measured through the surface adsorption of nitrogen at 77 K on a degassed surface. For the analysis, the raw sample is degassed at 120°C for 12 hours, while the carbonized sample is degassed at 200°C for 3 hours. Degassing is important as it removes surface-adsorbed moisture, residual organics, and gases, ensuring a more accurate measurement of surface area and porosity. BET surface area measurements are calculated by plotting the volume of N_2 gas adsorbed against the relative pressure. These measurements are critical because adsorption is a surface phenomenon.

Figure 2.24 illustrates the different types of isotherms obtainable from the BET method, each providing insights into the characteristics of the adsorbing surface:

Type 1 Isotherm: Represents a microporous biosorbent, showing an initial rapid increase in adsorption followed by a plateau, depicted by a concave curve. This suggests a surface that becomes saturated after a certain point.

Type 2 Isotherm: Also shows a microporous nature, but with multilayer adsorption. The curve has a concave shape, reflecting the increase in adsorption with respect to concentration.

Type 3 Isotherm: Exhibits a convex shape, indicating rare or unusual adsorption behaviour.

Type 4 Isotherm: Displays a hysteresis loop, which indicates capillary condensation within the mesoporous structure of the adsorbent.

Type 5 Isotherm: Suggests weak interactions between the adsorbate and adsorbent, with a porous structure.

Type 6 Isotherm: Shows non-porous multi-layer adsorption, represented graphically by steps, which indicates a process of stepwise adsorption onto the surface.

Each type of isotherm provides distinct information about the adsorbent's surface properties and its interactions with the adsorbate (Khalfaoui, 2003).

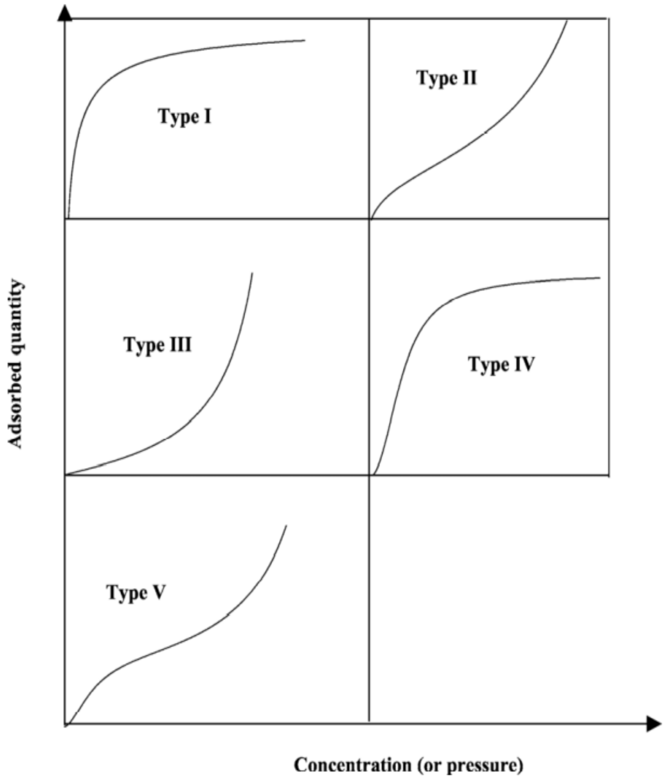

Figure 2.24 BET isotherm types (Khalfaoui, 2003)

Pathak et al. (2017) states that the surface of FP is porous and rough in nature, as evident from the SEM images. The BET surface area of OP (1.03 m^2/g) and CP (1.14 m^2/g) is low, in comparison to siliceous materials. The BET surface area of OP is in the range of 2.14–47.03 m^2/g. Low surface area is a characteristic of carbonaceous materials. The BET equation (Equation 2.5) is used to determine the distribution, micropore, and mesopore volumes.

$$\frac{1}{W((P_0 / P)-1)} = \frac{1}{W_m C} + \frac{C-1}{W_m C}\left(\frac{P}{P_0}\right)$$ Equation 2.5

W = weight of adsorbed
P/P_0 = relative pressure

W_m = weight of adsorbate
C = BET constant

2.21 Batch studies

There have been quite a few batch studies done on removal of Fe and Mn by adsorption from water. These authors have researched various agricultural and fruit peel waste as adsorbents and have studied the effect of pH, mass, biosorbent dosage, concentration, temperature, agitation speed and contact time.

2.21.1 Effect of pH

Many of the literature reviewed recorded optimum removal for iron and manganese at pH 4, 5 and 6. Tadepalli et al. (2016) investigated the effect of pH on iron (Fe) biosorption, testing a range from 2 to 8. They found that the optimal pH for maximum iron removal was 5, recommending that pH levels not exceed 6 to avoid the precipitation of insoluble ferric hydroxides, which hinder biosorption. At low pH values, the presence of hydronium ions surrounding the adsorbent reduces adsorption uptake. Conversely, increasing the pH decreases the competition from hydrogen ions, leading to improved adsorption efficiency.

Elsherif et al. (2017) studied a pH range from 2 –8 for Fe and states that in acidic ranges which is usually pH 3 and below, the metal adsorption was low. It was observed that the maximum adsorption occurred at pH between 5-6 for Fe. Lower pH values, less than pH 2, was not studied because it results in lower uptake of metal. At higher pH values (greater than pH 6) a decrease in percentage removal was observed.

Idrees et al. (2018) found that using a biochar adsorbent, manganese removal efficiency exceeded 80% at pH 6. Ali (2017) reported that the optimal pH for manganese removal using banana peel adsorbent was 7. However, at pH 8, the adsorption of manganese decreased due to the precipitation of hydroxide ions and manganese hydroxide, which can limit its availability for adsorption.

2.21.2 Effect of biosorbent dosage

Tadepalli et al. (2016) noted that increasing the dosage of biosorbent enhances the number of available binding sites for adsorption. This increase in adsorption sites correlates with a higher percentage of metal removal, as a greater amount of adsorbent provides more opportunities for interaction with the metal ions.

Elsherif et al. (2017) states that metal uptake by orange peel powder is a function of biosorbent dose. The metal uptake decreases with the biosorbent dose up to 1 g. Morad et al. (2012) also agrees with this finding and found that the removal percentage was constant after using 1 g of the adsorbent.

Zhang et al. (2014) reported that the biosorption efficiency for iron (Fe) and manganese (Mn) increased exponentially with higher adsorbent doses. They achieved maximum biosorption rates of 96% for Fe and 95% for Mn. However, at higher dosages, the biosorption efficiency plateaued, showing little additional increase beyond those maximum values.

It was seen that with higher adsorbent dosages there were more active sites, but excessive adsorbent dosage could decrease adsorption (Iftekhar et al., 2018).

2.21.3 Effect of concentration

Tadepalli (2016) observed that at high metal ion concentrations, the amount of metal adsorbed per unit weight of adsorbent (Q_e) increased. However, the percentage removal of metal ions decreased with rising concentrations. This indicates that as more metal ions are present, the binding sites on the adsorbent become saturated, limiting the effectiveness of the adsorption process.

Elsherif et al. (2017) studied the adsorption of Fe, Co, and Cu ions using orange peel powder in batch experiments. They found that adsorption was more effective at higher initial metal ion concentrations, though it was still feasible at lower concentrations. Overall, the adsorption efficiency increased as the initial concentration of metal ions rose.

Zhang et al. (2014) examined the effect of initial ion concentrations on the removal of Fe and Mn ions using rice husk ash as an adsorbent. They found that the percentage removal of these ions decreased exponentially as the initial concentration increased. This decline was attributed to the limited number of active sites on the adsorbent, which were insufficient to handle higher concentrations of metal ions.

Adekola et al. (2016) compared the adsorption behavior of iron and manganese using rice husk ash as a biosorbent. The study revealed that manganese showed a modest increase in adsorption with rising initial concentrations, whereas iron exhibited a substantially higher increase. The results demonstrated that rice husk ash had a greater adsorption capacity for iron, with 18.84 mg/g adsorbed at 100 ppm, compared to only 3.21 mg/g for manganese.

Rudi et al. (2020) noted that while the total adsorption capacity increases at higher initial concentrations of metal ions, the percentage removal of manganese ions decreases as the initial concentration increases. This suggests that as more manganese ions are present, there may be insufficient available binding sites on the adsorbent, leading to lower overall removal efficiency.

2.21.4 Effect of contact time

Shafiq et al. (2018) highlighted that a shorter contact time to achieve equilibrium in adsorption indicates the adsorbent's effectiveness. In water treatment processes, this is beneficial as it can lead to reduced operational costs and decreased processing time, making the overall treatment more efficient.

Tadepalli et al. (2016) conducted an experiment using 50 mg/L concentrations of copper (Cu) and iron (Fe) with 0.25 g of orange peel as the adsorbent, maintaining a pH of 6 for Cu and 5 for Fe at a constant temperature of 30°C. They observed that the rate of adsorption increased with contact time, reaching a point where a constant percentage removal indicated that the adsorption process had reached equilibrium. This suggests that the adsorbent effectively captures the metal ions until its binding sites are saturated.

Elsherif et al. (2017) conducted batch experiments to evaluate the effect of contact time on the adsorption of iron (Fe), cobalt (Co), and copper (Cu) using orange peel powder. They found that the percentage removal of Fe gradually increased until it plateaued at 30 minutes, leading them to use this contact time for subsequent experiments. Similarly, Zhang et al. (2014) observed that the percentage removal of Fe and manganese (Mn) on rice husk ash increased with contact time, reaching a maximum at 60 minutes.

Adekola et al. (2016) reported a rapid initial increase in the quantity of adsorbed Mn and Fe ions, with equilibrium achieved around 100 minutes for Mn and 50 minutes for Fe. Marque et al. (2013) noted that manganese removal using Moringa oleifera seeds increased with contact time, reaching optimum removal at just 5 minutes, with a 95% removal rate. Adeogun et al. (2013) found that maize husk adsorbent could remove 88% of manganese, achieving equilibrium within 30 minutes. These studies collectively emphasize the importance of contact time in optimizing metal adsorption processes.

2.21.5 Removal efficiencies

The removal efficiencies recorded for orange peels as an adsorbent for iron and manganese removal is quite high ranging from 84% to as high as 100%. Tadepalli et al. (2016) observed a maximum of 85 % metal ion removal for iron while Elsherif et al. (2017) observed a 95% iron removal. Surovka et al (2019) recorded a 96% manganese removal with orange peels as a biosorbent.

2.22 Modelling batch experimental data

2.22.1 Equilibrium adsorption isotherm

An adsorption isotherm is a mathematical model that defines the concentration relationship at equilibrium between the mass of a specific adsorbate in untreated water, the mass of adsorbate bound by the biosorbent and the mass of adsorbate remaining in solution when the biosorbent is saturated (Metcalf et al., 2004). The equilibrium relationship can be described by Equation 2.6:

$$\frac{x}{m} = q_e = \left(\frac{C_i - C_e}{m}\right) v \qquad \text{Equation 2.6}$$

Equilibrium is reached in batch mode when the solute concentration remains constant. At this point, equilibrium adsorption isotherms describe the relationship between the solute concentration and the amount adsorbed. Experimental data can produce various isotherm shapes, including linear, favourable, strongly favourable, irreversible, and unfavourable, as illustrated in Figure 2.25 (Kopsidas, 2016).

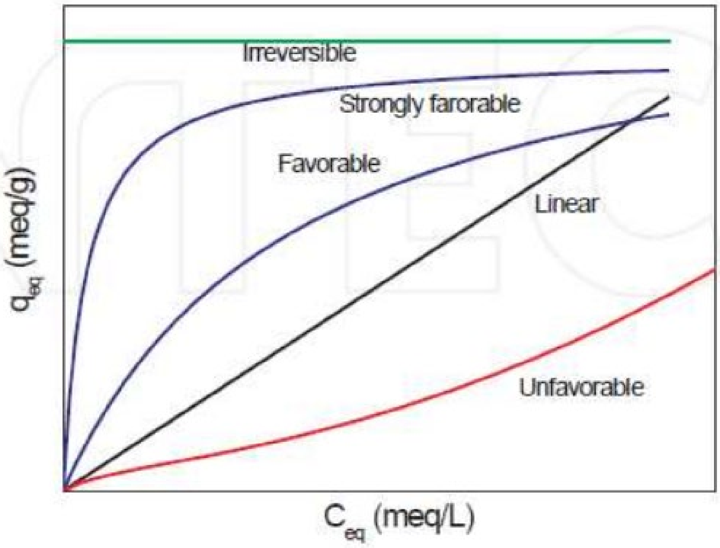

Figure 2.25 Adsorption isotherms (Kopsidas, 2016)

In the adsorption plot the linear isotherm starts from the origin and this linear isotherm facilitates the column modelling although it does not show a specific selectivity. In dynamic studies, a strongly favourable/ favourable isotherm is usually preferred because it indicates the adsorbent selectivity to the adsorbate. However, where regeneration is required, these isotherms may not be useful.

In the scale up procedure, mathematical modelling is an essential aspect especially when utilising data from laboratory experiments and then moving on through to pilot plant and then to industrial scale. The models assist with analysing and explaining experimental data such as identify mechanisms relevant to the process, predicting changes when varying operating parameters and when optimizing the process. In a case where an irreversible isotherm is observed indicated by a horizontal line, this means that a constant amount is absorbed, and no regeneration is possible. The factor of multicomponent effluent should be considered when designing a dynamic adsorption process (Kopsidas, 2016).

Various models are available to describe adsorption isotherms. These models help in comparing different biomasses under various operating conditions, as evidenced by the experimental data and the shape of the mathematical laws linked to the model. They offer valuable insights into metal uptake capacities and highlight differences in metal uptake across different types of adsorbents (Rashid, 2009).

Langmuir model:

The Langmuir isotherm assumes monolayer adsorption on a uniform surface with a finite number of adsorption sites. Once all the sites are occupied, no further adsorption can occur, and the system reaches saturation (Elsherif, 2017).

The Langmuir model takes the form as illustrated in Equation 2.7:

$$q_e = \frac{q_e K_L C_e}{1+K_L C_e} \qquad \text{Equation 2.7}$$

which may be linearized as per Equation 2.8:

$$\frac{C_e}{q_e} = \frac{1}{K_L q_m} + \frac{C_e}{q_m} \qquad \text{Equation 2.8}$$

where: Q_e = the amount of metal ion adsorbed at equilibrium per g of sorbent (mg/g) C_e = equilibrium concentration of metal ion in the solution (mg/L) K_L =Langmuir model constant (related to affinity of binding sites) q_m = Langmuir model constant (Rashid, 2009).

The key characteristics of the Langmuir isotherm parameters can be used to predict the affinity between the sorbate and sorbent through the separation factor, also known as the dimensionless equilibrium parameter (R_L). This parameter is expressed in equation 2.9 (Elsherif, 2017):

$$R_L = \frac{1}{1+bC_O} \qquad \text{Equation 2.9}$$

The value of R_L shows the type of Langmuir isotherm, if $R_L<0$ then it is unfavourable and if R_L is between 0 and 1 then it is favourable. If $R_L>1$, then it is irreversible (Elsherif, 2017).

Freundlich model:

The Freundlich isotherm model describes the adsorption process. This model applies to adsorption on heterogeneous surfaces (Elsherif, 2017).
The Freundlich model takes the form as illustrated in Equation 2.10:

$$q_e = K_F {C_e}^n$$ Equation 2.10

which may be linearized as per Equation 2.11:

$$lnq_e = lnK_F + nlnC_e$$ Equation 2.11

which: Q_e = the amount of metal ion adsorbed at equilibrium per g of sorbent (mg/g), K_F = Freundlich model constant, n = Freundlich model constant (Rashid, 2009).

2.22.2 Kinetic models

The adsorption kinetics is used to describe the adsorption process as it relates to time (Surovka, 2017).

Pseudo first order model:

To study the adsorption kinetics, it is essential to investigate the kinetic parameters of the adsorption process. The experimental results must be analysed using the formula that represents the pseudo-first-order kinetic model, which is expressed by equation 2.12. This equation helps describe how the rate of adsorption changes over time, providing insight into the adsorption mechanism and rate constants (Surovka, 2017):

$$ln(q_1 - q_t) = ln(q_1) - k_1 t$$ Equation 2.12

Where q is the amount adsorbed at equilibrium (mg/g), q_t is the amount adsorbed in time (mg/g), t is time, k_1 is adsorption rate.

Pseudo second order model:

The kinetic equation of the pseudo-second-order model is commonly used for analysing biosorption data. It is represented by equation 2.13, which helps describe the adsorption process assuming that the rate of adsorption is proportional to the square of the number of available sites on the adsorbent. This model is particularly useful for systems where the adsorption process is controlled by chemisorption (Surovka, 2017):

$$\frac{t}{q_t} = \frac{1}{k_2 {q_2}^2} + \frac{t}{q_2}$$ Equation 2.13

Where q is the amount adsorbed at equilibrium (mg/g), q_t is the amount adsorbed in time (mg/g), t is time, k_2 is the equation rate constant.

The pseudo-second-order model is based on the assumption that the rate-limiting step in the adsorption process may involve a combination of several mechanisms, which collectively describe the entire adsorption process. This is in contrast to the pseudo-first-order model, which assumes a simpler rate-determining mechanism (Surovka, 2017).

Intraparticle diffusion model:

The intraparticle diffusion model is commonly used to describe the adsorption process where solute molecules move from the solution into the solid. This model helps to understand the diffusion of particles within the biosorbent. The equation for the intraparticle diffusion models is given as equation 2.14 (Pholosi et al., 2020):

$$q_t = k_i t^{0.5} + C \qquad \text{Equation 2.14}$$

Where q is the amount adsorbed over time, C is the intercept, K_i is the rate constant, t is time.

2.23 Fixed bed column studies

A fixed bed is a column or pipe filled with packing material, which often includes adsorbents. Its primary purpose is to enhance the contact between two phases in a chemical process, facilitating efficient mass transfer or adsorption. The packed material in the bed allows the fluid to flow through while interacting with the adsorbent, thereby promoting the desired chemical or physical reaction (Kopsidas, 2016). The fixed bed reactor can be utilised for adsorption in large scale industrial applications and is seen as a commercially viable technique. See Table 2.10 detailing the specifications of an industrial fixed bed system.

Table 2.10 Specifications of an industrial fixed bed system

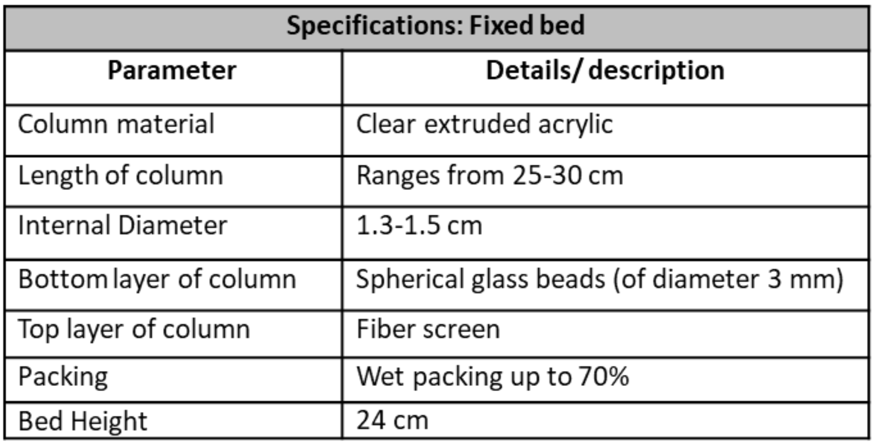

Specifications: Fixed bed	
Parameter	**Details/ description**
Column material	Clear extruded acrylic
Length of column	Ranges from 25-30 cm
Internal Diameter	1.3-1.5 cm
Bottom layer of column	Spherical glass beads (of diameter 3 mm)
Top layer of column	Fiber screen
Packing	Wet packing up to 70%
Bed Height	24 cm

In an industrial adsorption column, a predetermined amount of material is wet packed into the column and conditioned with a suitable solvent overnight. After conditioning, a test solution is passed through the column at a constant flow rate using a peristaltic pump. As the solution flows through the column, it adsorbs heavy metal ions. Samples are collected at specific time intervals to track the progress of the adsorption process. A schematic representation of the experimental setup for the fixed-bed adsorption column is shown in Figure 2.26 (Mahato et al., 2021).

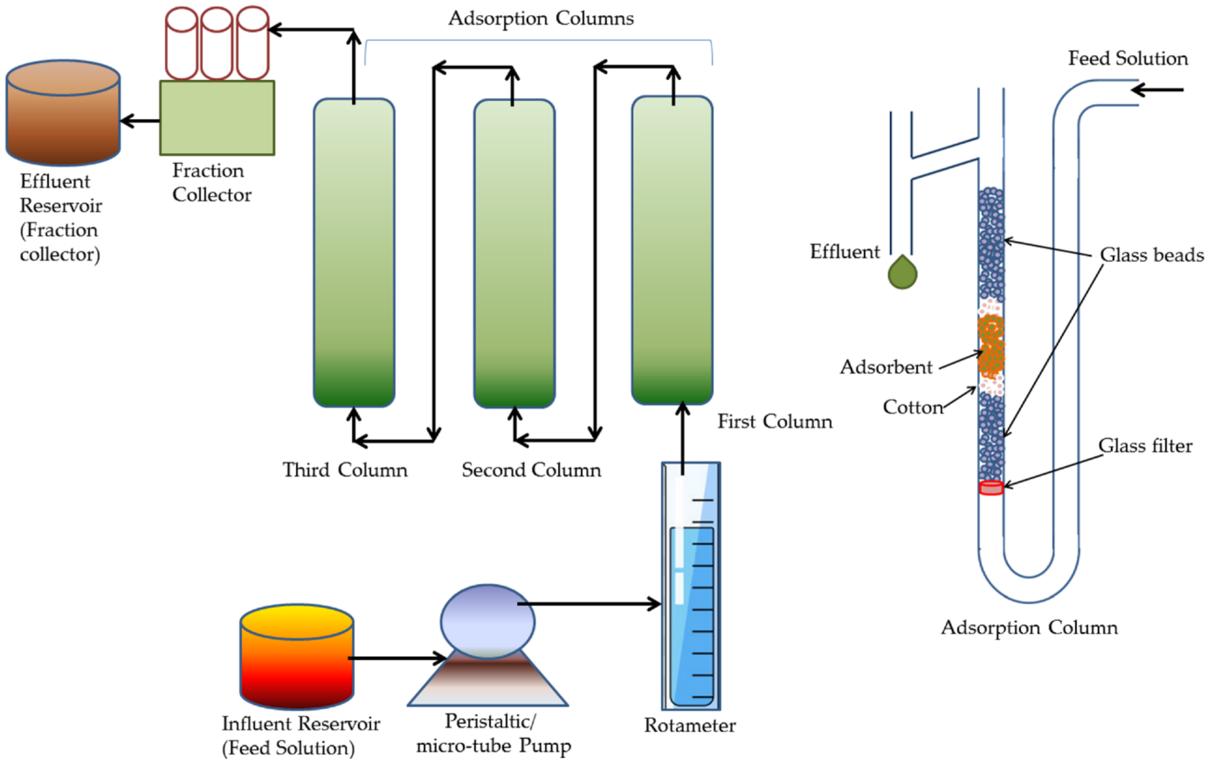

Figure 2.26 Schematic diagram of experimental set up for fixed bed column (Mahato et al., 2021)

The different mechanisms through which heavy metals and dyes are adsorbed onto the surface of biomass-derived biosorbents are illustrated in Figure 2.27.

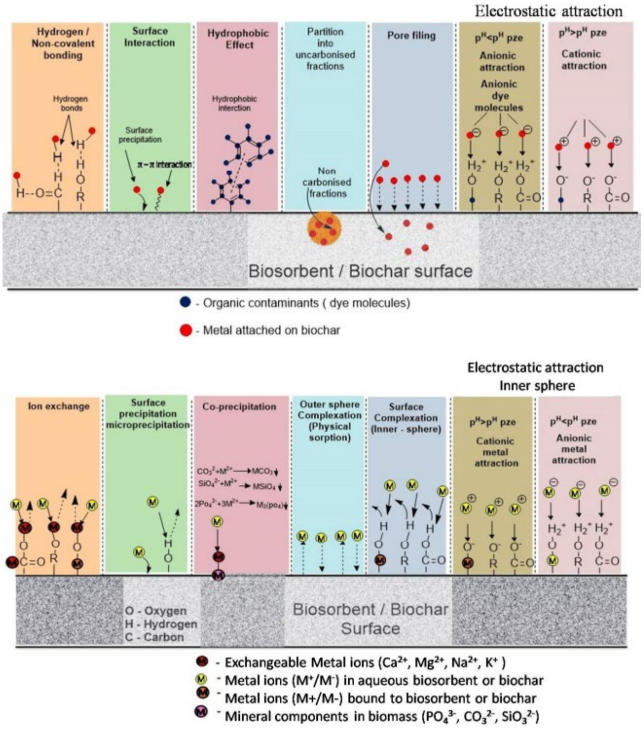

Figure 2.27 Different mechanisms through which heavy metals and dyes are adsorbed from industrial wastewater onto the surface of citrus biosorbents (Mahato et al., 2021).

The operating variables in batch studies are the same as that of column studies except in batch studies the effect of mass and the effect of agitation speed would be substituted by the effect of bed height and flow rate in column studies.

2.23.1 Effect of bed height

Chowdhury et al. (2012) found that increasing the bed height in the adsorption column resulted in longer breakthrough and exhaustion times. The study showed that varying bed depths affected both the shape and gradient of the breakthrough curves, with higher bed heights leading to increased adsorption efficiency. This is attributed to the greater mass of adsorbent available, which provides a larger surface area and enhances the volume of the treated solution. Overall, the findings underscore the importance of bed height in optimizing the adsorption process.

2.23.2 Effect of flow rate

Chowdhury et al. (2012) investigated the impact of feed flow rate on manganese (Mn) adsorption using a fixed adsorbent bed height of 4.5 cm and an inlet adsorbate concentration of 100 mg/L. They tested two flow rates: 1 mL/min and 3 mL/min. The results indicated that at higher flow rates, the adsorption column reached saturation more quickly, resulting in a steeper breakthrough curve and reduced overall adsorption uptake. Conversely, lower flow rates allowed for longer contact times and created shallower adsorption zones, leading to improved adsorption efficiency. This study highlights the critical role of flow rate in optimizing the adsorption process for manganese removal.

2.24 Modelling of fixed bed column data

The fixed-bed parameters are evaluated using breakthrough curves, with the results analysed through the mathematical models of Bohart–Adams, Thomas, and Yoon–Nelson (Trgo et al., 2011). Figure 2.28 depicts two operational zones: the initial mass transfer zone and the fresh adsorbent zone, which eventually leads to saturation. These zones help describe the progression of the adsorption process within the column.

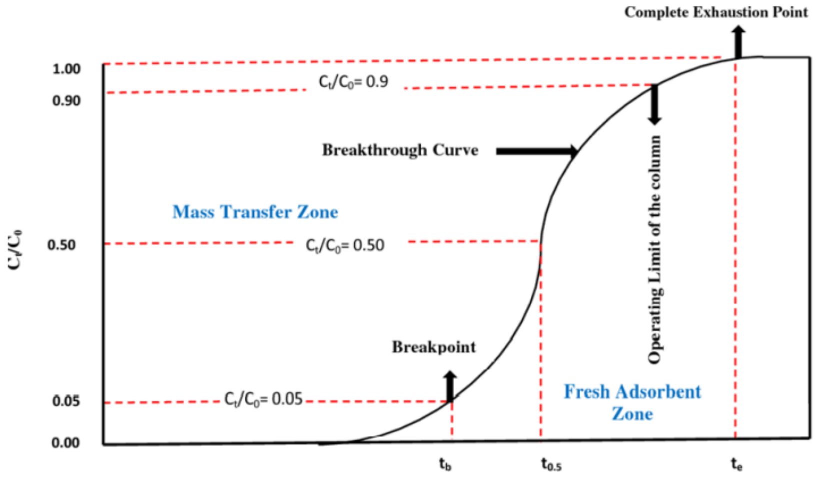

Figure 2.28 Break through curve in fixed bed column illustration (Chowdhury et al., 2012)

A breakthrough curve is a key element in column experiments, used to determine the maximum solid-phase concentration, which reflects the adsorbent's maximum adsorption capacity. The results obtained from these curves are essential for the design and operation of full-scale adsorption columns. Various models have been developed to serve this purpose.

2.24.1 Bohart-Adams model

This model is the simplest method for analysing fixed-bed systems, predicting the relationship between bed height and time. A linearized form of this model, which describes the time at the breakthrough point, is given in Equation 2.15 (Amin et al.,2017):

$$t = \frac{N_b}{C_O U}\, z - \frac{1}{K_a C_O} \ln\left(\frac{C_O}{C_b - 1}\right) \qquad \text{Equation 2.15}$$

2.24.2 Thomas model

The Thomas model, which is derived from the Langmuir model, is frequently applied to describe the behaviour of breakthrough curves in fixed-bed columns. It is widely used in industrial design to estimate the maximum adsorption capacity of the adsorbent. The linearized version of the Thomas model is represented by Equation 2.16. (Amin et al.,2017):

$$\ln\left(\frac{C_o}{C_t} - 1\right) = \frac{K_{TH} q_o m}{Q} - (K_{TH} C_o) t \qquad \text{Equation 2.16}$$

2.24.3 Yoon-Nelson model

The Yoon-Nelson model is a straightforward theoretical model grounded in adsorption theory, and it is useful for analysing breakthrough behaviour. The linearized version of the Yoon-Nelson model is expressed as per Equation 2.17 (Amin et al.,2017):

$$\ln \frac{C_t}{C_o - C_t} = K_{YN} t - T K_{YN} \qquad \text{Equation 2.17}$$

2.25 Fixed bed column design

The first step in the design of a fixed bed column system is the selection of an efficient and effective adsorbent. Thereafter, the focus is on equilibrium batch studies and the development of isotherms. Once the concentration of a solute remains constant then equilibrium is reached. Relationships at equilibrium are described by the adsorption isotherms and experimental data provides various isotherm shapes. The mathematical modelling is a vital aspect in the scale up procedure and adequate models can help to analyse and explain experimental data (Kopsidas, 2016).

The next step is the fixed-bed column studies. Fixed bed adsorption is the better suited option for practical application of the adsorption process however, mathematical modelling is more difficult than batch adsorption. In a fixed bed system, a solution is passed through the fixed bed of adsorbent where its composition is changed. This change is dependent on various factors such as the adsorbent properties and operating conditions. Breakthrough curves are developed by plotting the ratio C/C_o versus time (Kopsidas, 2016).

The breakthrough curve and concentration profile are shown in Figure 2.29. The region where the majority of the concentration change occurs is referred to as the mass-transfer zone. The boundaries of the breakthrough curve are typically defined by C/C_o values ranging from 0.05 to 0.95, which correspond to the breakpoint and saturation points. In most cases, $C_s = C_o$. When the concentration reaches the maximum allowable value, this is considered the breakpoint. At this point, the flow is halted, and the column is then regenerated (Kopsidas, 2016).

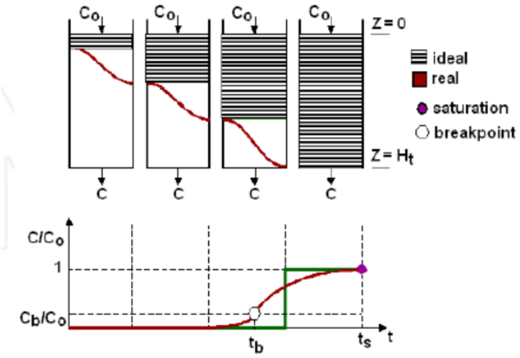

Figure 2.29 The breakthrough curve for the sorption process in fixed beds shows the concentration of the inlet solution (C_o), the concentration at breakthrough (C_b), the breakpoint time (t_b), and the saturation time (t_s) (Kopsidas, 2016)

In fixed bed columns, continuous solution feeding continues until equilibrium is reached, necessitating the selection of appropriate mathematical models to represent the equilibrium data. These models are crucial for designing and optimizing adsorption processes for industrial applications. The development of a breakthrough curve either through mathematical modelling or direct experimentation is vital for understanding and designing column adsorption systems. The breakthrough curve is a crucial element in fixed bed columns. Obtaining breakthrough curves experimentally is preferred as it often yields more accurate representations of an adsorption system. Ideal breakthrough curves exhibit an S-shape, indicating efficient adsorption behaviour. Deviations from this shape suggest inadequacies in the model. Collected model data is essential for validating mathematical models. Once validated, these models can be used for designing and optimizing adsorption systems. It should be noted that longer contact times enhance bed performance. This can be achieved by increasing bed height or decreasing flow rates. Optimal linear flow rates should align with laboratory results for effective scaling. The key parameters in column design are internal diameter and bed depth as well as maximum adsorption capacity. For scale-up experiments, both the internal diameter (D_i) and bed depth (H) should increase while maintaining a constant ratio (D_i/H). The maximum adsorption capacity (Q_{max}) represents the total number of available adsorption sites in the material. Developing a suitable model requires balancing accuracy with ease of use. Different models (e.g., Bohart-Adams, Yoon-Nelson, Thomas) can be applied even without isotherm data, but laboratory experiments are necessary to determine isotherms. Each model has its limitations and may require further development to improve performance. Fixed bed column design and operation depend on accurately modelling adsorption processes. The breakthrough curve serves as a critical tool for this purpose, and experimental validation of models is essential for optimizing industrial applications. Achieving efficient contact time and maintaining appropriate geometrical ratios are fundamental to successful design and operation in real-world scenarios (Kopsidas, 2016).

2.26 Activated carbon column design

This research intends to extend the principles behind the application of activated carbon (AC) columns in water treatment facilities by substituting AC with a suitable waste biomass. I have reviewed the process for development of industrial AC columns as a model to follow in respect to my column design. According to Rodriguez et al. (2015) when sizing AC columns it is important to consider the carbon depth, the number of contactors, the empty bed contact time, and the hydraulic loading rate. AC filters may be designed as up or downflow systems comprising of one or more vessels in series or in parallel. Furthermore, the core parameters illustrating the AC process are filter velocities, filter operation time, bed volume, carbon usage rate, Empty Bed Contact time and output volume.

According to Sincero et al. (2003) there are two methods that can be utilised for the scale up of a packed bed column namely, the scale up procedure approach or the kinetic approach. An advantage of using the kinetic approach is the fact that the breakthrough volume may be chosen in the design of a column. A breakthrough curve from a test column is essential and it is not possible to design a column accurately without this breakthrough curve for both approaches. Another recommendation is that the designer sizes the column as large as possible to reduce sidewall effects.

2.27 Conclusion

South Africa faces significant challenges in water quality and supply, particularly due to rapid industrialization and heavy metal contamination. Iron and manganese contaminants in borehole water arise from both natural geological processes and human activities, leading to health risks and aesthetic issues. Groundwater is essential for rural communities and represents a crucial alternative water source in the context of increasing water scarcity. Despite its potential, only 13% of South Africa's water supply comes from groundwater.

Enhanced management strategies are necessary to utilize this resource effectively. Recent droughts have heightened the demand for sustainable water management practices, including the use of groundwater. Various removal methods for iron and manganese exist, including conventional, biological, and nanotechnology-based approaches. However, many current methods may not be suitable for developing countries due to cost and complexity. South Africa's water legislation emphasizes integrated water resource management, but implementation challenges persist, particularly for rural populations relying on untreated groundwater. To ensure safe drinking water and enhance water security, there is a critical need for the development and adoption of effective, low-cost water treatment technologies. Municipalities must prioritize groundwater as a sustainable supply option while addressing the environmental impacts of industrialization. Enhanced education and investment in water management infrastructure are vital for improving public health and resilience against climate-induced water scarcity.

Various agricultural wastes, especially fruit peel waste (FPW), are identified as effective biosorbents for removing heavy metals from water. They are abundant, biodegradable, and inexpensive, making them superior to commercial adsorbents like activated carbon. The selection criteria for biosorbents include cost, availability, and environmental impact, with an emphasis on using waste materials to minimize environmental pollution and enhance sustainability. While traditional methods for contaminant removal exist, biosorption is noted for its lower operational costs and higher efficiency, particularly in developing countries where resources are limited. Biosorbents can be easily regenerated for multiple uses, further enhancing their cost-effectiveness and environmental benefits. The research emphasizes the importance of modifying agricultural wastes, particularly citrus peels, to enhance their adsorption capabilities for metal ion removal. Optimal conditions, including pH, concentration, and dosage, play critical roles in the effectiveness of biosorption processes. This approach not only provides a means for wastewater treatment but also promotes the recycling of agricultural by-products.

A study by Rao et al. (2011) highlighted the need for more studies on the optimization and real-world application of biosorption methods, particularly for enhancing the performance of modified biosorbents. Overall, the research underscores the potential of biosorption using agricultural and fruit waste as a viable solution for wastewater treatment and solid waste management, contributing to a more sustainable future.

Batch experiments examine the adsorption capacity of the proposed biosorbent. The experimental data provide an isotherm which indicate the adsorption behaviour. Common models for isotherm representation are the langmuir and freundlich models. In fixed bed column studies, breakthrough curves are assessed, and these are essential for understanding the adsorption process in columns. They illustrate the concentration of adsorbate over time and help in evaluating maximum adsorption capacity. Common models used for fixed bed analysis are Bohart-Adams, Thomas, and Yoon-Nelson Models.

Joseph et al. (2019) states that while substantial progress has been made in understanding biosorbents and their applications, gaps remain in the exploration of fixed-bed column models using agricultural or fruit peel wastes as biosorbents, real-world applications, and commercialization potential. The proposed study aims to fill these gaps by focusing on treating existing borehole water samples applied in column studies and evaluating the effectiveness of various biosorbents in practical settings.

Chapter 3 Research methodology

3.1 Introduction

This chapter provides a comprehensive outline of the methodology employed in the study, detailing each step from research design to material preparation as well as batch and column experimental processes. The procedures established a robust framework for assessing the biosorption capacity of carbonized orange peels in removing heavy metals from water. Figure 3.1 presents a flow diagram which summarises the research methodology.

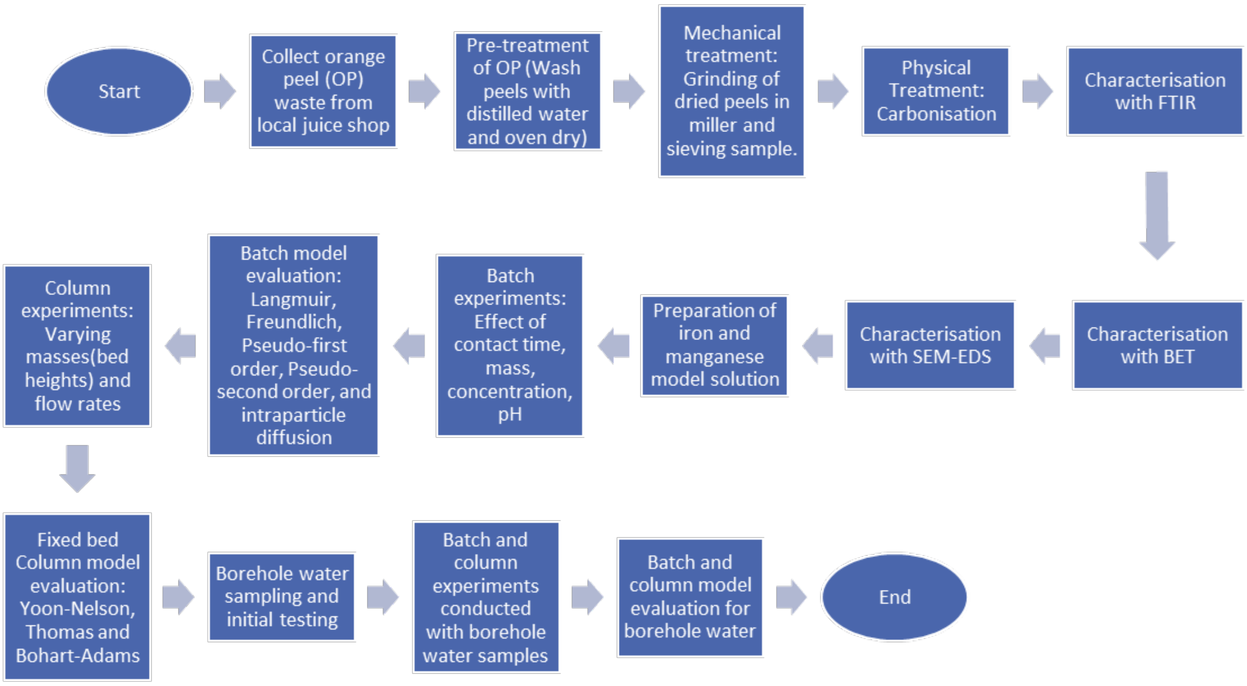

Figure 3.1 Flow diagram presenting research methodology used.

3.2 Research design

The purpose of this research study was to assess the iron and manganese removal efficiency of carbonized orange fruit peels when used as a biosorbent in borehole water with high concentrations of iron and manganese. The experimental set up and procedure entailed the collection and pre-treatment of biomaterials, characterization of the adsorbent material, and preparation of model fluid as well as the batch and column biosorption. An experimental based research design technique was applied in this study. Experiments were conducted in the laboratory, testing the biosorbent material through biosorption procedures in both batch and column studies. The research is of a comparative nature where different variables were tested and compared against each other as well as standard models for the batch and fixed-bed column design. Biosorbents produced from orange peels can be a sustainable and economically viable solution to the problem of treating iron and manganese laden borehole water.

3.3 Materials and methods

3.3.1 Study area

The study area is the Gateway wellfield in the Overstrand Municipality that consists of numerous boreholes with elevated levels of iron and manganese. The Municipality could utilise iron and manganese rich ground water reserves to supplement surface water resources. The Gateway well field typically has high iron concentrations ranging from 6–91 mg/l and manganese concentrations from 1-7 mg/l with an average pH 4. It was found that the Gateway wellfield generally had acidic pH values due to the low buffering capacity of the silica-rich rock (Peninsula formation). The study area consists of five production boreholes GWP02, GWE06, GWP12, GWP16 and GWP17, refer to Figure 3.2: locality plan indicating the borehole locations (Blignaut et al.,2015).

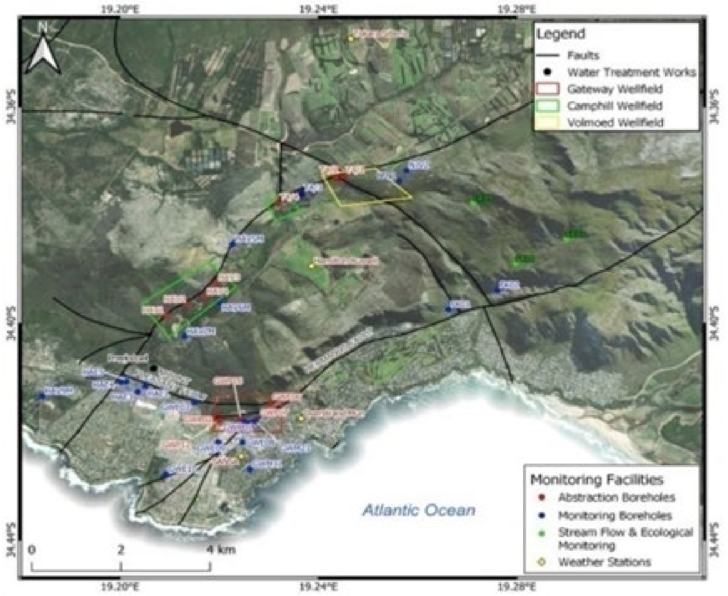

Figure 3.2 Locality plan indicating borehole locations

The Overstrand Municipality is a local municipality situated in the Western Cape province of South Africa, along the Atlantic coast between Cape Town and Cape Agulhas, within the Overberg District Municipality.

3.3.2 Sourcing and preparations

Fruit waste, specifically orange peels, was collected from a local juice shop and characterized. The peels were thoroughly washed with distilled water, then oven-dried at 80°C for 48 hours. After drying, the peels were physically processed by grinding in a mill and sieved through a 350 µm sieve to achieve a uniform particle size. Figures 3.3 a, b, c, and d illustrate the preparation process.

Figure 3.3 (a) Collected orange peel waste (b) Oven-dried orange peels (c) The grinding process in the miller machine (d) The sieving process

3.3.3 Cleaning of containers

A systematic cleaning process was completed where all containers used such as beakers, flasks, measuring cylinders etc. were thoroughly cleaned with detergent and tap water. Subsequently, they were rinsed with distilled water and then treated with nitric acid solution for up to 24-48 hours. Thereafter, the containers were given a final rinse and left to dry. This method ensured the removal of contaminants and prepared the containers for precise experiments.

3.3.4 Model fluid preparation

Two litres of 1000 ppm solutions were prepared containing either iron or manganese. Iron was prepared from Iron (III) Chloride ($FeCl_3$); using a mass of 5.792 g and manganese was prepared from Manganese (II) Chloride ($MnCl_2$); using a mass of 7.197 g. The salt was dissolved in approximately 200 mL of deionised water in a beaker. The solution was then quantitatively transferred into a 2 L volumetric flask and filled up to the mark. Thereafter, the solutions were diluted to prepare the 100 ppm, 50 ppm, 40 ppm, 30 ppm, 20 ppm, 10 ppm, and 5 ppm working concentrations. The pH of the solutions was adjusted to four and the experiments were conducted at room temperature to simulate the real borehole conditions.

3.3.5 Sampling

For initial testing, two 50 ml samples of each borehole were taken and put in clean labelled containers for easy identification. To stabilize the pH and thereby to prevent iron and manganese from precipitation before analysis in the laboratory, 0.5 ml of nitric acid was added to the samples. The sample bottles were then sealed. Subsequently, five separate 25 litre containers were filled with the borehole water which was to be used for experimental purposes. The pH of the samples was taken immediately on site and recorded as shown in Figure 3.4. It was assumed that all ferrous ions in the water samples remained unoxidized prior to laboratory testing. Visual observations for colour changes were made and recorded. The samples were transported to the University of Cape Town's Chemical Engineering Laboratory for same day analysis of iron and manganese. This approach ensured accurate measurement of the metal concentrations in the samples.

Figure 3.4 On site pH testing of the borehole water samples collected

To determine the final concentration of Fe and Mn in the water, the samples taken during the experiments were sent to be tested at the University of the Western Cape’s Chemical Sciences Department. The testing machine used was the ICP-OES: Inductively Coupled Plasma - Optical Emission Spectrometry (Figure 3.5). A standard pH meter was used to test the pH of the simulated metal ion solution and the borehole water.

Figure 3.5 ICP-OES machine used for water sample analysis

3.4 Groundwater characteristics

Groundwater was collected directly from the pipes connected to the boreholes, and the results of the groundwater analysis are presented in Table 3.1. The analysis revealed high concentrations of iron and manganese, indicating that the groundwater must undergo treatment before it can be used. The maximum concentrations of iron and manganese in the Gateway Boreholes exceeded the recommended aesthetic and chronic limits for both raw and drinking water quality. The aesthetic limits are 0.3 mg/L for iron (Fe) and 0.1 mg/L for manganese (Mn), while the chronic limits are 2 mg/L for Fe and 0.4 mg/L for Mn. Based on these maximum values, it can be concluded that the water from these boreholes requires pre-treatment before being suitable for drinking.

Table 3.1 Borehole characteristics

	GWP 02	GWP12	GWP16	GWP17	GWE06
pH	3.25	5.72	3.61	5.51	3.48
Iron (mg/l)	38.3	42.8	91	23	7.8
Manganese (mg/l)	5.8	6.8	5.9	2.5	3.5

3.5 Treatment/ modifications to orange peels (Carbonization)

The raw fruit peels were carbonized in a Pyrotherm tube furnace at 600°C under an argon flow rate of 10 L/min. The OP was loaded into a steel tube and placed inside the furnace, where it underwent thermal treatment in the absence of oxygen for 120 minutes. After the heating process, the material was allowed to cool for 12 hours. Figure 3.6 shows the pyrotherm tube furnace used for carbonization.

Figure 3.6 Pyrotherm tube furnace

3.6 Techniques for characterisation

The biosorbent was characterized using several techniques. Scanning Electron Microscopy (SEM) was employed to assess the surface morphology of the biosorbents, while Electron Dispersive Spectroscopy (EDS) was used to analyse the elemental composition of the biosorbent before and after biosorption, specifically to detect the presence of iron and manganese. Fourier Transform Infrared (FTIR) spectroscopy was utilised to identify the chemical structure and functional groups of the biosorbent. Additionally, the surface area, pore size, and volume of the biosorbent were measured using Brunauer-Emmett-Teller (BET) analysis. Pathak et al. (2017) did extensive studies utilizing the SEM, FTIR and BET characterization methods to assist with characterizing biosorbents. Figure 3.7 illustrates the biosorbent powder before carbonization (raw orange peel powder) and after carbonization (carbonized orange peel powder).

Figure 3.7 Biosorbent powder before carbonization and after carbonization

3.6.1 Scanning Electron Microscopy (SEM) & Electron Dispersive Spectroscopy (EDS)

Scanning Electron Microscopy (SEM) was conducted using an Auriga SEM at the University of the Western Cape. Prior to the SEM analysis the samples were dried in a conventional oven at 120°C overnight. The samples were then coated with a thin layer of gold palladium (Au:Pd) which is the sputter coating or carbon coating process required for SEM analysis. This coating serves multiple purposes: improving conductivity, enhancing image quality, protecting the sample, and reducing charging effects. The micrographs were taken at 50K magnifications. Electron Dispersive Spectroscopy (EDS) was also done to evaluate the biosorbents before and after biosorption to ascertain the presence of iron and manganese qualitatively and quantitatively before and after biosorption from the borehole water source.

3.6.2 Fourier Transform infrared (FTIR) Spectroscopy

FTIR was conducted at the Stellenbosch University and was used to identify and characterize the biosorbent based on its molecular vibrations. The resulting spectrum displays absorption peaks corresponding to specific wavelengths, allowing the identification of functional groups, and assisted in assessing molecular structure. Peaks in the spectrum are often correlated with bond types (e.g., C=O, N-H, O-H). FTIR spectra of raw orange peels (ROP) and carbonised orange peels (COP), both before and after adsorption were recorded with an FTIR spectrometer (Perkin Elmer UATIR-FTIR, Llantrisant UK). 0.1 g of the powder sample was used to carry out the experiments and measurements were captured between 4000 cm^{-1} to 500 cm^{-1}.

3.6.3 Brunauer Emmet Teller (BET)

BET surface area and pore analysis was conducted at University of Cape Town, Analytical laboratory in the Department of Chemical Engineering. The instrument used to analyse the samples was a Tristar II (Micrometrics Instrument Corporation, USA) running on TriStar II 3020 V3.02 and this measured through adsorption of nitrogen, the surface area, pore size distribution and volume of the biosorbent samples. The samples were degassed at 120°C overnight under vacuum on a VacPrep 061 unit. Thereafter, the nitrogen physisorption analysis on Tristar II 3020 was done. Degassing was done to remove contaminants from the surface and pores. The BET equation was applied to determine the distribution, micropore, and mesopore volumes, refer to equation 2.5.

3.7 Batch experiments

Preliminary batch experiments were done to test that carbonised orange peels could reduce iron and manganese concentrations in borehole water. The effect of mass, contact time, ion concentrations, and pH were done in batch mode. A 1000 ppm model fluid containing either Fe or Mn was prepared. The solutions were then diluted to prepare the 100 ppm, 50 ppm, 40 ppm, 30 ppm, 20 ppm, 10 ppm and 5 ppm concentrations for varying concentration tests. For varying masses an amount of either 0.05, 0.1, 0.2, 0.3, 0.5 and 1 g was tested. The pH of the solutions was adjusted to pH 4 with either NaOH or HCl and the experiments were conducted at room temperature to simulate real borehole water conditions. For the varying pH studies values of 2.5 and 4 were tested for Fe. This was done due to preliminary work on the pH experiments which showed that iron precipitated above pH 4. Literature studies done by Elsherif (2017) and Tadepalli et al. (2016) suggested studies in moderately acidic pH to suppress precipitates. Based on the literature, pH 2.5 and 4 was selected for the study. Furthermore, the narrow pH aligned with the pH values for the sampled borehole water, which was chosen to be left in the sampled condition to replicate their natural state. All batch experiments were conducted at room temperature to simulate real borehole conditions. Typically, a weighed amount of biosorbent was contacted by shaking in a sample shaker at 150 rpm with a known concentration of Fe and Mn ions in a given volume overnight. The adsorbed samples were then filtered through Whatman No 1 filter paper and analysed for residual metal ions. The borehole water samples underwent the same batch treatment. Figure 3.8 shows the sample shaking and the filtering process.

Figure 3.8 Sample shaking and filtering of solutions

The percentage and quantity adsorbed were calculated according to Equation 2.18:

$$\% \, adsorption = \frac{C_i - C_e}{C_i} \, x \, 100 \qquad \text{Equation } 2.18$$

3.7.1 Effect of biosorbent mass

The effect of dosage was assessed by varying the amount of biosorbent used. Different quantities (0.05, 0.1, 0.2, 0.3, 0.5, and 1 g) of the biosorbent were added to 30 ml of either Fe or Mn solution at pH 4 in a 50 ml tube. The mixture was then shaken for 24 hours at 150 rpm in a sample shaker. Afterward, the effluent was filtered using Whatman filter paper and collected in a 50 ml tube. The concentration of the elements in the filtered solution was analysed using an Inductively Coupled Plasma - Optical Emission Spectrometer (ICP-OES). The percentage of adsorption was then plotted against the different biosorbent masses.

3.7.2 Effect of contact time

The effect of contact time on the adsorption process was investigated by varying the contact time in batch mode, with durations of 1, 3, 5, 10, 15, 20, 30, 45, 60, and 90 minutes. A biosorbent dosage of 0.3 g and a 100 mg/L ion solution were added to plastic jars, each containing 30 ml of solution at pH 4, and placed in a shaker set at 150 rpm. After the designated contact time, the biosorbent was filtered out, and the remaining solution was analysed using an Inductively Coupled Plasma - Optical Emission Spectrometer (ICP-OES). The results were used to assess the impact of contact time on the biosorption process.

3.7.3 Effect of metal concentration

The effect of initial concentration on the adsorption process was examined by varying the solution concentration between 5, 10, 20, 30, 40, 50, and 100 mg/L, using 0.3 g of biosorbent in 30 ml of the solution at pH 4. The samples were placed in a shaker overnight at 150 rpm and then filtered. The results were used to evaluate the equilibrium models of the biosorption process.

3.7.4 Effect of pH

The effect of pH was determined by varying the pH to 2.5 and 4 for a 100 ppm Fe solution, using 0.3 g of the biosorbent in a 30 ml solution. The pH of the solutions was adjusted with either NaOH or HCl. The reason for the selection of the chosen pH range is due to iron precipitation at values higher than 4 as this will restrict the biosorption studies and at pH values less than 2.5 the overall active sites on the biosorbent surface become positive which results in a lower uptake of metal. However, the adsorption of manganese is not problematic at lower pH levels and thus studies was not conducted in varying the pH of manganese. Additionally, the intention of this study is to remove Fe an Mn from real municipal BH water with an average pH 4.

3.7.5 Modelling of batch biosorption data

Adsorption isotherms were used to illustrate the relationship between the equilibrium concentration and the amount of adsorbate adsorbed at equilibrium. The Langmuir and Freundlich models were applied to compare the performance of the biosorbents. The data for this analysis was obtained from the concentration variation studies. The Langmuir model assumes that adsorption occurs in a monolayer on a surface with a finite number of adsorption sites, while the Freundlich model assumes adsorption occurs in multiple layers, with non-uniformity present.

Kinetic studies were conducted to determine the adsorption rate. Contact time was varied, with durations of 1, 3, 5, 10, 15, 20, 30, 45, 60, and 90 minutes. A biosorbent dosage of 0.3 g and a 100 mg/L ion solution were added to plastic jars, each containing 30 ml of solution at pH 4, and placed in a shaker set at 150 rpm. After the specified contact time, the biosorbent was filtered out, and the remaining solution was analysed using an Inductively Coupled Plasma - Optical Emission Spectrometer (ICP-OES). The results were used to populate the kinetic mathematical models: pseudo-first-order, pseudo-second order, and intraparticle diffusion.

3.8 Fixed bed column experiments

Fixed-bed column studies were carried out using a plastic column with an internal diameter of 1.7 cm and a height of 20 cm. The column was packed with filter paper, cut to a 1.7 cm diameter, along with cotton and carbonized biosorbent. Borehole water was passed through the column at different flow rates and bed heights. Samples were then collected at different time intervals for analysis. The experiments used varying bed heights (0.3 g, 0.5 g, and 1 g) and flow rates (10, 15, and 20 ml/min). All fixed bed experiments were carried out at room temperature to simulate real borehole conditions. Figure 3.9 demonstrates the fixed bed set up for the column experiments.

Figure 3.9 Fixed bed set-up for column experiments

3.8.1 Modelling of column biosorption data

From the equilibrium data, a breakthrough curve was derived to analyse and describe the performance of the adsorption process in the fixed-bed column. Four response factors were applied: Breakpoint time (TB), Fractional Bed Utilization (FBU), Saturation time (TS), and Volume of effluent treated per gram (VS). TB represents the time required to reach 5% of the inlet concentration, while TS refers to the time taken for the effluent to reach 95% of the inlet concentration. Fixed bed models, including the Bohart-Adams model, Thomas model, and Yoon-Nelson model, were applied to interpret the results. The best-performing model was selected, and based on this, the scaled-up design could be developed for municipal application.

3.9 Fixed bed column design

The adsorption performance was evaluated using breakthrough curves, which are generated by plotting the ratio of the concentration of the solution at a given time (C) to the initial concentration (C0), i.e., (C/C0), against time (t). These curves provided valuable information about the breakthrough and saturation points. By analysing the area under the curve, we determined the length of the used and unused portions of the bed. When the C/C0 ratio reached one, the column was considered saturated, signalling the termination of the adsorption process. The plot of C/C0 versus time formed an 'S'-shaped curve, known as the breakthrough curve, as shown in Figure 3.10. The steepness of the curve varied depending on the specific conditions of the fixed-bed column studies (Thirunavukkarasu et al., 2021). Chowdhury et al. (2012) also used the fixed bed experiments to describe the adsorption process and found that it worked well.

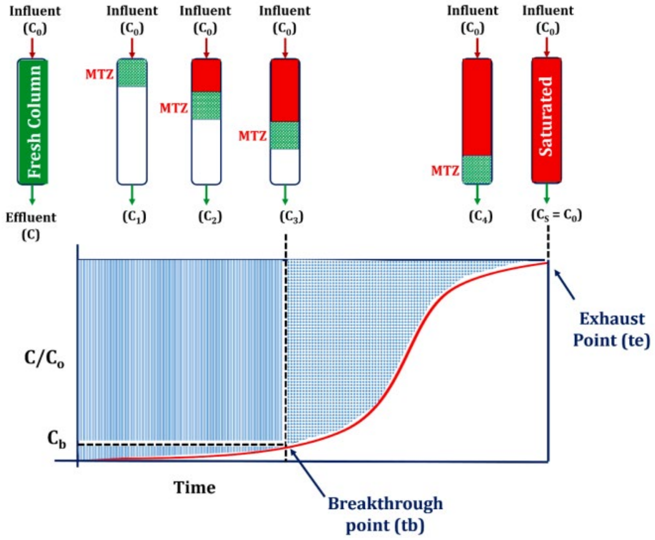

Figure 3.10 The breakthrough curve, obtained from the plot of C/C_0 versus time, and its relationship with the movement of the Mass Transfer Zone (MTZ) along the length of the column (Thirunavukkarasu et al., 2021)

3.10 Conclusion

This chapter outlined the methodology used in this study detailing each step in the process. The study was conducted at the Gateway wellfield in Overstrand Municipality, known for elevated iron (6–91 mg/L) and manganese (1–7 mg/L) levels compared to the World Health Organisation limits for drinking water. The orange peels were collected, washed, oven-dried, ground, sieved and carbonised. Laboratory containers were meticulously cleaned using detergents, rinsed, and treated with nitric acid to eliminate contaminants. Solutions of iron and manganese (model fluid) were prepared at specific concentrations (1000 ppm diluted to lower concentrations) with pH adjusted to 4 to simulate real borehole conditions. Initial borehole water samples were collected, stabilized with nitric acid, and analysed immediately to prevent oxidation. Iron and manganese concentrations were determined using Inductively Coupled Plasma - Optical Emission Spectrometry (ICP-OES). Various characterisation techniques were completed to analyse the structure, morphology, and elemental composition of the proposed biosorbent. Thereafter, batch and column experiments were done to assess the performance of the biosorbent in both batch and column setup while investigating various process parameters. The following chapters will present the results and findings from the batch and column experiments conducted.

Chapter 4 Structural characterisation of the biosorbent

4.1 Introduction

This chapter presents the characterization results of both raw and carbonized adsorbents using Scanning Electron Microscopy (SEM), Fourier Transform Infrared Spectroscopy (FTIR), and Brunauer-Emmett-Teller (BET) analysis. For the characterization, 1 g of the biosorbent was added to 200 ml of borehole water to adsorb iron and manganese metals, followed by subsequent analysis. The elemental composition obtained through SEM-EDS is also provided and discussed. The raw, non-carbonised sample was found to be poor in its ability to adsorb Fe and Mn and so gave rise to water of poor quality (Fe and Mn content was above legally allowed limits).

4.2 SEM-EDS for surface morphology and elemental analysis of biosorbent

The surface structure of the biosorbent, both before and after carbonization and adsorption, was examined using Scanning Electron Microscopy (SEM). SEM is an effective method for analySing the surface morphology of a biosorbent. The SEM images shown in Figures 1a, 1b, 2a, and 2b were captured at a magnification of 50K. The unmodified biosorbent (Figure 1a) has a heterogeneous, uneven, and rough surface texture. After carbonization (Figure 2a), the surface appears to be covered with dust-like particles or filled with craters. The surface particles are asymmetrical, varying in diameter and shape, ranging from spherical to elongated flakes. The carbonization process appears to have altered the biosorbent's surface structure.

The raw biosorbent after adsorption (Figure 1b) possess some dust-like particles not seen in the raw biosorbent before adsorption (Figure 1a). The adsorption process seems to have completely transformed the microstructure of the raw biosorbent to a seemingly more homogenous and smoother surface. After adsorption, the pores of the biosorbent were filled with heavy metal ions, and the structural changes observed in the adsorbent can be attributed to the interaction with these metal ions. This is because the OP has bound the metals in the water sample.

The carbonised biosorbent before adsorption (Figure 2a) possesses a rough surface with some small, filled craters and the surface particles vary in size and shape and shows a few dust-like particles. While the carbonised biosorbent after adsorption (Figure 2b) shows flaky microparticles. The surface of the biosorbent seems to be more homogenous. Pathak et al. (2017) also found the surface of OP to be rough with some fibers that were spread throughout the surface.

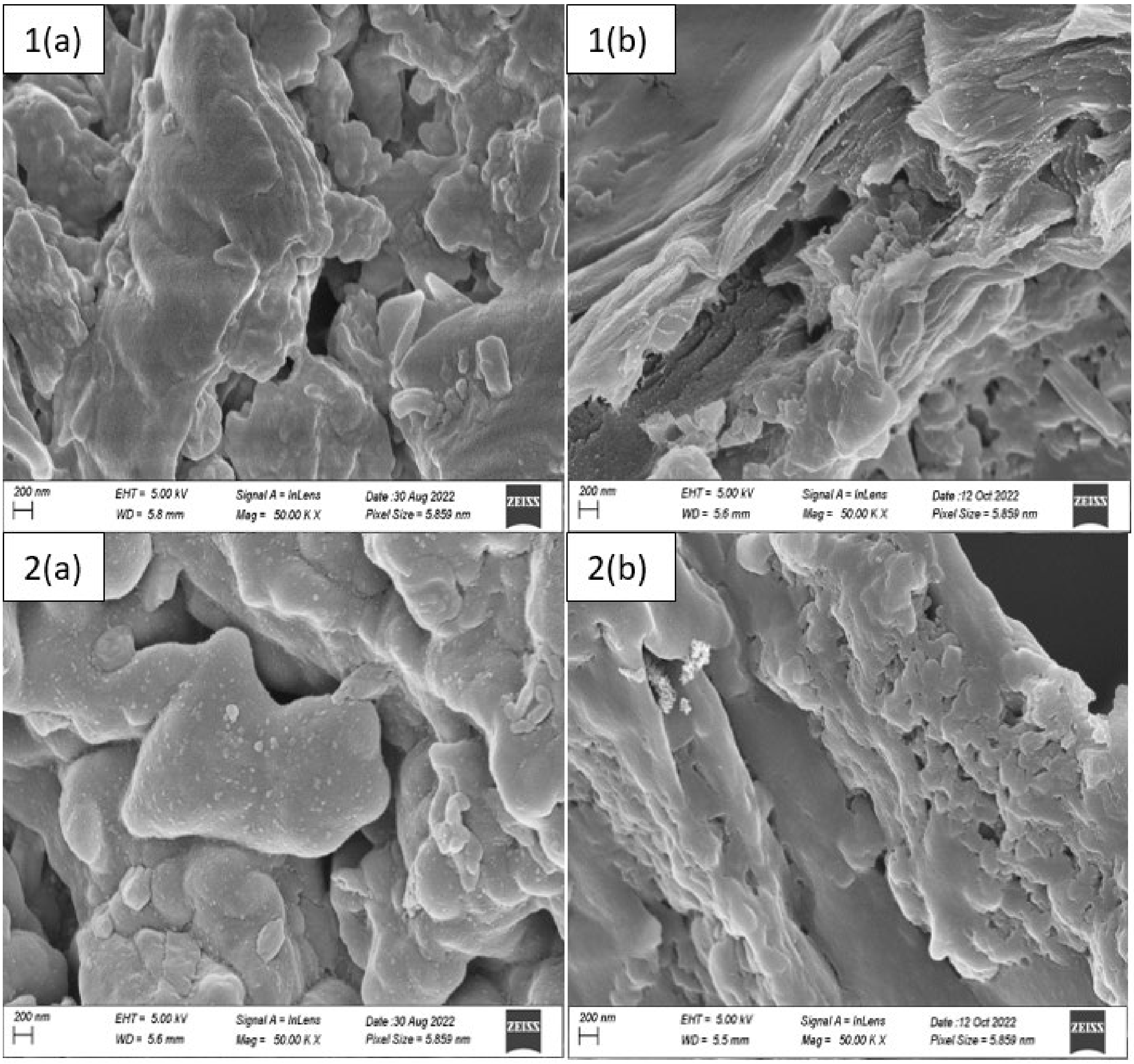

Figure 4.1 SEM micrographs of 1) ROP 2) COP (a) before adsorption (b) after adsorption

EDS in conjunction with SEM was used to determine the elemental composition of the biosorbent samples before and after biosorption. The EDS results indicated a high percentage of carbon (C) and oxygen (O), consistent with the expected composition of an organic matrix. This finding suggests that the material analysed predominantly consists of organic compounds, likely reflecting its biological origin. The O content of the carbonised sample was significantly lower than the raw sample. Before biosorption, the biomass showed a small amount of Fe and no Mn present in the elemental composition. After treatment, the Fe ions in the sample increased and Mn ions were now present. The present Fe ions in the ROP was 0.02% and after treatment the Fe ions present increased to 0.09%. For the COP the Fe ions present before adsorption was 0.05% and this increased to 0.23% after adsorption. This is an indication that absorptive removal of the metal ions from the aqueous solution is evident for both Fe and Mn. This work clearly shows that carbonisation of the raw sample can improve biosorption by nearly 3-fold. It was also noted that there was nitrogen (N) and chlorine (Cl) present in the raw sample after adsorption which was not contained in any of the other samples this could possibly be due to functional groups that were present in the raw sample which allowed for bonding with N and Cl containing compounds. These functional groups might have been completely broken down in the carbonised samples rendering these samples unable to adsorb the N and Cl compounds. Phosphorous and sulphur appeared in both samples after adsorption. A typical EDS spectrum is shown in Figure 4.2 while a summary of EDS results is presented in Table 4.1.

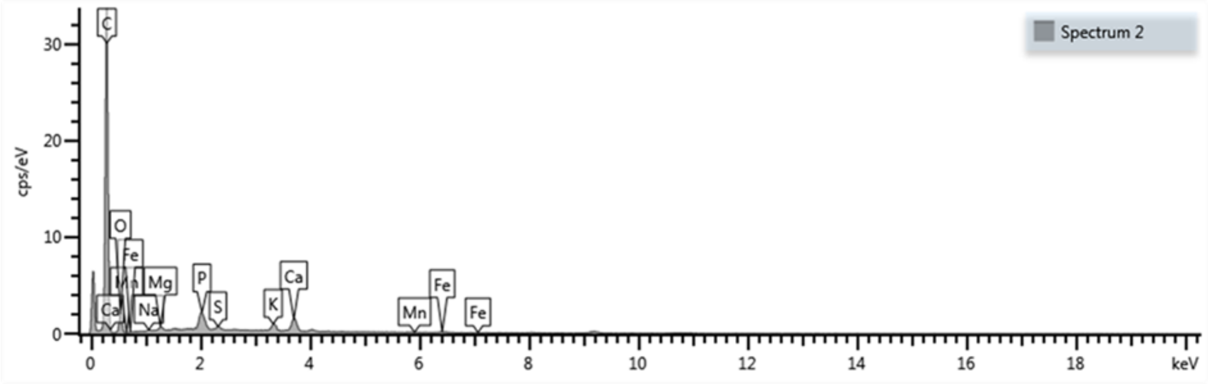

Figure 4.2 EDS spectrum

Table 4.1 Energy Dispersive X-ray Spectroscopy (EDS) data of raw and carbonised biosorbents before and after adsorption

Sample description	C	N	O	Na	Mg	P	S	Cl	K	Ca	Mn	Fe	Cu
ROP before adsorption	61.1		37.84	0.03	0.06	0.42	0.03		0.54	0.3		0.02	0.1
ROP after adsorption	61.5	2.1	35.21	0.06	0.13			0.02	0.05	0.42	0.02	0.04	
COP before adsorption	80.24		17.32	0.08	0.3				1.13	0.79		0.05	0.1
COP after adsorption	87.47		10.41	0.07	0.17	0.55	0.14		0.36	0.73	0.01	0.07	

4.3 FTIR for identifying the various functional groups on biosorbent surface

FTIR was employed to analyse the chemical structure of the biosorbent by identifying the functional groups present. The FTIR spectra of the biosorbents ROP and COP, both before and after adsorption, are shown in Figures 4.3 1(a) – 4.3 2(b). Figures 4.3 1(a) and 1(b) illustrate the morphology of ROP before and after adsorption. A variety of functional group bands were identified on the surface of the biosorbent. The wide and intense adsorption peak at 3380 can be attributed to stretching in O-H and can be H-bonded or carboxylic acids. Between 3000-2850, a weak peak of 2935 which can be attributed to stretching in C-H and is an alkane functional group. Then sharp-medium bands at 1728 and 1599, can be attributed to C=O due to either aldehyde or a ketone and C=C due to alkene and often implies an aromatic ring respectively. Then a strong band at 1018 is seen and can be attributed to a C-O band and can be due to the presence of esters. These findings are similar to Pathak et al. (2017) who found intense bands indicating the presence of alcohol, phenol, carboxylic group, amines, amides, ketones, ester, ether, and amino acid group in OP. Pathak et al. (2017) also stated that no peaks between the regions 2220 and 2260 cm^{-1} would be present, which suggests the absence of cyanide groups which this work confirms.

The FTIR spectrum for COP showed a complete elimination of peaks previously seen in ROP. There was no significant or observable difference in the FTIR spectrum of ROP and COP before and after application for the sorption of Fe and Mn. This indicates that the adsorption of Mn, Fe, P, S ions were non-chemical in nature (no chemical bonds were formed between the adsorbate (COP) and the adsorbents. However, although the shape of the COP after adsorption remained similar to that of the COP sample before adsorption it was observed that the percentage transmittance or intensity was lower for the COP sample before adsorption.

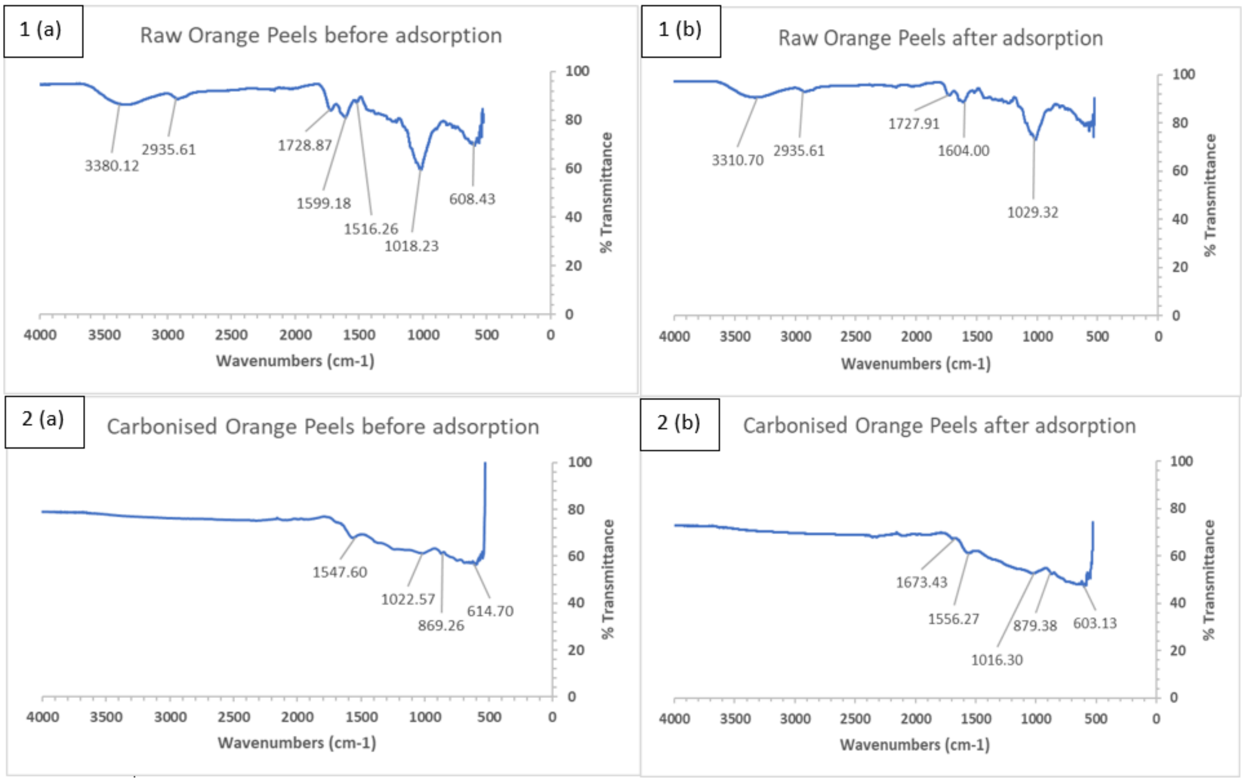

Figure 4.3 FTIR spectrum of 1) ROP and 2) COP (a) before and (b) after adsorption

4.4 BET for surface area and pore analysis of the biosorbent

BET N_2 (77k) adsorption/desorption isotherms were used to evaluate the adsorbents in terms of the surface area, pore size and volume. Barrett-Joyner-Halenda (BJH) is also a testing technique that is used to determine the pore size and volume analysis. A summary of the characterisation of ROP and COP is presented in Table 4.3. All samples exhibited a Type II isotherm indicating that they are macro-porous adsorbents as seen in Figure 4.4.

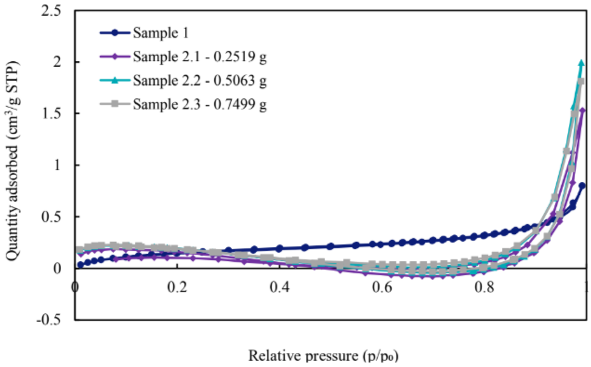

Figure 4.4 Plot of adsorption and desorption isotherms for samples

Table 4.2 Classification of pores (Shafiq et al., 2017)

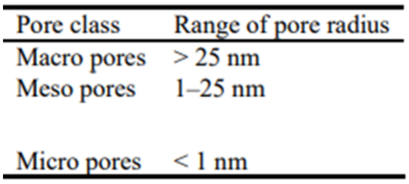

Pore class	Range of pore radius
Macro pores	> 25 nm
Meso pores	1–25 nm
Micro pores	< 1 nm

However, the IUPAC standards define Macro-porous as > 50 nm, mesoporous as between 2-50 nm and microporous as < 2nm.

The BET surface areas of both the ROP (0.57m²/g) and COP (0.96 m²/g) were found to be quite low, and this agrees with Pathak et al. (2017) who also found that the BET surface area of OP to be very low at 1.03 m²/g, when compared to siliceous materials. He attributed the low surface area to the operational complexity of degassing lignocellulosic samples and further stated that the low surface area is a characteristic feature of carbonaceous materials. Though the surface area of the ROP and COP adsorbents are very low it should be noted that carbonisation of ROP at 600°C resulted in an increase in the surface area of the COP. The surface area of COP is almost two times that of ROP. These very low surface areas suggest that low adsorption capabilities of the COP adsorbent will be observed when compared to other high surface area adsorbents like activated carbon. Future work for these OP should involve drying, selective etching with acids/bases and carbonizing at 800, 900, and 1000°C to see if these treatment regimens will give COP's with higher surface areas than that witnessed at 600°C. It is also observed that the BJH pore widths shows significant improvement with carbonisation of ROP at 600°C.

Table 4.3 BET information

	ROP	**COP**
BET surface area (m²/g)	0.57	0.96
Pore diameter (Å)	68	97
BJH Pore width (Å)	73	310
Pore volume (cm³/g)	0.001	0.002

4.5 Conclusion

SEM images of ROP and COP revealed varying degrees of porosity and particle distribution. However, no clear correlation could be established between the SEM images and the treatment protocols applied. EDS analysis confirmed the presence of Fe and Mn on the surfaces of both ROP and COP after biosorption. FTIR analysis of ROP indicated the presence of functional groups such as carboxylic, alkane, aldehyde, alkene, ketones, and ester. The thermal treatment through carbonization resulted in a significant removal of the characteristic peaks of ROP. The BET surface areas of both ROP and COP were found to be very low, which is typical for carbonaceous materials. The surface area of the ROP is seen to increase with carbonization, an occurrence which should help increase the adsorption capability of the resultant COP.

Chapter 5 Biosorbent performance in batch studies

In this chapter the results of the adsorption capabilities of the biosorbent applied in batch studies are presented for both iron and manganese in model fluid and borehole water.

5.1 Batch studies

The experimental parameters that were optimised are pH, adsorbent dosage, concentration, and contact time.

5.1.1 Effect of concentration

Fe and Mn ion adsorption onto orange peel powder was studied using various initial metal ion concentrations for the model fluid ranging from 5 mg/L to 100 mg/L. Experiments were also conducted using 200 ppm, 300 ppm, 500 ppm, 700 ppm and 1000 ppm, however, the experimental data was discarded due to precipitates forming in the solutions at these higher concentrations. Studies were also conducted with the actual borehole water samples and can be seen in Figures 5.1 (e) and (f).

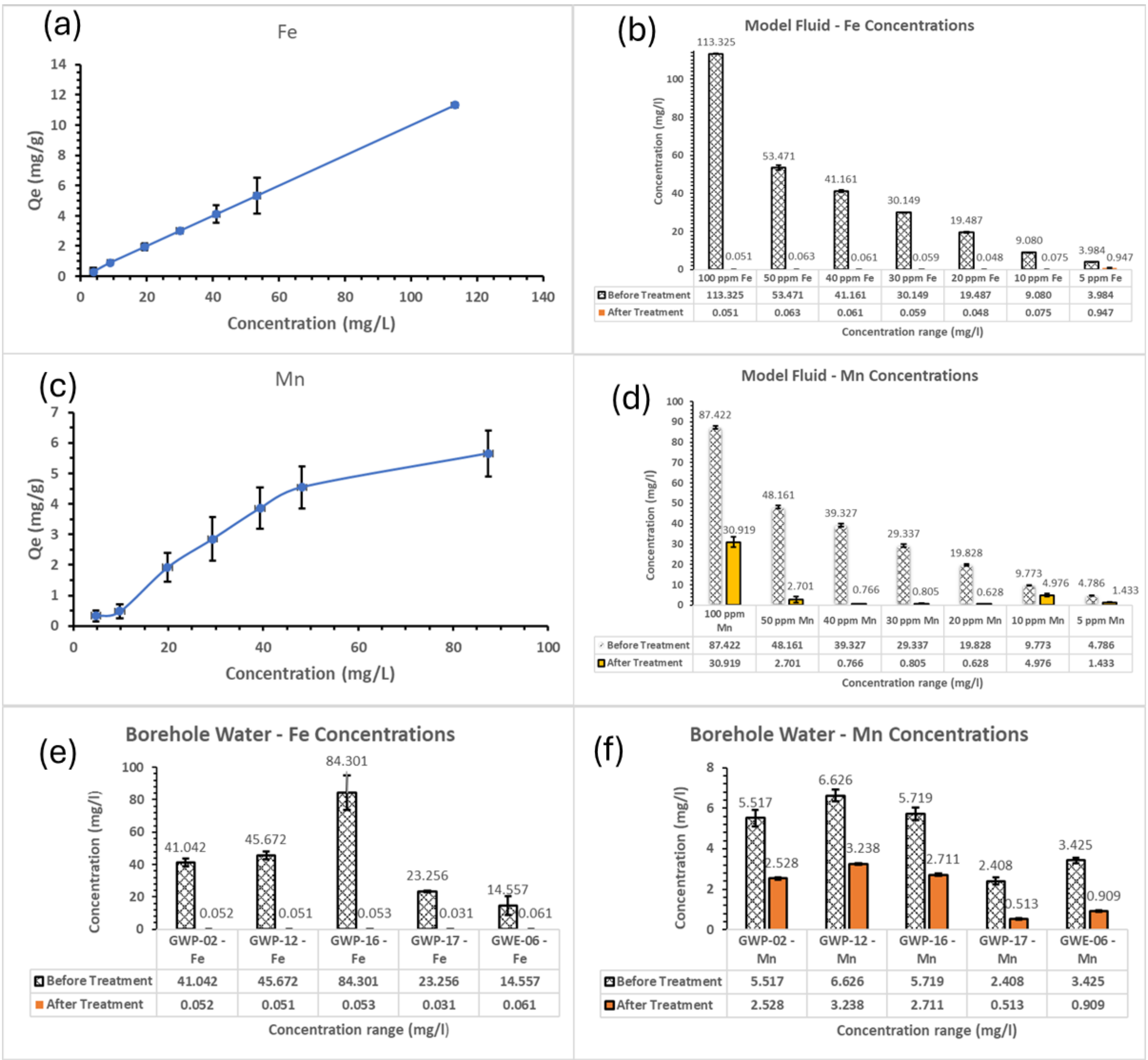

(b)

	100 ppm Fe	50 ppm Fe	40 ppm Fe	30 ppm Fe	20 ppm Fe	10 ppm Fe	5 ppm Fe
▨ Before Treatment	113.325	53.471	41.161	30.149	19.487	9.080	3.984
■ After Treatment	0.051	0.063	0.061	0.059	0.048	0.075	0.947

Concentration range (mg/l)

(d)

	100 ppm Mn	50 ppm Mn	40 ppm Mn	30 ppm Mn	20 ppm Mn	10 ppm Mn	5 ppm Mn
▨ Before Treatment	87.422	48.161	39.327	29.337	19.828	9.773	4.786
■ After Treatment	30.919	2.701	0.766	0.805	0.628	4.976	1.433

Concentration range (mg/l)

(e)

	GWP-02 - Fe	GWP-12 - Fe	GWP-16 - Fe	GWP-17 - Fe	GWE-06 - Fe
▨ Before Treatment	41.042	45.672	84.301	23.256	14.557
■ After Treatment	0.052	0.051	0.053	0.031	0.061

Concentration range (mg/l)

(f)

	GWP-02 - Mn	GWP-12 - Mn	GWP-16 - Mn	GWP-17 - Mn	GWE-06 - Mn
▨ Before Treatment	5.517	6.626	5.719	2.408	3.425
■ After Treatment	2.528	3.238	2.711	0.513	0.909

Concentration range (mg/l)

Figure 5.1 Effect of concentration (a) and (b) Fe in the model fluid, (c) and (d) Mn in the model fluid, (e) and (f) Fe and Mn in the borehole water

The experiments for effect of concentration were carried out with model fluid at pH 4. The relation between metal ion adsorption (mg/g) and initial metal ion concentration (mg/L) for the model fluid is shown in Figures 5.1 (a) and (c) for Fe and Mn respectively. It is observed that Q_e increases as the metal ion concentration increases where 5 mg/l was 0.311 mg/g and 100 mg/l was 11.33 mg/g. For Fe it was observed that the percentage removal is constant at 99% removal except for 5 mg/l which was at 76%. It was also observed that the iron concentration seems to increase linearly. The iron concentrations are significantly removed as opposed to the manganese concentrations. This could be attributed to the biosorbent's structure and surface characteristics relative to iron and manganese. Manganese still showed acceptable percentage removals ranging from 40%-97%.

Figures 5.1 (b) and (d) presents the concentration of the metals (mg/l) in the model fluid before and after adsorption for Fe and Mn respectively. These figures show the corresponding reduction in iron concentrations of the model fluid with little to no iron left while the manganese concentrations varied markedly with initial concentration. The percentage removal for Mn reached a plateau at around 40 ppm after which the removal efficiency decreases. It is seen that the model fluid for Fe performed remarkably well when compared to Mn. Figures 5.1 (e) and (f) indicates a similar trend for the five borehole water samples, where the biosorbent removed practically all the iron in the borehole water while significantly high amounts of manganese were still present in the water after treatment. This is notable as the removal of iron has been constant even in a binary system where there is simultaneous removal of iron and manganese.

5.1.2 Effect of pH

The pH of the solution is a vital aspect in the adsorption process. Previous studies found that acidic conditions, pH<2.5, metal adsorption was low. The pH of the borehole water was tested, and it was found to be an average of pH 4. The aim of this study was to successfully treat the borehole water and therefore the experimental conditions were centred around the characteristics of the borehole water to simulate real conditions. Iron was a challenging metal as precipitation occurred at pH values higher than 5 which restricted the adsorption studies as discovered in preliminary experiments conducted. Therefore, the removal of Fe in some of the BH samples could be attributed to metal iron precipitation. The effect of pH was determined by varying the pH of the model fluid to 2.5 and 4 for Fe. Presented in Figure 5.2 is the effect of pH on the biosorption for Fe at pH 2.5 and 4. A study was not conducted varying the pH of manganese as this metal was not found to be problematic within the pH range of 3-5 and as presented in numerous previous studies it was found that Mn only precipitates at a high pH 8 which would not restrict the adsorption study. It was observed that adsorption increases for Fe at the higher pH value 4 and the percentage absorbed for iron remains at 99-100%. Therefore, all remaining experiments were carried out at pH 4.

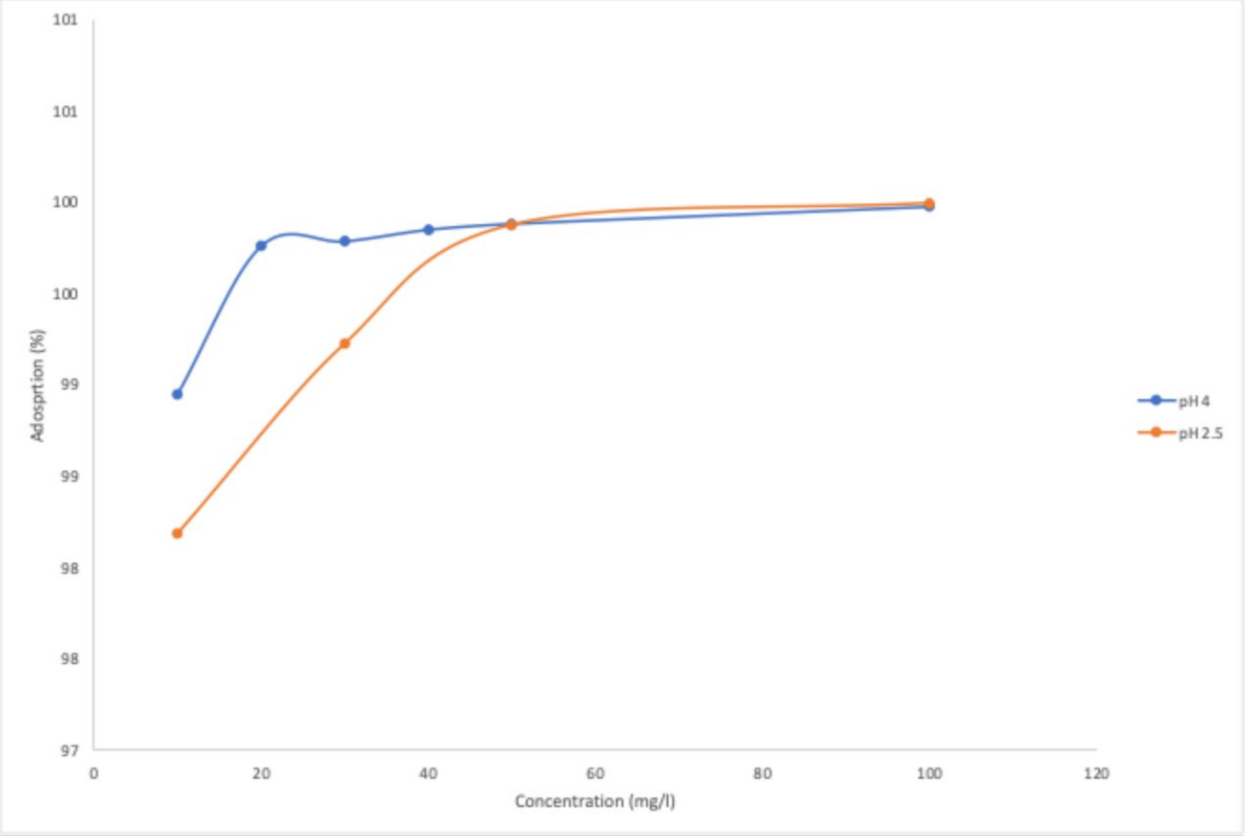

Figure 5.2 Effect of pH on the biosorption of COP for Fe at pH 4 and pH 2.5

5.1.3 Effect of adsorbent dose

The adsorbent dose plays a crucial role in determining the biosorbent's capacity for a specific initial ion concentration. While the adsorption of iron by orange peel remained unaffected by variations in adsorbent mass, the adsorption of manganese was significantly influenced by the initial biosorbent dose. The percentage of manganese removed from the solution reduced markedly (when dose was doubled from 0.05 g) but rose steadily as the dose increased, reaching a pseudo-plateau at 0.5 g. As a result, subsequent adsorption experiments were conducted with a dose of 0.3 g to balance efficient biomass use with the consistent adsorption of iron ions. The adsorbent dose significantly affects the economic feasibility of the adsorption process, emphasizing the importance of maximizing removal efficiency with the least amount of adsorbent.

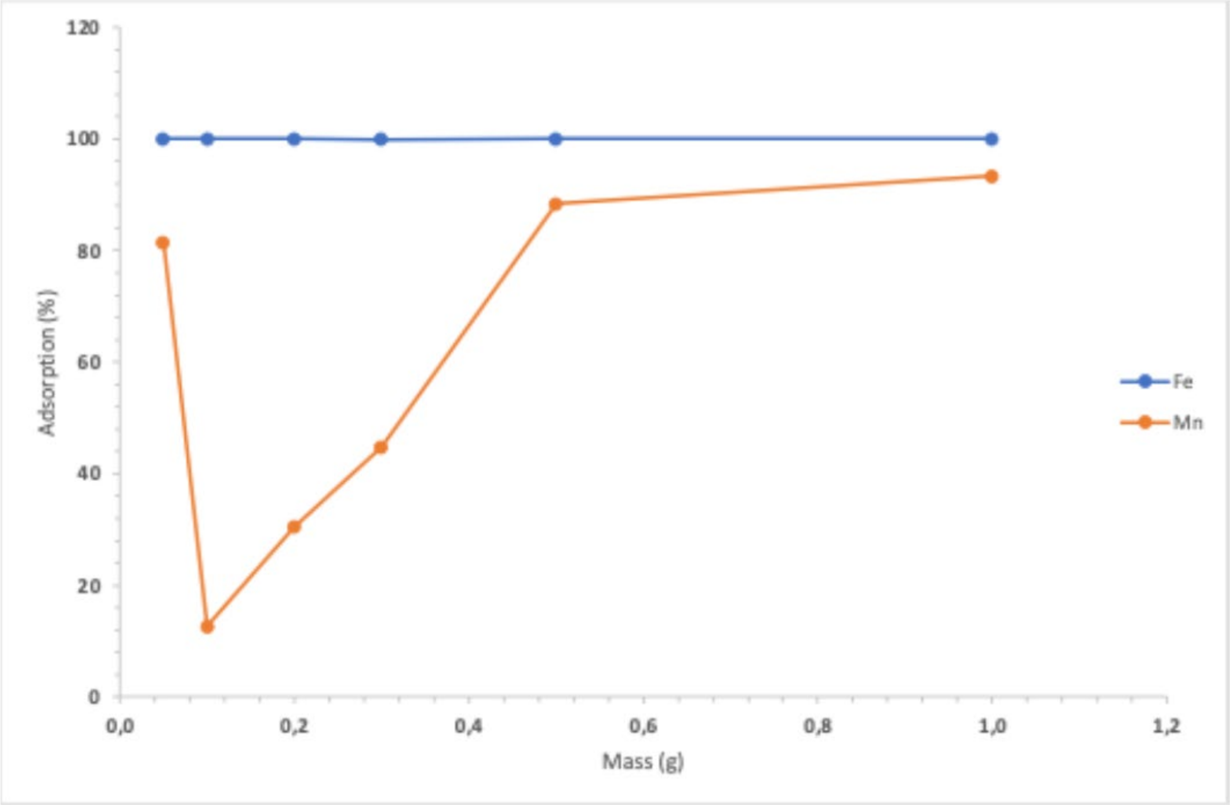

Figure 5.3 Effect of adsorbent dose as a function of percentage adsorbed for Fe and Mn

5.1.4 Effect of contact time

The time taken for a batch system to reach equilibrium is a valuable factor to consider therefore the effect of contact time was investigated. In Figures 5.4 (a) and (b) it is seen that the adsorption for iron is instantaneous and stays constant while for manganese there is desorption over time. The adsorption reaches a maximum at 10 mins after which desorption occurs until it reaches equilibrium around 40 mins. Therefore, all other experiments were conducted at 40 mins as this was seen as the optimal contact time for Mn

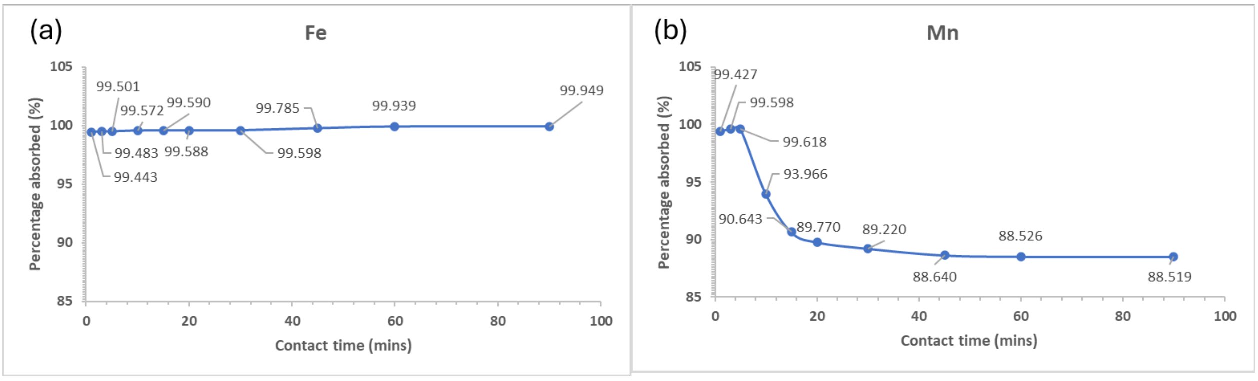

Figure 5.4 Effect of contact time as a function of percentage adsorbed for Fe and Mn

5.2 Modelling: Isotherm models

The isotherm models are used to describe the characteristics of the biosorbent and to explain the biosorbent performance. The Langmuir and Freundlich models were used to compare and analyse the experimental data. Figure 5.5 (a) and (b) presents the Langmuir biosorption isotherm for iron and manganese adsorption and Figure 5.6 (a) and (b) shows the Freundlich biosorption for iron and manganese adsorption. For the Langmuir isotherm the biosorbent was more favourable towards manganese adsorption and gave a marginally better result where the regression coefficient was 0.9964 in comparison to iron which was 0.9944. The Freundlich model was also more favourable towards manganese adsorption with a regression coefficient of 0.9681 while iron was 0.9641. Overall, both isotherm models showed an excellent fit to the experimental data (R^2>0.9) with high regression coefficients for both Fe and Mn. Table 5.2 presents the isotherm model parameters, the R_L values for Fe (0.016) and Mn (0.033) in the Langmuir model indicates that the adsorption is favourable for both metals. A comparison of Q_{max} values against all the literature using orange peels as a biosorbent can be seen in Table 5.1. The Q_{max} findings of this work aligns with the work done by Elsherif (2017) and Adebayo (2016) who found Q_{max} values of 12.26 mg/g and 9.1 mg/g for iron respectively. There was only one study found on manganese done by Surovka et al. (2017) who found Q_{max} at a value three times higher than the results found in this study. Overall, the results compared well with the findings in the literature.

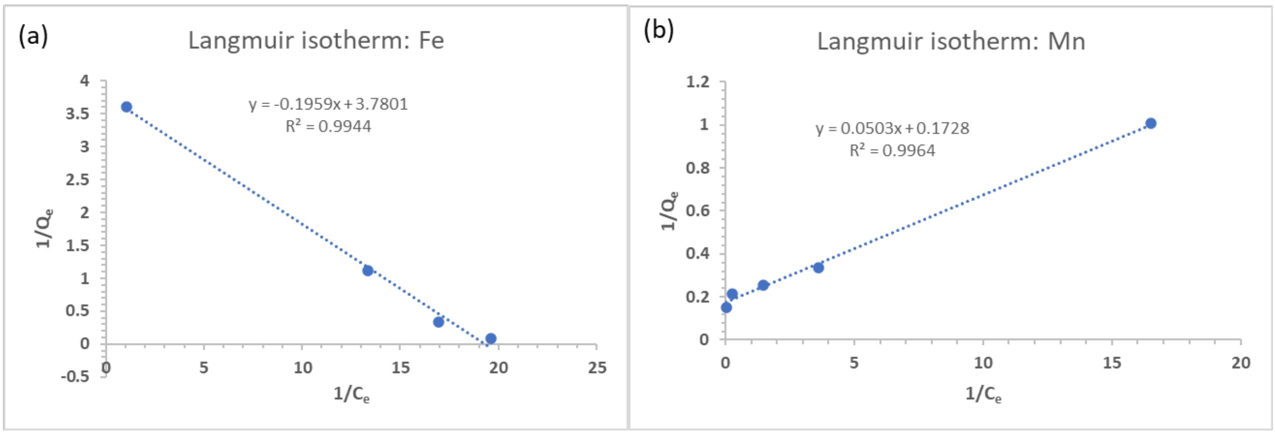

Figure 5.5 Langmuir biosorption isotherm for the adsorption of (a) iron and (b) manganese on COP

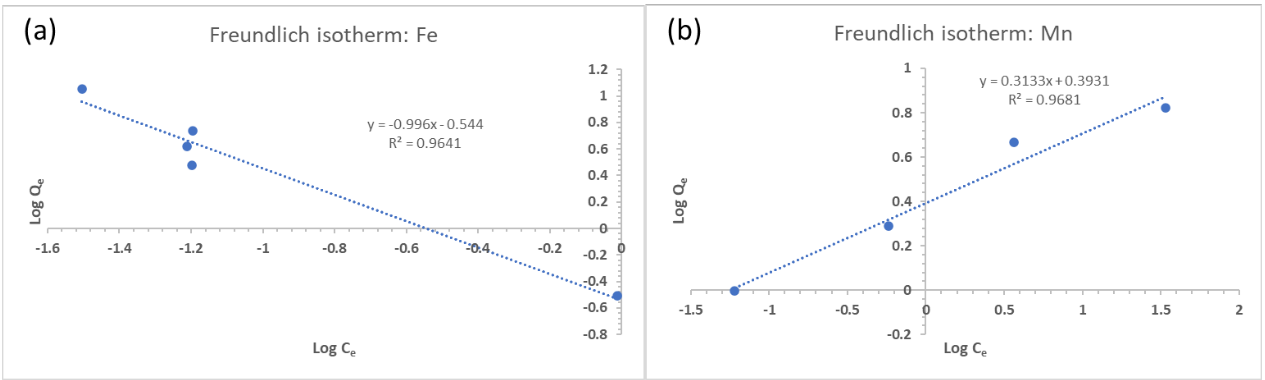

Figure 5.6 Freundlich model isotherm for the adsorption of (a) iron and (b) manganese on COP

Table 5.1 Q_{max} values for Fe and Mn versus literature findings

Author/s and Year of publication	**Title of paper**	**Q_{max} values**	
		Fe	**Mn**
This study	Iron and manganese removal from borehole water using carbonised orange peels as a biosorbent	11.32 mg/g	4.9 mg/g
Tadepalli et al., 2016	Removal of Cu (II) and Fe (II) from Industrial waste water using orange peel as adsorbent in batch mode operation	Not stated	
Elsherif, 2017	Removal of Fe (III), Cu (II), and Co (II) from Aqueous Solutions by Orange Peels Powder: Equilibrium Study	12.26 mg/g	
Mamun et al., 2019	A Comparative Study of the Adsorption Capacity of Tea Leaves and Orange Peel for the Removal of Fe (III) Ion from Wastewater	0.037 mg/g	
Adebayo et al.,2016	Biosorption of Fe (II) and Cd (II) ions from aqueous solution using a low cost Adsorbent from Orange Peels	6.9 mg/g (Modified orange peel) 9.1 mg/g (Activated orange peel)	
Surovka et al.,2017	Sorption of Iron, Manganese, and Copper from Aqueous Solution Using Orange Peel: Optimization, Isothermic, Kinetic, and Thermodynamic Studies	8.35 mg/g	15.95 mg/g
Rashid, 2009	Removal of Heavy Metals in Aqueous Solution Using Banana and OrangePeels	8.2 mg/g	
Nandeshwar et al., 2015	Green activated carbons from different waste materials for the removal of iron from real wastewater samples of Nag River, India	Not stated	

Table 5.2 Isotherm parameters

Isotherm model	Parameters	Iron	Manganese
Langmuir	Q (mg/g)	0.26	19.88
	K_L	-19.29	0.29
	R_L	0.016	0.033
	R^2	0.9944	0.9964
Freundlich	K_F	0.28	2.47
	n	-1.00	3.19
	R^2	0.9641	0.9681

5.3 Modelling: Kinetic models

Kinetic models were also done to better understand the biosorption performance of carbonised orange peels in the removal of Fe and Mn in water and thus was performed by utilising the contact time experimental data. The mathematical models used was the pseudo first order, pseudo second order and the intraparticle diffusion models. The model constants were determined from a linear graph as presented in Figure 5.7 (a) and (b) for iron and manganese respectively. Table 5.3 summarises the results for the three kinetic models. It was observed that the Pseudo second order presented the best fit with excellent regression coefficients that indicates a linear relationship. The pseudo second order predicted Q_e as 10 mg/g and the experimental Q_e was calculated as 11.3 mg/g for Fe. For Mn the predicted Q_e is 4.9 mg/g while the experimental Q_e was calculated to be 5.3 mg/g.

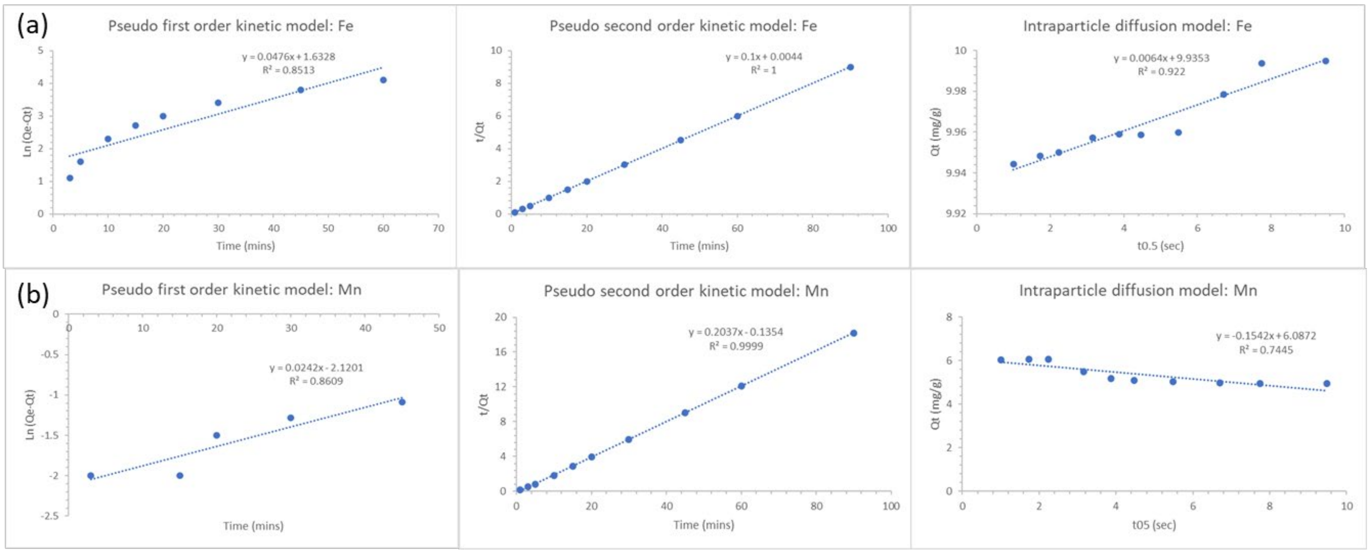

Figure 5.7 Kinetic models: Pseudo first order, pseudo second order and intraparticle diffusion for (a) iron and (b) manganese

Table 5.3 Kinetic models parameters

Kinetic model	Parameters	Iron	Manganese
Pseudo first order kinetics	Q_e (mg/g)	5.1182	0.1200
	K_1	-0.0476	-0.0242
	R^2	0.9084	0.8609
Pseudo second order kinetics	Q_e (mg/g)	10	4.9
	K_2	2.2727	-0.3065
	R^2	1	0.9999
Intraparticle diffusion	K_2	0.0064	-0.1542
	R^2	0.9220	0.7445

5.4 Conclusion

In the effect of concentration experiments it was observed that there was a constant percentage removal for iron and the iron concentrations were significantly reduced after treatment while the manganese concentrations varied with initial concentration. The iron performed well in both the model fluid and the borehole water adsorption experiments when compared to manganese. The iron removal has been constant even in a binary system where there is simultaneous removal of iron and manganese. In the pH studies it was observed that adsorption increases for Fe at the higher pH value 4 and the percentage absorbed for iron remains at 99-100%. The effect of adsorbent dose revealed that the adsorption of iron was unaffected by the mass of the adsorbent. However, manganese adsorption was significantly impacted by the biosorbent dose. In the effect of contact time experiments, it is seen that the adsorption for iron is instantaneous and stays constant while for manganese there is desorption over time.

In the biosorption isotherms, it was found that both isotherm models showed an excellent fit to the experimental data ($R^2>0.9$) with high regression coefficients for both Fe and Mn. In the kinetic modelling, it was observed that the pseudo second order predicted Q_e as 10 mg/g and the experimental Q_e was calculated as 11.3 mg/g for Fe. For Mn the predicted Q_e is 4.9 mg/g while the experimental Q_e was calculated to be 5.3 mg/g. Therefore, for the description of the experimental data, it is preferable to use the pseudo-second order model. These findings imply that Fe and Mn adsorption is primarily physical and occurs in a way that is driven by surface interactions. The good fit to both Langmuir and Freundlich suggests that the adsorbent has heterogenous surface characteristics, with both well-defined and variable adsorption sites. This means that the adsorption process might involve a combination of monolayer adsorption at specific sites and multilayer adsorption on other, more heterogenous sites. In addition, the FTIR analysis revealed that the adsorption of Fe and Mn is non-chemical which indicates that the adsorption is physical adsorption rather than chemical adsorption. The pseudo second-order kinetic model is often associated with chemical adsorption, but it doesn’t always imply that the process is purely chemical as it can also describe physical adsorption particularly when surface interactions dominate the adsorption process. While the Langmuir model can also describe both physical and chemical adsorption.

From the results obtained carbonised orange peel powder was found to be effective in biosorption. The biosorbent was successfully applied on various municipal borehole water, when examining GWP17 it is observed that an initial concentration of 2 mg/l was reduced to 0.5 mg/l for Mn and an initial concentration of 23 mg/l was reduced to 0.03 mg/l for iron. The carbonised orange peel powder (COPP) proved to be successful in the removal of Fe and Mn in batch studies and therefore column studies was also performed utilising COPP which is presented in the following chapter. The raw data for batch studies are presented in Appendix A.

Chapter 6 Biosorbent performance in column studies

6.1 Introduction

Fixed bed column studies were conducted using COP to evaluate the effects of mass (bed height) and flow rate with a prepared model fluid. Subsequently, municipal borehole water was treated in the column system using COP. From the equilibrium data, breakthrough curves were derived to assess and describe the adsorption process performance in the fixed bed column. Four parameters were analysed: the breakpoint time of the adsorbent (tb), fractional bed utilization (FBU), saturation time (ts), and the volume of water treated per gram of adsorbent (Vs) across three masses (bed heights) and three flow rates. To model the biosorption process, three mathematical models were applied: Bohart-Adams, Thomas, and Yoon-Nelson. These models were compared to determine the best fit for treating the borehole water. The results of the column tests are presented for manganese adsorption in this section. The column work for iron did not produce useful data because the design column removed 99-100% of iron in the model water for this study. While this is an ideal situation with respect to the borehole water treatment required the data could not be modelled to predict the breaking at saturation point. Therefore, only the results for manganese, whose concentration was substantially lower than iron, was presented here. See Appendix B for the column experimental data.

6.2 Optimization of parameters

Table 6.1 shows a summary of the performance of the biosorbent which includes the effect of mass and flowrate as well as all the response factors. Highlighted in Table 6.1 is the optimal conditions for maximum biosorbent uptake at saturation for manganese.

Table 6.1 Summary of the performance of manganese adsorption experiments

Parameter	**Experimental conditions**			**Response factors**					
	C_i (mg/l)	**W (g)**	**Q (ml/min)**	**t_b (min)**	**t_s (min)**	**V_s(ml/g)**	**q_b (mg/g)**	**q_s (mg/g)**	**FBU**
0.2 g Mn	11.1	0.2	10	1	4	0.08	0.022	0.089	0.250
0.3 g Mn	11.1	0.3	10	2	10	0.30	0.067	0.333	0.200
1 g Mn	11.1	1	10	6	22	2.20	0.666	2.442	0.273
10 ml/min Mn	11.1	0.3	10	2	22	0.66	0.067	0.733	0.091
15 ml/min Mn	11.1	0.3	15	2	22	0.44	0.100	1.099	0.091
20 ml/min Mn	11.1	0.3	20	2	22	0.33	0.133	1.465	0.091
Borehole water	7.1	0.3	10	2	10	0.30	0.075	0.375	0.200

6.2.1 Effect of flow rate

Figure 6.1 shows the breakthrough curves for varying flow rates. The flow rates were varied from 10, 15 and 20 ml/min and the breakthrough curves showed that the breakpoint time and saturation time is the same for all three flow rates at 2 and 22 minutes, respectively. It can be concluded that the adsorption capacity of the biosorbent is not limited by the flow rate under the conditions tested. This finding aligns with the experimental work done by Ghorbani et al. (2018), on the adsorption of sulfur who agrees that flow rate effects is negligible.

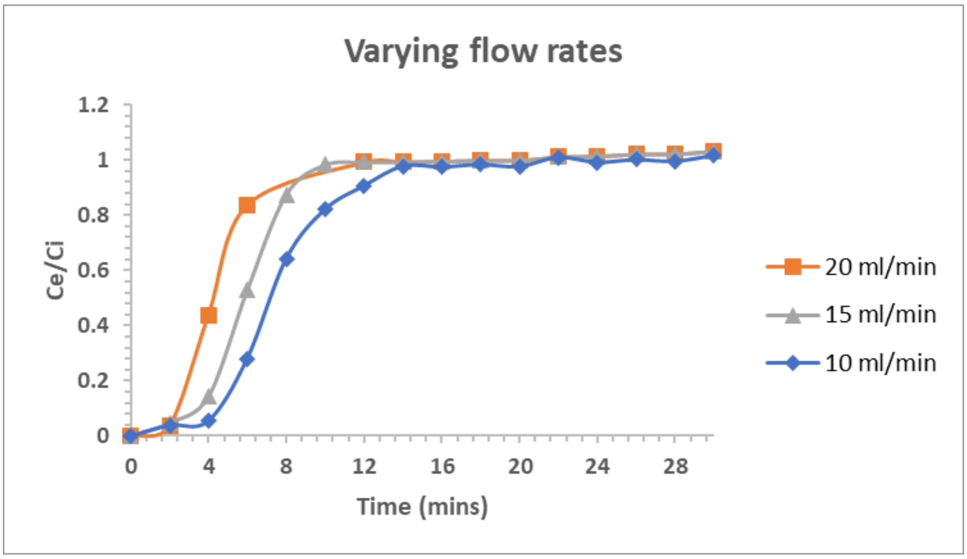

Figure 6.1 Varying flow rates

6.2.2 Effect of mass

Figure 6.2 presents the breakthrough curves for three different biosorbent masses: 0.2 g, 0.3 g, and 1 g, used to evaluate the effect of mass at a pH of 4, a concentration of 10 ppm, and a flow rate of 10 ml/min. The breakthrough curves indicate that both the breakpoint time and saturation time increase with increasing biosorbent mass. For 0.2 g of biosorbent, the breakpoint time and saturation time were 1 and 4 minutes, respectively. For 0.3 g, the breakpoint and saturation times were 2 and 10 minutes, respectively, and for 1 g, they were 6 and 22 minutes, respectively. The shape and gradient of the breakthrough curves varied significantly with mass. It is clear that a greater mass offers more adsorbent for metal binding, allowing for the treatment of a larger volume of liquid and extending the breakthrough time. These results align with the findings of Chowdhury et al. (2012), which observed that higher bed heights (masses) resulted in a higher percentage of adsorption. This can be attributed to an expansion of the mass transfer zone and a larger surface area for adsorption.

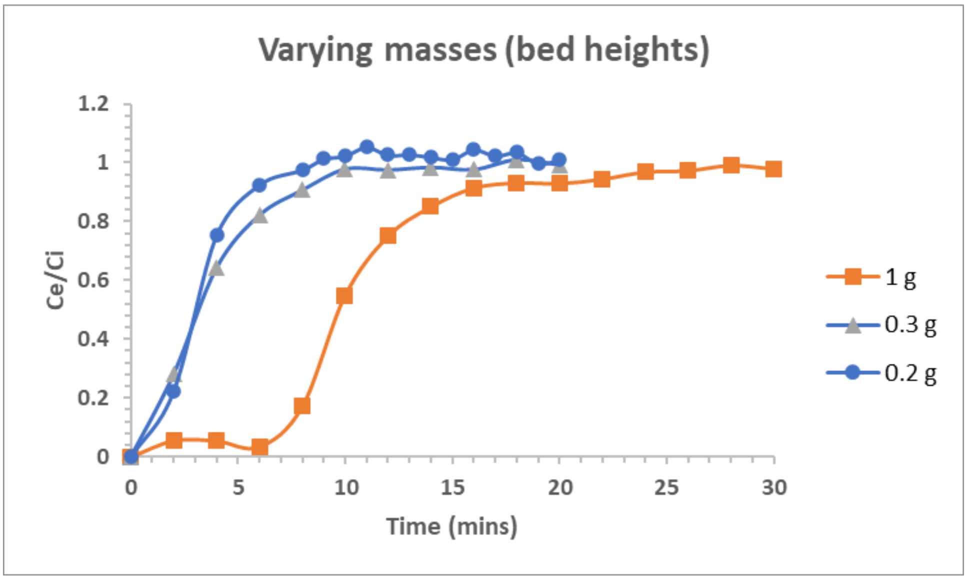

Figure 6.2 Varying masses/bed heights.

6.3 Modelling- Fixed bed models

Fixed bed models were employed to describe the biosorption performance and develop the breakthrough curves. The three mathematical models applied were the Bohart-Adams, Thomas, and Yoon-Nelson models. The linearized data derived from the breakthrough curves are shown in Figure 6.3. This section presents the results of the column tests conducted for manganese adsorption.

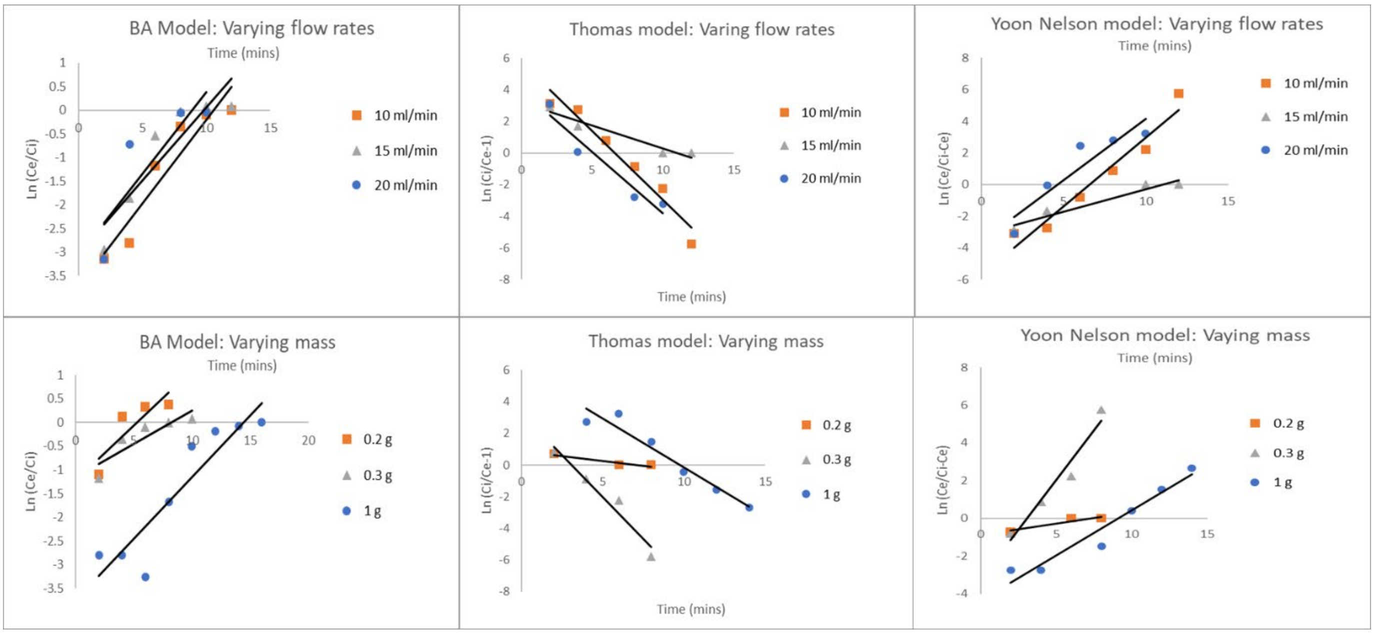

Figure 6.3 Modelling the effect of flow rates and mass for the Bohart-Adams, Thomas, and Yoon-Nelson models.

6.3.1 Modelling of data for effect of mass on column adsorption

Table 6.2 presents a summary of the parameters of the three mathematical models. The highest regression coefficients were observed for the 0.3 g mass, where the regression coefficients were 0.9688 for Thomas and Yoon-Nelson. Although it is observed from Figure 6.3 that all three models fit the data, it can be argued that the Yoon Nelson showed a better fit with regressions of 0.8929, 0.9688 and 0.9482 for the 0.2 g, 0.3 g and 1g respectively.

The Bohart-Adams model coefficient is K_{ba} as presented in Table 6.2. The K_{ba} coefficient for the varying masses of 0.2 g, 0.3 g and 1 g was 0.0210, 0.0128 and 0.0234 respectively and the quantity absorbed, N_0 was 51.23, 12.51 and 5.73 respectively. For the Thomas model coefficient, K_{TH} it was found that for varying masses values of 0.0136,0.0464 and 0.0484 was calculated and the Q_{th} values were 3.9971,1.2656 and 0.1.1662 respectively. The Yoon Nelson model coefficient is K_{YN} and it was found to be 0.1515,0.5151 and 0.4159 for 0.2 g, 0.3 g and 1 g respectively.

6.3.2 Modelling of data for effect of flow rate on column adsorption

The model with the best fitting regression was the Thomas model with regressions of 0.9706, 0.9834 and 0.8751 for the varying flow rates of 10, 15 and 20 ml/min respectively. Overall, the lower flow rates exhibited better regression fit with 0.8946, 0.9706 and 0.9484 for 10 ml/min where it was observed that the Yoon-Nelson and Thomas models fits the low flow rates the best.

The Bohart-Adams model coefficient is K_{BA} as presented in Table 6.2. The K_{BA} coefficient for the varying flow rates of 10, 15 and 20 ml/min was 0.0318, 0.0277 and 0.0311 respectively and the quantity absorbed, N_0 was 31.06, 40.58 and 60.85 respectively. For the Thomas model coefficient, K_{TH} it was found that for varying masses values of 0.0534, 0.0684 and 0.0548 was calculated and the q_{th} values were 2.8830, 3.3625 and 4.4091 respectively. The Yoon Nelson model coefficient is K_{YN} and it was found to be 0.5922, 0.7587 and 0.6082 for 10, 15 and 20 ml/min respectively.

Table 6.2 Summary of the parameters for the Thomas, Bohart-Adams and Yoon Nelson models

Experimental conditions			**Thomas model**			**Bohart-Adams model**			**Yoon Nelson model**			
C_i (mg/L)	**W** (g)	**Q** (ml/min)	**K_{TH}** (ml/mg/min)	**Q_{TH}** (mg/g)	**R^2**	**K_{BA}** (ml/mg/min)	**N_o** (mg/L)	**R^2**	**t_{50}** (min)	**K_{YN}** L/mg	**R^2**	**Exp. Q_s** (mg/g)
11.1	0.2	10	0.013	3.997	0.892	0.021	51.238	0.741	7.202	0.151	0.892	0.178
11.1	0.3	10	0.046	1.265	0.968	0.012	12.512	0.780	3.421	0.515	0.968	0.333
11.1	1	10	0.048	1.166	0.926	0.023	5.732	0.843	10.086	0.415	0.948	2.442
11.1	0.3	10	0.053	2.883	0.970	0.031	31.060	0.894	7.792	0.592	0.948	0.733
11.1	0.3	15	0.068	3.362	0.983	0.027	40.589	0.834	6.059	0.758	0.938	1.099
11.1	0.3	20	0.054	4.409	0.875	0.031	60.850	0.729	5.446	0.608	0.850	1.465
7.1	0.3	10	0.061	1.633	0.957	0.007	8.195	0.889	4.218	0.701	0.892	0.375

6.4 Application of biosorbent to municipal borehole water

A fixed bed study was conducted using 0.3 g of COP on municipal borehole water containing both iron and manganese at 10 ml/min. Figure 6.4 shows the breakthrough curve obtained. The breakpoint and saturation times were 2 mins and 10 mins respectively. The quantity absorbed at breakpoint and saturation point was 0.075 and 0.375 mg/g respectively. Mathematical models developed using the experimental data were applied to borehole water to identify the model that best predicts the fixed-bed data. The models used were the Bohart-Adams, Thomas, and Yoon-Nelson. The borehole water sample had a concentration of 7 ppm, while the model fluid contained a concentration of 11.1 ppm as they closely approximated the borehole water conditions. The results of the models were plotted alongside the borehole water data and are shown in Figure 6.4. Among the models, the Yoon Nelson model provided the best fit to the experimental data for the borehole water. These findings align with the results reported by Fila et al. (2023). The biosorbent demonstrated effective performance on borehole water, achieving removal to 0.05 mg/L from an initial concentration of 91 mg/L for iron while the initial concentration for manganese was reduced from 7 mg/L to 2mg/L. Figure 6.5 (a) and (b) illustrates the borehole water before and after treatment, respectively. Prior to treatment, the borehole water appears orange, likely due to the high iron and manganese concentrations imparting its distinct colour. After treatment, the water becomes clear, indicating the effective removal of impurities.

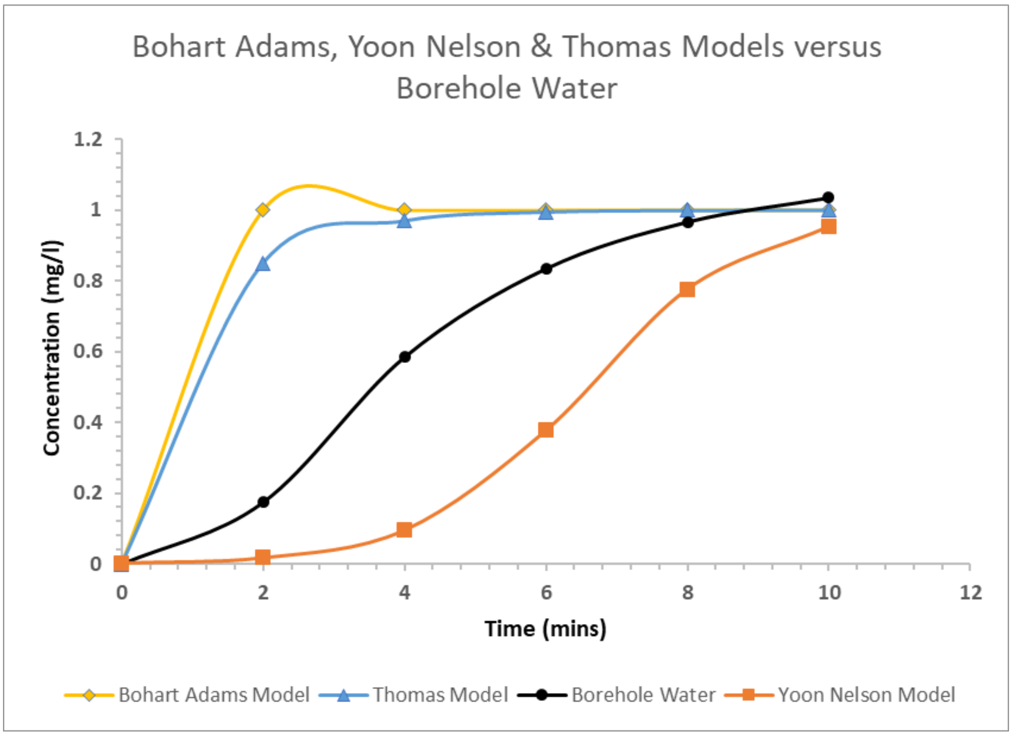

Figure 6.4 Adsorption of Mn from BH

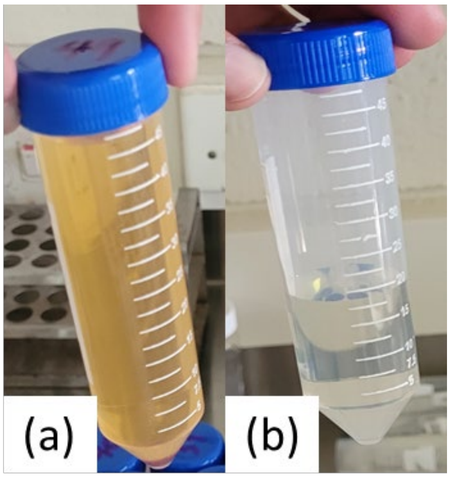

Figure 6.5 Borehole water (a) before treatment (b) after treatment

6.5 Column Model design

For the design of the fixed bed column system the carbonised orange peels was selected as an appropriate adsorbent. Thereafter, batch systems in equilibrium and the development of the isotherms were done as the mathematical modelling has a key role in the scale up procedure. The models were analysed, and experimental data explained. It was concluded that the COP was able to successfully remove iron and manganese.

The next phase involved conducting column studies in the fixed-bed system. Breakthrough plots were presented and analysed, and mathematical models were developed, as these models are crucial for designing adsorption processes in fixed-bed columns. To simulate the dynamic removal of heavy metal ions in the fixed-bed columns, a mathematical analysis of the system was carried out, and S-shaped experimental curves were evaluated. The models used in the analysis include the Bohart-Adams model, Yoon-Nelson model, and Thomas model. A summary of these models is presented in Table 6.3.

Table 6.3 Summary of the mathematical models for effect of mass, flow rate and the borehole water

		Bohart-Adams equation	**R^2_{BA}**	**Thomas equation**	**R^2_{TH}**	**Yoon-Nelson equation**	**R^2_{YN}**
Mass (g)	**0.2**	$y = 0.2326x-1.3352$	0.741	$y = -0.1515x+1.0911$	0.892	$y = 0.1515x-1.0911$	0.892
	0.3	$y = 0.142x-1.2674$	0.780	$y = -0.5151x+1.7619$	0.968	$y = 0.5151x-1.7619$	0.968
	1	$y = 0.2602x-3.8578$	0.843	$y = -0.5375x+5.6472$	0.926	$y = 0.4159x-4.1947$	0.948
Flow rate (ml/min)							
	10	$y = 0.3525x-3.8360$	0.894	$y = -0.5922x+4.6144$	0.970	$y = 0.8708x-5.7266$	0.948
	15	$y = 0.3071x-3.1249$	0.834	$y = -0.7587x+4.5966$	0.983	$y = 0.2874x-3.1578$	0.938
	20	$y = 0.3453x-3.1732$	0.729	$y = -0.6082x+3.6238$	0.875	$y = 0.7749x-3.5968$	0.850
Borehole water		$y = 0.093x-0.8710$	0.889	$y = -0.7631x+2.9915$	0.957	$y = 0.2373x-1.7082$	0.892

6.6 Conclusion

The maximum biosorption achieved in the experiments for manganese (Mn) was 1.465 mg/g with a biosorbent mass of 0.3 g. The column study results showed that the biosorbent's performance is significantly influenced by mass (bed heights). A greater mass offers more adsorbent for metal binding, allowing for the treatment of a larger volume of liquid and extending the breakthrough time. However, it was found that the adsorption capacity of the biosorbent is not limited by the flow rate under the conditions tested. The fixed-bed models (Bohart-Adams, Thomas, and Yoon-Nelson) were compared, and the linearized data and regression analysis revealed that both the Yoon Nelson and Thomas model fits the experimental data. However, the Yoon Nelson model provided the best fit for the adsorption process. The Thomas model had predicted a maximum adsorption of 4.409 mg/g however the actual experimental quantity adsorbed was 1.465 mg/g, the difference could be attributed to the fact that the Thomas model assumes ideal conditions where all adsorbent sites are fully utilised and does not account for the adsorbate-adsorbent interaction complexity or multi-layer adsorption. The biosorbent was successfully applied to treat municipal borehole water, reducing manganese and iron concentrations. Data from the column studies can be found in Appendix B.

The study demonstrated that carbonized orange peels can effectively reduce iron and manganese concentrations, suggesting their potential as a sustainable solution for treating contaminated borehole water. Breakthrough curves were generated to analyse the adsorption efficiency in fixed bed setups, allowing for the development of scaled-up design for municipal applications. The findings support the use of carbonized orange peels as a potentially economically viable biosorbent for treating iron and manganese-laden borehole water, contributing to water reuse strategies in South Africa.

Chapter 7 Conclusions and recommendations

7.1 Introduction

The aim of this work was to investigate the application of carbonised orange peels for the adsorption of iron and manganese from borehole water in batch and column studies. The iron and manganese were successfully removed from model fluid as well as municipal borehole water. This chapter draws on the conclusion of the experimental work and recommendations for future research work.

7.2 Summary of results

Orange peels were carbonised in a tube furnace at 600^{o}C under argon at 10 L/min flow rate for 120 minutes. Thereafter, the biosorbent was characterised using SEM, FTIR and BET, a comparison was done between the raw orange peels and the carbonised orange peels. The efficiency of the carbonised treatment was then evaluated by biosorption experiments.

SEM images of ROP and COP revealed varying degrees of porosity and particle distribution. However, no clear correlation could be established between the SEM images and the treatment protocols applied. EDS analysis confirmed the presence of Fe and Mn on the surfaces of both ROP and COP after biosorption. The EDS findings shows that carbonisation of the raw sample can improve biosorption by nearly 3-fold. There were no significant differences in the FTIR spectrum of ROP and COP before and after application for the sorption of Fe and Mn. This indicates that the adsorption of Mn and Fe ions were non-chemical in nature. FTIR analysis of ROP indicated the presence of functional groups such as carboxylic, alkane, aldehyde, alkene, ketones, and ester. The BET surface areas of both ROP and COP were found to be very low, which is typical for carbonaceous materials. The surface area of the ROP is seen to increase with carbonization, an occurrence which should help increase the adsorption capability of the resultant COP.

The biosorption capacity at equilibrium were 11 mg/g and 5 mg/g for iron and manganese respectively. Iron proved to be a challenge to work with, however, the removal thereof by carbonised orange peels was surprisingly good with constant removal percentages between 98-100% while manganese removal was 70-75%. Iron removal was consistent even in a binary system where there was simultaneous removal of iron and manganese. The iron performed well in both the model fluid and the borehole water adsorption experiments when compared to manganese. It was concluded that carbonised orange peels had a higher capacity for iron removal than manganese which was in agreement with the study by Adekola et. al (2016). In the batch experiments, the influence of operating variables was investigated, and the optimal conditions for biosorbent mass and pH were found to be 0.3 g and pH 4, respectively. The adsorption data were analysed using isotherm models, and the equilibrium data were best described by the Langmuir isotherm model. In the kinetic modelling, it was observed that the pseudo second order predicted Q_e as 10 mg/g and the experimental Q_e was calculated as 11.3 mg/g for Fe. For Mn the predicted Q_e is 4.9 mg/g while the experimental Q_e was calculated to be 5.3 mg/g. Therefore, for the description of the experimental data, it is preferable to use the pseudo-second order model.

Carbonized orange peel (COP) was also used in column studies, and the column biosorption data were subjected to mathematical modelling. Among the models tested, the Yoon-Nelson model provided the best fit for the data. Column studies revealed that the breakpoint and saturation point were directly proportional to the column mass while not limited by the flow rate under the conditions tested. The biosorbent demonstrated effective performance on borehole water, achieving removal to 0.05 mg/L from an initial concentration of 91 mg/L for iron while the initial concentration for manganese was reduced from 7 mg/L to 2mg/L. Although, the removal of both iron and manganese was statically significant, only iron was successfully reduced to below the drinking water standards required by the World Health Organisation in both the single and binary system. Even though manganese concentrations are still above the limit for drinking water, the final concentrations fall within a range that is reported to not include any health effects but causes severe staining which is aesthetically unacceptable.

7.3 Conclusions

In conclusion, it was determined that carbonized orange peel (COP) is an effective biosorbent for the removal of Fe and Mn ions from borehole water. The biosorbent successfully treated municipal borehole water, achieving adsorption capacities of 11 mg/g for iron and 5 mg/g for manganese. The results suggest that orange peel fruit waste, sourced from a local juice shop, can serve as a valuable adsorbent for removing Fe and Mn. Therefore, COP is proposed as a promising, environmentally friendly option for water treatment in municipal application.

7.4 Recommendations for further studies

Although this study successfully achieved its objectives, there are a few limitations to note which needs to be examined in future studies such as desorption, regeneration, scaled-up designs as well as the need for the development of multiple fixed-bed columns operating in series or parallel configurations to address the removal of multiple pollutants simultaneously. Furthermore, a detailed cost analysis should be conducted to ascertain the financial viability of using fruit peel waste as a biosorbent with specific emphasis on scale-up costs to determine the practical and economic viability for real-world applications. There is a substantial body of batch research on the use of biosorbents but the application of a suitable biomass in column studies remains an area of ongoing scientific investigation. The biosorption process requires advanced development and further improvements in the area of column studies and real-world applications.

References

Abdel Maksoud, M.I.A., Elgarahy, A.M., Farrell, C., Al-Muhtaseb, A.H., Rooney, D.W. and Osman, A.I. (2020). Insight on water remediation application using magnetic nanomaterials and biosorbents. Coordination Chemistry Reviews, [online] 403, p.213096.

Abdul Rashid, Z., 2009. Removal of Heavy Metals in Aqueous Solution Using Banana and Orange Peels.

Adebayo, G.B., Mohammed, A.A. and Sokoya, S.O., 2016. Biosorption of Fe (II) and Cd (II) ions from aqueous solution using a low-cost adsorbent from orange peels. *Journal of Applied Sciences and Environmental Management*, *20*(3), pp.702-714.

Adekola, F.A., Hodonou, D.S.S. and Adegoke, H.I. (2014). Thermodynamic and kinetic studies of biosorption of iron and manganese from aqueous medium using rice husk ash. Applied Water Science, 6(4), pp.319–330.

Ahmad, A., Khatoon, A., Mohd-Setapar, S.-H., Kumar, R. and Rafatullah, Mohd. (2015). Chemically oxidized pineapple fruit peel for the biosorption of heavy metals from aqueous solutions. Desalination and Water Treatment, 57(14), pp.6432–6442.

Bakari, S. (2017). Why is South Africa Still a Developing Country? [online] mpra.ub.uni-muenchen.de. Available at: https://mpra.ub.uni-muenchen.de/80763/.

Basson, L., Bronkhorst, S., Fordyce, N. and Pengelly, C. (n.d.). Water - 2018 Market Intelligence Report - 18 Roeland Street, Cape Town, 8001, South Africa Editorial and review. [online] Available at: https://greencape.co.za/wp-content/uploads/2022/10/GreenCape-Water-MIR-FINAL-20180405-3.pdf [Accessed 6 Oct. 2022].

Braune, E., Adams, S. Cobbing, J.E., Fourie, F. and Riemann, K., 2015. Critical reflections on 20 years of groundwater research, development and implementation in South Africa. *South African Journal of Geology*, *118*(1), pp.5-16.

City of Cape Town (2018). WATER SERVICES AND THE CAPE TOWN URBAN WATER CYCLE. [online] Available:https://resource.capetown.gov.za/documentcentre/Documents/Graphics%20and%20educational%20material/Water%20Services%20and%20Urban%20Water%20Cycle.pdf.

Chowdhury, Z. Z., Zain, S. M., Rashid, A. K., Rafique, R. F., Khalid, K., Breakthrough Curve Analysis for Column Dynamics Sorption of Mn(II) Ions from Wastewater by Using *Mangostana garcinia* Peel-Based Granular-Activated Carbon, *Journal of Chemistry*, 2012, 959761, 8 pages, 2013.

Constantin Muhire and Jay Rwaka Itete (2021). Adsorptive Removal of Manganese from Water Intended for Consumption by Use of Cost-effective Gisenyi Volcanic Rocks. Research Square (Research Square).

Elsherif, K.M., Ewlad-Ahmed, A.M.S. and Treban, A.A.S., 2017. Biosorption studies of Fe (III), Cu (II), and Co (II) from aqueous solutions by olive leaves powder. *Applied Journal of Environmental Engineering Science*, *3*(4), pp.J-Envir.

Emenike, P.C.; Omole, D.O.; Ngene, B.U.; Tenebe, I.T., (2016). Potentiality of agricultural adsorbent for the sequestering of metal ions from wastewater. Global J. Environ. Sci. Manage.

García-Mendieta, A., Olguín, M.T. and Solache-Ríos, M. (2012). Biosorption properties of green tomato husk (Physalis philadelphica Lam) for iron, manganese and iron–manganese from aqueous systems. Desalination, 284, pp.167–174.

García-Mendieta, A., Olguín, M.T. and Solache-Ríos, M. (2012). Biosorption properties of green tomato husk (Physalis philadelphica Lam) for iron, manganese and iron–manganese from aqueous systems. Desalination, 284, pp.167–174.

Joomag. (n.d.). Water, Sewage & Effluent January February 2019. [online] Available at: https://viewer.joomag.com/water-sewage-effluent-january-february 2019/0957439001548740878?short& [Accessed 6 Oct. 2022].

Joseph, L., Jun, B.-M., Flora, J.R.V., Park, C.M. and Yoon, Y. (2019). Removal of heavy metals from water sources in the developing world using low-cost materials: A review. Chemosphere, [online] 229, pp.142–159.

Jun, B.-M., Kim, S., Heo, J., Park, C.M., Her, N., Jang, M., Huang, Y., Han, J. and Yoon, Y. (2018). Review of MXenes as new nanomaterials for energy storage/delivery and selected environmental applications. Nano Research, 12(3), pp.471–487.

Khan, N., le Roes-Hill, M., Welz, P., Grandin, K., Kudanga, T., van Dyk, S., Ohlhoff, C., van Zyl, W.H. (Emile) and Pletschke, B. (2015). Fruit waste streams in South Africa and their potential role in developing a bio-economy. South African Journal of Science, 111(5/6).

Khatri, N., Tyagi, S. and Rawtani, D. (2017). Recent strategies for the removal of iron from water: A review. Journal of Water Process Engineering, [online] 19, pp.291–304.

Lim, A.P. and Aris, A.Z. (2013). A review on economically adsorbents on heavy metals removal in water and wastewater. Reviews in Environmental Science and Bio/Technology, 13(2), pp.163–181. Local Municipality, South Africa. Unpublished thesis.

Mahato, N., Agarwal, P., Mohapatra, D., Sinha, M., Dhyani, A., Pathak, B., Tripathi, M.K. and Angaiah, S. (2021). Biotransformation of Citrus Waste-II: Biosorbent Materials for Removal of Dyes, Heavy Metals and Toxic Chemicals from Polluted Water. Processes, 9(9), p.1544.

Mahato, N., Sharma, K., Sinha, M., Baral, E.R., Koteswararao, R., Dhyani, A., Hwan Cho, M. and Cho, S. (2020). Biosorbents, industrially important chemicals and novel materials from citrus processing waste as a sustainable and renewable bioresource: A review. Journal of Advanced Research, 23, pp.61–82.

Mamun, K.R. and Chakrabarty, S., 2019. A Comparative Study of the Adsorption Capacity of Tea Leaves and Orange Peel for the Removal of Fe (III) Ion from Wastewater. *Journal of Chemical Health Risks*, *9*(2).

Mnisi, R. 2011. An Assessment of the Water and Sanitation Problems in New Forest, Bushbuckridge.

Mutula, J. (n.d.). University of Nairobi Department of civil and construction engineering iron removal from borehole water: A case study of Kiambu Town [online]. Available at: https://civil.uonbi.ac.ke/sites/default/files/cae/engineering/civil/JOSEPH%20MUTULA%20JOSEPH_1.pdf [Accessed 6 Oct. 2022].

Nandeshwar, S.N., Mahakalakar, A.S., Gupta, R.R. and Kyzas, G.Z. (2016). Green activated carbons from different waste materials for the removal of iron from real wastewater samples of Nag River, India. Journal of Molecular Liquids, 216, pp.688–692.

Nandeshwar, S.N., Mahakalakar, A.S., Gupta, R.R. and Kyzas, G.Z. (2016). Green activated carbons from different waste materials for the removal of iron from real wastewater samples of Nag River, India. Journal of Molecular Liquids, 216, pp.688–692.

Ntshoko, Z. (n.d.). Low-cost pineapple peel biosorbent for the removal of aqueous cobalt from textile wastewater effluent. Thesis [Accessed 6 Oct. 2021].

O'Hehir, M. (2009). Chemical-free Iron Removal and Disinfection Unit of Drinking Water for Single House Application.

Pascu, D.-E., Pascu(Neagu), M., Traistaru, G.A., Nechifor, A.C. and Miron, A.R. (2015). Iron and manganese removal from drinking water. Journal of Electrochemical Science and Engineering.

Pathak, P.D., Mandavgane, S.A. and Kulkarni, B.D. (2015). Fruit peel waste as a novel low-cost bio adsorbent. Reviews in Chemical Engineering, 31(4).

Pathak, P.D., Mandavgane, S.A. and Kulkarni, B.D. (2017). Fruit Peel Waste:Characterization and its Potential Uses. Current Science, [online] 113(03), p.444.

Pholosi, A., Naidoo, E.B. and Ofomaja, A.E., 2020. Batch and continuous flow studies of Cr (VI) adsorption from synthetic and real wastewater by magnetic pine cone composite. *Chemical Engineering Research and Design*, *153*, pp.806-818.

Ramachandra, T V & N, Ahalya & RD, Kanamadi. (2005). Biosorption: Techniques and Mechanisms. CES Technical Report 110.

Rodríguez-Galán, M., Baena-Moreno, F.M., Vázquez, S., Arroyo-Torralvo, F., Vilches, L.F. and Zhang, Z. (2019). Remediation of acid mine drainage. Environmental Chemistry Letters, 17(4), pp.1529–1538.

Rudi, N.N., Muhamad, M.S., Te Chuan, L., Alipal, J., Omar, S., Hamidon, N., Abdul Hamid, N.H., Mohamed Sunar, N., Ali, R. and Harun, H. (2020). Evolution of adsorption process for manganese removal in water via agricultural waste adsorbents. Heliyon, 6(9), p.e05049.

Schwarzenbach, R.P., Egli, T., Hofstetter, T.B., von Gunten, U. and Wehrli, B. (2010). Global Water Pollution and Human Health. Annual Review of Environment and Resources, [online] 35(1), pp.109–136.

South African Department of Water Affairs and Forestry and CSIR (South Africa). Environmental Services (1996). South African water quality guidelines. Volume 1, Domestic use. Editorial: Pretoria: The Department.

Surovka, D. and Pertile, E., 2017. Sorption of Iron, Manganese, and Copper from Aqueous Solution Using Orange Peel: Optimization, Isothermic, Kinetic, and Thermodynamic Studies. *Polish Journal of Environmental Studies*, *26*(2).

Thirunavukkarasu, A., Nithya, R. and Sivashankar, R. (2021). Continuous fixed-bed biosorption process: A review. Chemical Engineering Journal Advances, 8, p.100188.

Tobiason, J.E., Bazilio, A., Goodwill, J., Mai, X. and Nguyen, C. (2016). Manganese Removal from Drinking Water Sources. Current Pollution Reports, 2(3), pp.168–177.

Water: Facts and Futures Rethinking South Africa’s Water Future. (2016). Available at: https://wwfafrica.awsassets.panda.org/downloads/wwf009_waterfactsandfutures_report_web__lowres_.pdf [Accessed 6 Oct. 2022].

Appendices

Appendix A. Data for Batch studies

Table A 1: Data for effect of mass on biosorption of Fe and Mn

Solution Description	Volume (L)	Ci (mg/L)	Ce (mg/l)	Ci -Ce	Qe (mg/g)	Mass (g)	Percentage absorbed (%)	Ce/Qe	Log Ce	Log Qe
100 ppm Fe model fluid (0.05 g)	0.03	96.553	0.002	96.551	57.930	0.050	99.998	0.000	-2.710	1.763
100 ppm Fe model fluid (0.1 g)	0.03	96.553	0.002	96.550	28.965	0.100	99.998	0.000	-2.623	1.462
100 ppm Fe model fluid (0.2 g)	0.03	96.553	0.004	96.549	14.482	0.200	99.996	0.000	-2.413	1.161
100 ppm Fe model fluid(0.3 g)	0.03	113.393	0.061	113.331	11.333	0.300	99.946	0.005	-1.211	1.054
100 ppm Fe model fluid (0.5 g)	0.03	113.393	0.060	113.333	6.800	0.500	99.947	0.009	-1.221	0.833
100 ppm Fe model fluid (1 g)	0.03	113.393	0.057	113.335	3.400	1.000	99.949	0.017	-1.241	0.531
100 ppm Mn model fluid (0.05 g)	0.03	61.319	11.417	49.903	29.942	0.050	81.382	0.381	1.058	1.476
100 ppm Mn model fluid (0.1 g)	0.03	61.319	53.577	7.742	2.323	0.100	12.626	23.066	1.729	0.366
100 ppm Mn model fluid (0.2 g)	0.03	61.319	42.647	18.672	2.801	0.200	30.450	15.227	1.630	0.447
100 ppm Mn model fluid (0.3 g)	0.03	61.319	33.831	27.489	2.749	0.300	44.829	12.307	1.529	0.439
100 ppm Mn model fluid (0.5 g)	0.03	61.319	7.153	54.167	3.250	0.500	88.335	2.201	0.854	0.512
100 ppm Mn model fluid (1 g)	0.03	61.319	4.093	57.227	1.717	1.000	93.325	2.384	0.612	0.235
Borehole water - Fe (0.2 g)	0.03	42.800	0.366	42.434	6.365	0.200	99.144	0.058	-0.436	0.804
Borehole water - Fe (0.1 g)	0.03	42.800	0.492	42.308	12.692	0.100	98.850	0.039	-0.308	1.104
Borehole water - Fe (0.05 g)	0.03	42.800	0.135	42.665	25.599	0.050	99.686	0.005	-0.871	1.408
Borehole water - Mn (0.2 g)	0.03	7.500	6.300	1.200	0.180	0.200	16.000	35.000	0.799	-0.745
Borehole water - Mn (0.1 g)	0.03	10.300	6.300	4.000	1.200	0.100	38.835	5.250	0.799	0.079
Borehole water - Mn (0.05 g)	0.03	11.400	6.300	5.100	3.060	0.050	44.737	2.059	0.799	0.486

Table A 2: Data for effect of contact time on biosorption of Fe and Mn

Solution Description	Time (mins)	Volume (L)	Ci (mg/L)	Ce (mg/l)	Ci -Ce	Qe (mg/g)	Mass (g)	Percentage absorbed (%)	Ce/Qe	Log Ce	Log Qe
100 ppm Fe model fluid (1 min)	1	0.03	100	0.557	99.443	9.944	0.300	99.443	0.056	-0.254	0.998
100 ppm Fe model fluid (3 mins)	3	0.03	100	0.517	99.483	9.948	0.300	99.483	0.052	-0.287	0.998
100 ppm Fe model fluid (5 mins)	5	0.03	100	0.499	99.501	9.950	0.300	99.501	0.050	-0.302	0.998
100 ppm Fe model fluid (10 mins)	10	0.03	100	0.428	99.572	9.957	0.300	99.572	0.043	-0.369	0.998
100 ppm Fe model fluid (15 mins)	15	0.03	100	0.410	99.590	9.959	0.300	99.590	0.041	-0.387	0.998
100 ppm Fe model fluid (20 mins)	20	0.03	100	0.412	99.588	9.959	0.300	99.588	0.041	-0.385	0.998
100 ppm Fe model fluid (30 mins)	30	0.03	100	0.402	99.598	9.960	0.300	99.598	0.040	-0.396	0.998
100 ppm Fe model fluid (45 mins)	45	0.03	100	0.215	99.785	9.978	0.300	99.785	0.022	-0.667	0.999
100 ppm Fe model fluid (60 mins)	60	0.03	100	0.061	99.939	9.994	0.300	99.939	0.006	-1.211	1.000
100 ppm Fe model fluid (90 mins)	90	0.03	100	0.051	99.949	9.995	0.300	99.949	0.005	-1.292	1.000
100 ppm Mn model fluid (1 mins)	1	0.03	61	0.573	60.427	6.043	0.300	99.061	0.095	-0.242	0.781
100 ppm Mn model fluid (3 mins)	3	0.03	61	0.402	60.598	6.060	0.300	99.341	0.066	-0.396	0.782
100 ppm Mn model fluid (5 mins)	5	0.03	61	0.382	60.618	6.062	0.300	99.374	0.063	-0.418	0.783
100 ppm Mn model fluid (10 mins)	10	0.03	61	6.034	54.966	5.497	0.300	90.108	1.098	0.781	0.740
100 ppm Mn model fluid (15 mins)	15	0.03	61	9.357	51.643	5.164	0.300	84.661	1.812	0.971	0.713
100 ppm Mn model fluid (20 mins)	20	0.03	61	10.230	50.770	5.077	0.300	83.230	2.015	1.010	0.706
100 ppm Mn model fluid (30 mins)	30	0.03	61	10.780	50.220	5.022	0.300	82.328	2.147	1.033	0.701
100 ppm Mn model fluid (45 mins)	45	0.03	61	11.360	49.640	4.964	0.300	81.377	2.289	1.055	0.696
100 ppm Mn model fluid (60 mins)	60	0.03	61	11.474	49.526	4.953	0.300	81.190	2.317	1.060	0.695
100 ppm Mn model fluid (90 mins)	90	0.03	61	11.481	49.519	4.952	0.300	81.179	2.319	1.060	0.695
Borehole water - Fe (1 min)	1	0.03	100	0.016	99.984	9.998	0.300	99.984	0.002	-1.796	1.000
Borehole water - Fe (3 mins)	3	0.03	100	0.879	99.121	9.912	0.300	99.121	0.089	-0.056	0.996
Borehole water - Fe (5 mins)	5	0.03	100	0.820	99.180	9.918	0.300	99.180	0.083	-0.086	0.996
Borehole water - Fe (10 mins)	10	0.03	100	0.569	99.431	9.943	0.300	99.431	0.057	-0.245	0.998
Borehole water - Fe (15 mins)	15	0.03	100	0.572	99.428	9.943	0.300	99.428	0.058	-0.243	0.998
Borehole water - Fe (20 mins)	20	0.03	100	2.570	97.430	9.743	0.300	97.430	0.264	0.410	0.989
Borehole water - Fe (30 mins)	30	0.03	100	2.036	97.964	9.796	0.300	97.964	0.208	0.309	0.991
Borehole water - Fe (45 mins)	45	0.03	100	1.719	98.281	9.828	0.300	98.281	0.175	0.235	0.992
Borehole water - Fe (60 mis)	60	0.03	100	1.990	98.010	9.801	0.300	98.010	0.203	0.299	0.991
Borehole water - Fe (90 mins)	90	0.03	100	1.048	98.952	9.895	0.300	98.952	0.106	0.020	0.995
Borehole water - Mn (1 min)	1	0.03	100	2.096	97.904	9.790	0.300	97.904	0.214	0.321	0.991
Borehole water - Mn (3 mins)	3	0.03	100	7.015	92.985	9.299	0.300	92.985	0.754	0.846	0.968
Borehole water - Mn (5 mins)	5	0.03	100	10.156	89.844	8.984	0.300	89.844	1.130	1.007	0.953
Borehole water - Mn (10 mins)	10	0.03	100	12.415	87.585	8.759	0.300	87.585	1.417	1.094	0.942
Borehole water - Mn (15 mins)	15	0.03	100	10.694	89.306	8.931	0.300	89.306	1.197	1.029	0.951
Borehole water - Mn (20 mins)	20	0.03	100	11.472	88.528	8.853	0.300	88.528	1.296	1.060	0.947
Borehole water - Mn (30 mins)	30	0.03	100	11.393	88.607	8.861	0.300	88.607	1.286	1.057	0.947
Borehole water - Mn (45 mins)	45	0.03	100	10.224	89.776	8.978	0.300	89.776	1.139	1.010	0.953
Borehole water - Mn (60 mis)	60	0.03	100	11.741	88.259	8.826	0.300	88.259	1.330	1.070	0.946
Borehole water - Mn (90 mins)	90	0.03	100	7.352	92.648	9.265	0.300	92.648	0.794	0.866	0.967

Table A 3: Data for effect of concentration on biosorption of Fe and Mn

Solution Description	Volume (L)	Ci (mg/L)	Ce	Ci -Ce	Qe	Mass (g)	% absorbed	Ce/Qe	Log Ce	Log Qe
100 ppm Fe model fluid	0.03	113.3927	0.0313	113.3614	11.3361	0.3	99.9724	0.0028	-1.5043	1.0545
50 ppm Fe model fluid	0.03	54.5869	0.0637	54.5232	5.4523	0.3	99.8833	0.0117	-1.1959	0.7366
40 ppm Fe model fluid	0.03	41.6758	0.0615	41.6143	4.1614	0.3	99.8525	0.0148	-1.2113	0.6192
30 ppm Fe model fluid	0.03	30.1850	0.0633	30.1217	3.0122	0.3	99.7904	0.0210	-1.1989	0.4789
20 ppm Fe model fluid	0.03	19.6859	0.0490	19.6368	1.9637	0.3	99.7509	0.0250	-1.3095	0.2931
10 ppm Fe model fluid	0.03	9.1122	0.0973	9.0150	0.9015	0.3	98.9324	0.1079	-1.0120	-0.0450
5 ppm Fe model fluid	0.03	4.0851	0.9727	3.1124	0.3112	0.3	76.1889	3.1253	-0.0120	-0.5069
100 ppm Mn model fluid	0.03	86.8287	33.8308	52.9979	5.2998	0.3	61.0373	6.3834	1.5293	0.7243
50 ppm Mn model fluid	0.03	47.7074	3.6475	44.0598	4.4060	0.3	92.3544	0.8279	0.5620	0.6440
40 ppm Mn model fluid	0.03	39.6750	0.8133	38.8616	3.8862	0.3	97.9500	0.2093	-0.0897	0.5895
30 ppm Mn model fluid	0.03	29.6362	0.9623	28.6740	2.8674	0.3	96.7531	0.3356	-0.0167	0.4575
20 ppm Mn model fluid	0.03	20.2422	0.7099	19.5323	1.9532	0.3	96.4928	0.3635	-0.1488	0.2908
10 ppm Mn model fluid	0.03	9.9001	5.9424	3.9577	0.3958	0.3	39.9762	15.0149	0.7740	-0.4026
5 ppm Mn model fluid	0.03	4.7468	1.1593	3.5875	0.3587	0.3	75.5765	3.2316	0.0642	-0.4452
GWP-02 - Fe	0.03	42.8254	0.0566	42.7688	4.2769	0.3	99.8679	0.0132	-1.2475	0.6311
GWP-12 - Fe	0.03	47.2175	0.0534	47.1641	4.7164	0.3	99.8869	0.0113	-1.2724	0.6736
GWP-16 - Fe	0.03	91.0040	0.0596	90.9445	9.0944	0.3	99.9345	0.0066	-1.2249	0.9588
GWP-17 - Fe	0.03	23.7670	0.0358	23.7312	2.3731	0.3	99.8495	0.0151	-1.4464	0.3753
GWE-06 - Fe	0.03	18.0715	0.0615	18.0100	1.8010	0.3	99.6599	0.0341	-1.2114	0.2555
GWP-02 - Mn	0.03	5.0529	2.5955	2.4573	0.2457	0.3	48.6323	10.5625	0.4142	-0.6095
GWP-12 - Mn	0.03	6.2787	3.2989	2.9798	0.2980	0.3	47.4587	11.0710	0.5184	-0.5258
GWP-16 - Mn	0.03	5.3587	2.7828	2.5759	0.2576	0.3	48.0700	10.8030	0.4445	-0.5891
GWP-17 - Mn	0.03	2.2258	0.5566	1.6692	0.1669	0.3	74.9939	3.3344	-0.2545	-0.7775
GWE-06 - Mn	0.03	3.2759	0.9463	2.3296	0.2330	0.3	71.1138	4.0620	-0.0240	-0.6327
200 ppm Fe model fluid	Precipitates present in solution									
300 ppm Fe model fluid	Precipitates present in solution									
500 ppm Fe model fluid	Precipitates present in solution									
700 ppm Fe model fluid	Precipitates present in solution									
1000 ppm Fe model fluid	Precipitates present in solution									

Table A 4: Data for effect of pH on biosorption of Fe

Solution Description	pH	Volume (L)	Ci (mg/L)	Ce (mg/L)	Ci -Ce	Qe (mg/g)	Mass (g)	% absorbed	Ce/Qe	Log Ce	Log Qe
10 ppm Fe model fluid	4	0.03	9.1122	0.0973	9.0150	0.9015	0.3	98.9324	0.1079	-1.0120	-0.0450
30 ppm Fe model fluid	4	0.03	30.1850	0.0633	30.1217	3.0122	0.3	99.7904	0.0210	-1.1989	0.4789
50 ppm Fe model fluid	4	0.03	54.5869	0.0637	54.5232	5.4523	0.3	99.8833	0.0117	-1.1959	0.7366
100 ppm Fe model fluid	4	0.03	113.3927	0.0313	113.3614	11.3361	0.3	99.9724	0.0028	-1.5043	1.0545
10 ppm Fe model fluid	2.5	0.03	6.8453	0.1289	6.7164	0.6716	0.3	98.1164	0.1920	-0.8896	-0.1729
30 ppm Fe model fluid	2.5	0.03	30.8514	0.2865	30.5649	3.0565	0.3	99.0715	0.0937	-0.5429	0.4852
50 ppm Fe model fluid	2.5	0.03	57.1419	0.0570	57.0849	5.7085	0.3	99.9002	0.0100	-1.2441	0.7565
100 ppm Fe model fluid	2.5	0.03	96.5527	0.0070	96.5457	9.6546	0.3	99.9928	0.0007	-2.1551	0.9847

Appendix B. Data for Column studies

Table B 1: Data for effect of mass on column biosorption for Mn – mass 0.2 g

Time (mins)	Volume (L)	Mass (g)	Ci (mg/L)	Ce (mg/L)	Ci-Ce	Qe (mg/g)	Ce/Qe	Log Ce	Log Qe	% Adsorbed	Ce/Ci
1	0.015	0.2	15	3.32684	11.6732	0.875	3.800	0.522	-0.058	1.751	0.222
2	0.015	0.2	15	11.2808	3.7192	0.279	40.442	1.052	-0.554	0.558	0.752
3	0.015	0.2	15	13.8801	1.1199	0.084	165.254	1.142	-1.076	0.168	0.925
4	0.015	0.2	15	14.6384	0.3616	0.027	539.764	1.165	-1.567	0.054	0.976
5	0.015	0.2	15	14.7709	0.2291	0.017	859.648	1.169	-1.765	0.034	0.985
6	0.015	0.2	15	15.2136	-0.2136	-0.016	-949.663	1.182	#NUM!	-0.032	1.014
7	0.015	0.2	15	15.4595	-0.4595	-0.034	-448.589	1.189	#NUM!	-0.069	1.031
8	0.015	0.2	15	15.4787	-0.4787	-0.036	-431.132	1.190	#NUM!	-0.072	1.032
9	0.015	0.2	15	15.1973	-0.1973	-0.015	-1027.018	1.182	#NUM!	-0.030	1.013
10	0.015	0.2	15	15.3534	-0.3534	-0.027	-579.264	1.186	#NUM!	-0.053	1.024
11	0.015	0.2	15	15.8054	-0.8054	-0.060	-261.657	1.199	#NUM!	-0.121	1.054
12	0.015	0.2	15	15.3925	-0.3925	-0.029	-522.887	1.187	#NUM!	-0.059	1.026
13	0.015	0.2	15	15.4279	-0.4279	-0.032	-480.732	1.188	#NUM!	-0.064	1.029
14	0.015	0.2	15	15.2899	-0.2899	-0.022	-703.226	1.184	#NUM!	-0.043	1.019
15	0.015	0.2	15	15.1748	-0.1748	-0.013	-1157.498	1.181	#NUM!	-0.026	1.012
16	0.015	0.2	15	15.6787	-0.6787	-0.051	-308.014	1.195	#NUM!	-0.102	1.045
17	0.015	0.2	15	15.3492	-0.3492	-0.026	-586.071	1.186	#NUM!	-0.052	1.023
18	0.015	0.2	15	15.5244	-0.5244	-0.039	-394.722	1.191	#NUM!	-0.079	1.035
19	0.015	0.2	15	14.9633	0.0367	0.003	5436.258	1.175	-2.560	0.006	0.998
20	0.015	0.2	15	15.1511	-0.1511	-0.011	-1336.960	1.180	#NUM!	-0.023	1.010
21	0.015	0.2	15	15.2400	-0.2400	-0.018	-846.667	1.183	#NUM!	-0.036	1.016
22	0.015	0.2	15	15.4381	-0.4381	-0.033	-469.850	1.189	#NUM!	-0.066	1.029
23	0.015	0.2	15	15.2771	-0.2771	-0.021	-735.094	1.184	#NUM!	-0.042	1.018
24	0.015	0.2	15	14.9567	0.0433	0.003	4605.604	1.175	-2.488	0.006	0.997
25	0.015	0.2	15	14.9725	0.0275	0.002	7259.394	1.175	-2.686	0.004	0.998
26	0.015	0.2	15	14.9725	0.0275	0.002	7259.394	1.175	-2.686	0.004	0.998
27	0.015	0.2	15	14.9725	0.0275	0.002	7259.394	1.175	-2.686	0.004	0.998
28	0.015	0.2	15	14.9725	0.0275	0.002	7259.394	1.175	-2.686	0.004	0.998
29	0.015	0.2	15	14.9725	0.0275	0.002	7259.394	1.175	-2.686	0.004	0.998
30	0.015	0.2	15	14.9725	0.0275	0.002	7259.394	1.175	-2.686	0.004	0.998
31	0.015	0.2	15	14.9725	0.0275	0.002	7259.394	1.175	-2.686	0.004	0.998
32	0.015	0.2	15	14.9725	0.0275	0.002	7259.394	1.175	-2.686	0.004	0.998
33	0.015	0.2	15	14.9725	0.0275	0.002	7259.394	1.175	-2.686	0.004	0.998
34	0.015	0.2	15	14.9725	0.0275	0.002	7259.394	1.175	-2.686	0.004	0.998
35	0.015	0.2	15	14.9725	0.0275	0.002	7259.394	1.175	-2.686	0.004	0.998
36	0.015	0.2	15	14.9725	0.0275	0.002	7259.394	1.175	-2.686	0.004	0.998
37	0.015	0.2	15	14.9725	0.0275	0.002	7259.394	1.175	-2.686	0.004	0.998
38	0.015	0.2	15	14.9725	0.0275	0.002	7259.394	1.175	-2.686	0.004	0.998
39	0.015	0.2	15	14.9725	0.0275	0.002	7259.394	1.175	-2.686	0.004	0.998
40	0.015	0.2	15	14.9725	0.0275	0.002	7259.394	1.175	-2.686	0.004	0.998

Table B 2: Data for effect of mass on column biosorption for Mn – mass 0.3 g

Time (mins)	Volume (L)	Mass (g)	Ci (mg/L)	Ce (mg/L)	Ci-Ce	Qe (mg/g)	Ce/Qe	Log Ce	Log Qe	Ce/Ci	% Adsorbed
2	0.015	0.3	11.1	3.08871	8.01129	0.4006	7.7109	0.4898	-0.3973	0.2783	72.1738
4	0.015	0.3	11.1	7.06091	4.03909	0.2020	34.9629	0.8489	-0.6947	0.6361	36.3882
6	0.015	0.3	11.1	9.02979	2.07021	0.1035	87.2355	0.9557	-0.9850	0.8135	18.6505
8	0.015	0.3	11.1	9.96871	1.13129	0.0566	176.2362	0.9986	-1.2475	0.8981	10.1918
10	0.015	0.3	11.1	10.7542	0.3458	0.0173	621.9896	1.0316	-1.7622	0.9688	3.1153
12	0.015	0.3	11.1	10.7213	0.3787	0.0189	566.2160	1.0302	-1.7227	0.9659	3.4117
14	0.015	0.3	11.1	10.8187	0.2813	0.0141	769.1930	1.0342	-1.8519	0.9747	2.5342
16	0.015	0.3	11.1	10.7352	0.3648	0.0182	588.5526	1.0308	-1.7390	0.9671	3.2865
18	0.015	0.3	11.1	11.105	-0.005	-0.0003	-44420.0000	1.0455	#NUM!	1.0005	-0.0450
20	0.015	0.3	11.1	10.9076	0.1924	0.0096	1133.8462	1.0377	-2.0168	0.9827	1.7333
22	0.015	0.3	11.1	11.0107	0.0893	0.0045	2466.0022	1.0418	-2.3502	0.9920	0.8045
24	0.015	0.3	11.1	10.9467	0.1533	0.0077	1428.1409	1.0393	-2.1155	0.9862	1.3811
26	0.015	0.3	11.1	11.1848	-0.0848	-0.0042	-2637.9245	1.0486	#NUM!	1.0076	-0.7640
28	0.015	0.3	11.1	11.0537	0.0463	0.0023	4774.8164	1.0435	-2.6354	0.9958	0.4171
30	0.015	0.3	11.1	11.1133	-0.0133	-0.0007	-16711.7293	1.0458	#NUM!	1.0012	-0.1198
32	0.015	0.3	11.1	11.0732	0.0268	0.0013	8263.5821	1.0443	-2.8729	0.9976	0.2414
34	0.015	0.3	11.1	10.9802	0.1198	0.0060	1833.0885	1.0406	-2.2226	0.9892	1.0793
36	0.015	0.3	11.1	10.8594	0.2406	0.0120	902.6933	1.0358	-1.9197	0.9783	2.1676
38	0.015	0.3	11.1	11.0073	0.0927	0.0046	2374.8220	1.0417	-2.3340	0.9916	0.8351
40	0.015	0.3	11.1	10.9857	0.1143	0.0057	1922.2572	1.0408	-2.2430	0.9897	1.0297
42	0.015	0.3	11.1	10.6874	0.4126	0.0206	518.0514	1.0289	-1.6855	0.9628	3.7171
44	0.015	0.3	11.1	10.7512	0.3488	0.0174	616.4679	1.0315	-1.7585	0.9686	3.1423
46	0.015	0.3	11.1	10.9547	0.1453	0.0073	1507.8734	1.0396	-2.1388	0.9869	1.3090
48	0.015	0.3	11.1	10.9661	0.1339	0.0067	1637.9537	1.0401	-2.1742	0.9879	1.2063
50	0.015	0.3	11.1	10.6936	0.4064	0.0203	526.2598	1.0291	-1.6921	0.9634	3.6613
52	0.015	0.3	11.1	-	#VALUE!	#VALUE!	#VALUE!	#VALUE!	#VALUE!	#VALUE!	#VALUE!
54	0.015	0.3	11.1	-	#VALUE!	#VALUE!	#VALUE!	#VALUE!	#VALUE!	#VALUE!	#VALUE!
56	0.015	0.3	11.1	-	#VALUE!	#VALUE!	#VALUE!	#VALUE!	#VALUE!	#VALUE!	#VALUE!
58	0.015	0.3	11.1	10.8102	#REF!	#REF!	#REF!	#REF!	#REF!	#REF!	#REF!
60	0.015	0.3	11.1	10.7910	#REF!	#REF!	#REF!	#REF!	#REF!	#REF!	#REF!

Table B 3: Data for effect of mass on column biosorption for Mn – mass 1 g

Time (mins)	Volume (L)	Mass (g)	Ci (mg/L)	Ce (mg/L)	Ci-Ce	Qe (mg/g)	Ce/Qe	Log Ce	Log Qe	Ce/Ci	% Adsorbed
2	0.015	1	11.1	0.6089	10.4911	0.1574	3.8693	-0.2155	-0.8031	0.0549	94.5144
4	0.015	1	11.1	0.6051	10.4949	0.1574	3.8438	-0.2182	-0.8029	0.0545	94.5486
6	0.015	1	11.1	0.3829	10.7171	0.1608	2.3820	-0.4169	-0.7938	0.0345	96.5502
8	0.015	1	11.1	1.8768	9.2232	0.1383	13.5660	0.2734	-0.8590	0.1691	83.0917
10	0.015	1	11.1	6.0343	5.0657	0.0760	79.4133	0.7806	-1.1193	0.5436	45.6371
12	0.015	1	11.1	8.2529	2.8471	0.0427	193.2478	0.9166	-1.3695	0.7435	25.6495
14	0.015	1	11.1	9.3577	1.7423	0.0261	358.0617	0.9712	-1.5828	0.8430	15.6963
16	0.015	1	11.1	10.0613	1.0387	0.0156	645.7623	1.0027	-1.8074	0.9064	9.3577
18	0.015	1	11.1	10.2532	0.8468	0.0127	807.2115	1.0109	-1.8961	0.9237	7.6288
20	0.015	1	11.1	10.2303	0.8697	0.0130	784.2014	1.0099	-1.8845	0.9216	7.8351
22	0.015	1	11.1	10.3954	0.7046	0.0106	983.5746	1.0168	-1.9760	0.9365	6.3477
24	0.015	1	11.1	10.6604	0.4396	0.0066	1616.6818	1.0278	-2.1809	0.9604	3.9604
26	0.015	1	11.1	10.7111	0.3889	0.0058	1836.1361	1.0298	-2.2341	0.9650	3.5036
28	0.015	1	11.1	10.9068	0.1932	0.0029	3763.5611	1.0377	-2.5379	0.9826	1.7405
30	0.015	1	11.1	10.7806	0.3194	0.0048	2250.1774	1.0326	-2.3196	0.9712	2.8775
32	0.015	1	11.1	10.5050	0.5950	0.0089	1177.0308	1.0214	-2.0494	0.9464	5.3604
34	0.015	1	11.1	10.6900	0.4100	0.0062	1738.2114	1.0290	-2.2111	0.9631	3.6937
36	0.015	1	11.1	10.7000	0.4000	0.0060	1783.3333	1.0294	-2.2218	0.9640	3.6036
38	0.015	1	11.1	10.8800	0.2200	0.0033	3296.9697	1.0366	-2.4815	0.9802	1.9820
40	0.015	1	11.1	10.8600	0.2400	0.0036	3016.6667	1.0358	-2.4437	0.9784	2.1622
42	0.015	1	11.1	10.9000	0.2000	0.0030	3633.3333	1.0374	-2.5229	0.9820	1.8018
44	0.015	1	11.1	10.9500	0.1500	0.0023	4866.6667	1.0394	-2.6478	0.9865	1.3514
46	0.015	1	11.1	11.1100	-0.0100	-0.0001	-74066.6667	1.0457	#NUM!	1.0009	-0.0901
48	0.015	1	11.1	11.2300	-0.1300	-0.0020	-5758.9744	1.0504	#NUM!	1.0117	-1.1712
50	0.015	1	11.1	11.2900	-0.1900	-0.0028	-3961.4035	1.0527	#NUM!	1.0171	-1.7117
52	0.015	1	11.1	11.3602	-0.2602	-0.0039	-2910.6328	1.0554	#NUM!	1.0234	-2.3441
54	0.015	1	11.1	11.1609	-0.0609	-0.0009	-12217.7340	1.0477	#NUM!	1.0055	-0.5486
56	0.015	1	11.1	11.0779	0.0221	0.0003	33417.4962	1.0445	-3.4795	0.9980	0.1991
58	0.015	1	11.1	10.9836	0.1164	0.0017	6290.7216	1.0407	-2.7580	0.9895	1.0486
60	0.015	1	11.1	11.4738	-0.3738	-0.0056	-2046.3349	1.0597	#NUM!	1.0337	-3.3676

Table B 4: Data for effect of flow rate on column biosorption for Mn – flow rate 10 ml/min

Time (mins)	Volume (L)	Mass (g)	Ci (mg/L)	Ce (mg/L)	Ci-Ce	Qe (mg/g)	Ce/Qe	Log Ce	Log Qe	Ce/Ci	% Adsorbed
2	0.015	0.3	11.1	0.4280	10.6720	0.5336	0.8021	-0.3686	-0.2728	0.0386	96.1441
4	0.015	0.3	11.1	0.6051	10.4949	0.5247	1.1531	-0.2182	-0.2801	0.0545	94.5486
6	0.015	0.3	11.1	3.0887	8.0113	0.4006	7.7109	0.4898	-0.3973	0.2783	72.1738
8	0.015	0.3	11.1	7.0609	4.0391	0.2020	34.9629	0.8489	-0.6947	0.6361	36.3882
10	0.015	0.3	11.1	9.0298	2.0702	0.1035	87.2355	0.9557	-0.9850	0.8135	18.6505
12	0.015	0.3	11.1	9.9687	1.1313	0.0566	176.2362	0.9986	-1.2475	0.8981	10.1918
14	0.015	0.3	11.1	10.7542	0.3458	0.0173	621.9896	1.0316	-1.7622	0.9688	3.1153
16	0.015	0.3	11.1	10.7213	0.3787	0.0189	566.2160	1.0302	-1.7227	0.9659	3.4117
18	0.015	0.3	11.1	10.8187	0.2813	0.0141	769.1930	1.0342	-1.8519	0.9747	2.5342
20	0.015	0.3	11.1	10.7352	0.3648	0.0182	588.5526	1.0308	-1.7390	0.9671	3.2865
22	0.015	0.3	11.1	11.1050	-0.0050	-0.0003	-44420.0000	1.0455	#NUM!	1.0005	-0.0450
24	0.015	0.3	11.1	10.9076	0.1924	0.0096	1133.8462	1.0377	-2.0168	0.9827	1.7333
26	0.015	0.3	11.1	11.0107	0.0893	0.0045	2466.0022	1.0418	-2.3502	0.9920	0.8045
28	0.015	0.3	11.1	10.9467	0.1533	0.0077	1428.1409	1.0393	-2.1155	0.9862	1.3811
30	0.015	0.3	11.1	11.1848	-0.0848	-0.0042	-2637.9245	1.0486	#NUM!	1.0076	-0.7640
32	0.015	0.3	11.1	11.0537	0.0463	0.0023	4774.8164	1.0435	-2.6354	0.9958	0.4171
34	0.015	0.3	11.1	11.1133	-0.0133	-0.0007	-16711.7293	1.0458	#NUM!	1.0012	-0.1198
36	0.015	0.3	11.1	11.0732	0.0268	0.0013	8263.5821	1.0443	-2.8729	0.9976	0.2414
38	0.015	0.3	11.1	10.9802	0.1198	0.0060	1833.0885	1.0406	-2.2226	0.9892	1.0793
40	0.015	0.3	11.1	10.8594	0.2406	0.0120	902.6933	1.0358	-1.9197	0.9783	2.1676
42	0.015	0.3	11.1	11.0073	0.0927	0.0046	2374.8220	1.0417	-2.3340	0.9916	0.8351
44	0.015	0.3	11.1	10.9857	0.1143	0.0057	1922.2572	1.0408	-2.2430	0.9897	1.0297
46	0.015	0.3	11.1	10.6874	0.4126	0.0206	518.0514	1.0289	-1.6855	0.9628	3.7171
48	0.015	0.3	11.1	10.7512	0.3488	0.0174	616.4679	1.0315	-1.7585	0.9686	3.1423
50	0.015	0.3	11.1	10.9547	0.1453	0.0073	1507.8734	1.0396	-2.1388	0.9869	1.3090
52	0.015	0.3	11.1	10.9661	0.1339	0.0067	1637.9537	1.0401	-2.1742	0.9879	1.2063
54	0.015	0.3	11.1	10.6936	0.4064	0.0203	526.2598	1.0291	-1.6921	0.9634	3.6613
56	0.015	0.3	11.1	10.8102	0.2898	0.0145	746.0455	1.0338	-1.8389	0.9739	2.6108
58	0.015	0.3	11.1	10.7910	0.3090	0.0155	698.4466	1.0331	-1.8111	0.9722	2.7838
60	0.015	0.3	11.1	11.4738	-0.3738	-0.0187	-613.9005	1.0597	#NUM!	1.0337	-3.3676
62	0.015	0.3	11.1	11.2808	-0.1808	-0.0090	-1248.0119	1.0523	#NUM!	1.0163	-1.6286
64	0.015	0.3	11.1	11.3921	-0.2921	-0.0146	-780.1178	1.0566	#NUM!	1.0263	-2.6312
66	0.015	0.3	11.1	11.5033	-0.4033	-0.0202	-570.4041	1.0608	#NUM!	1.0363	-3.6337
68	0.015	0.3	11.1	11.6146	-0.5146	-0.0257	-451.3863	1.0650	#NUM!	1.0464	-4.6362
70	0.015	0.3	11.1	11.7259	-0.6259	-0.0313	-374.6892	1.0691	#NUM!	1.0564	-5.6387

Table B 5: Data for effect of flow rate on column biosorption for Mn – flow rate 15 ml/min

Time (mins)	Volume (L)	Mass (g)	Ci (mg/g)	Ce (mg/L)	Ci-Ce	Qe (mg/g)	Ce/Qe	Log Ce	Log Qe	Ce/Ci	% Adsorbed
2	0.015	0.3	11.1	0.5230	10.5770	0.5289	0.9889	-0.2815	-0.2767	0.0471	95.2883
4	0.015	0.3	11.1	1.5624	9.5376	0.4769	3.2762	0.1938	-0.3216	0.1408	85.9247
6	0.015	0.3	11.1	5.8064	5.2936	0.2647	21.9378	0.7639	-0.5773	0.5231	47.6897
8	0.015	0.3	11.1	9.6133	1.4867	0.0743	129.3240	0.9829	-1.1288	0.8661	13.3937
10	0.015	0.3	11.1	10.8094	0.2906	0.0145	743.9367	1.0338	-1.8377	0.9738	2.6180
12	0.015	0.3	11.1	10.9110	0.1890	0.0095	1154.6032	1.0379	-2.0246	0.9830	1.7027
14	0.015	0.3	11.1	10.9230	0.1770	0.0088	1234.2373	1.0383	-2.0531	0.9841	1.5946
16	0.015	0.3	11.1	10.9450	0.1550	0.0077	1412.2581	1.0392	-2.1107	0.9860	1.3964
18	0.015	0.3	11.1	10.9870	0.1130	0.0056	1944.6018	1.0409	-2.2480	0.9898	1.0180
20	0.015	0.3	11.1	10.9860	0.1140	0.0057	1927.3684	1.0408	-2.2441	0.9897	1.0270
22	0.015	0.3	11.1	11.1200	-0.0200	-0.0010	-11120.0000	1.0461	#NUM!	1.0018	-0.1802
24	0.015	0.3	11.1	11.1480	-0.0480	-0.0024	-4645.0000	1.0472	#NUM!	1.0043	-0.4324
26	0.015	0.3	11.1	11.2330	-0.1330	-0.0067	-1689.1729	1.0505	#NUM!	1.0120	-1.1982
28	0.015	0.3	11.1	11.2360	-0.1360	-0.0068	-1652.3529	1.0506	#NUM!	1.0123	-1.2252
30	0.015	0.3	11.1	11.3560	-0.2560	-0.0128	-887.1875	1.0552	#NUM!	1.0231	-2.3063
32	0.015	0.3	11.1	11.4860	-0.3860	-0.0193	-595.1295	1.0602	#NUM!	1.0348	-3.4775
34	0.015	0.3	11.1	11.4950	-0.3950	-0.0198	-582.0253	1.0605	#NUM!	1.0356	-3.5586
36	0.015	0.3	11.1	11.7450	-0.6450	-0.0323	-364.1860	1.0699	#NUM!	1.0581	-5.8108
38	0.015	0.3	11.1	11.8560	-0.7560	-0.0378	-313.6508	1.0739	#NUM!	1.0681	-6.8108
40	0.015	0.3	11.1	10.3500	0.7500	0.0375	276.0000	1.0149	-1.4260	0.9324	6.7568
42	0.015	0.3	11.1	11.1000	0.0000	0.0000	#DIV/0!	1.0453	#NUM!	1.0000	0.0000
44	0.015	0.3	11.1	11.2600	-0.1600	-0.0080	-1407.5000	1.0515	#NUM!	1.0144	-1.4414
46	0.015	0.3	11.1	11.3300	-0.2300	-0.0115	-985.2174	1.0542	#NUM!	1.0207	-2.0721
48	0.015	0.3	11.1	11.9600	-0.8600	-0.0430	-278.1395	1.0777	#NUM!	1.0775	-7.7477
50	0.015	0.3	11.1	11.5100	-0.4100	-0.0205	-561.4634	1.0611	#NUM!	1.0369	-3.6937

Table B 6: Data for effect of flow rate on column biosorption for Mn – flow rate 20 ml/min

Time (mins)	Volume (L)	Mass (g)	Ci (mg/g)	Ce (mg/L)	Ci-Ce	Qe (mg/g)	Ce/Qe	Log Ce	Log Qe	Ce/Ci	% Adsorbed
2	0.015	0.3	11.1	0.4250	10.6750	0.5338	0.7963	-0.3716	-0.2727	0.0383	96.1712
4	0.015	0.3	11.1	4.8217	6.2783	0.3139	15.3599	0.6832	-0.5032	0.4344	56.5612
6	0.015	0.3	11.1	9.2100	1.8900	0.0945	97.4603	0.9643	-1.0246	0.8297	17.0270
12	0.015	0.3	11.1	10.9110	0.1890	0.0095	1154.6032	1.0379	-2.0246	0.9830	1.7027
14	0.015	0.3	11.1	10.9230	0.1770	0.0088	1234.2373	1.0383	-2.0531	0.9841	1.5946
16	0.015	0.3	11.1	10.9450	0.1550	0.0077	1412.2581	1.0392	-2.1107	0.9860	1.3964
18	0.015	0.3	11.1	10.9870	0.1130	0.0056	1944.6018	1.0409	-2.2480	0.9898	1.0180
20	0.015	0.3	11.1	10.9860	0.1140	0.0057	1927.3684	1.0408	-2.2441	0.9897	1.0270
22	0.015	0.3	11.1	11.1200	-0.0200	-0.0010	-11120.0000	1.0461	#NUM!	1.0018	-0.1802
24	0.015	0.3	11.1	11.1480	-0.0480	-0.0024	-4645.0000	1.0472	#NUM!	1.0043	-0.4324
26	0.015	0.3	11.1	11.2330	-0.1330	-0.0067	-1689.1729	1.0505	#NUM!	1.0120	-1.1982
28	0.015	0.3	11.1	11.2360	-0.1360	-0.0068	-1652.3529	1.0506	#NUM!	1.0123	-1.2252
30	0.015	0.3	11.1	11.3560	-0.2560	-0.0128	-887.1875	1.0552	#NUM!	1.0231	-2.3063
32	0.015	0.3	11.1	11.4000	-0.3000	-0.0150	-760.0000	1.0569	#NUM!	1.0270	-2.7027
34	0.015	0.3	11.1	11.4627	-0.3627	-0.0181	-632.0761	1.0593	#NUM!	1.0327	-3.2676
36	0.015	0.3	11.1	11.5254	-0.4254	-0.0213	-541.8618	1.0617	#NUM!	1.0383	-3.8324
38	0.015	0.3	11.1	11.5881	-0.4881	-0.0244	-474.8248	1.0640	#NUM!	1.0440	-4.3973
40	0.015	0.3	11.1	11.6508	-0.5508	-0.0275	-423.0501	1.0664	#NUM!	1.0496	-4.9622

Appendix C. BH Column data for Fe and Mn

Table C 1: BH Column data for Fe

Time (mins)	Volume (L)	Mass (g)	Ci (mg/L)	Ce (mg/L)	Ci-Ce	Qe (mg/g)	Ce/Qe	Log Ce	Log Qe	Ce/Ci	% Adsorbed
2	0.015	0.3	100	0.0150	99.9850	4.9993	0.0030	-1.8239	0.6989	0.0002	99.9850
4	0.015	0.3	100	0.8790	99.1210	4.9561	0.1774	-0.0560	0.6951	0.0088	99.1210
6	0.015	0.3	100	0.2900	99.7100	4.9855	0.0582	-0.5376	0.6977	0.0029	99.7100
8	0.015	0.3	100	0.8200	99.1800	4.9590	0.1654	-0.0862	0.6954	0.0082	99.1800
10	0.015	0.3	100	0.5600	99.4400	4.9720	0.1126	-0.2518	0.6965	0.0056	99.4400
12	0.015	0.3	100	0.8680	99.1320	4.9566	0.1751	-0.0615	0.6952	0.0087	99.1320
14	0.015	0.3	100	0.5720	99.4280	4.9714	0.1151	-0.2426	0.6965	0.0057	99.4280
16	0.015	0.3	100	2.7140	97.2860	4.8643	0.5579	0.4336	0.6870	0.0271	97.2860
18	0.015	0.3	100	2.5780	97.4220	4.8711	0.5292	0.4113	0.6876	0.0258	97.4220
20	0.015	0.3	100	2.5010	97.4990	4.8750	0.5130	0.3981	0.6880	0.0250	97.4990
22	0.015	0.3	100	2.5230	97.4770	4.8739	0.5177	0.4019	0.6879	0.0252	97.4770
24	0.015	0.3	100	2.0690	97.9310	4.8966	0.4225	0.3158	0.6899	0.0207	97.9310
26	0.015	0.3	100	2.3210	97.6790	4.8840	0.4752	0.3657	0.6888	0.0232	97.6790
28	0.015	0.3	100	1.8450	98.1550	4.9078	0.3759	0.2660	0.6909	0.0185	98.1550
30	0.015	0.3	100	2.0360	97.9640	4.8982	0.4157	0.3088	0.6900	0.0204	97.9640
32	0.015	0.3	100	1.8400	98.1600	4.9080	0.3749	0.2648	0.6909	0.0184	98.1600
34	0.015	0.3	100	1.6920	98.3080	4.9154	0.3442	0.2284	0.6916	0.0169	98.3080
36	0.015	0.3	100	1.9200	98.0800	4.9040	0.3915	0.2833	0.6906	0.0192	98.0800
38	0.015	0.3	100	2.0100	97.9900	4.8995	0.4102	0.3032	0.6902	0.0201	97.9900
40	0.015	0.3	100	1.9120	98.0880	4.9044	0.3899	0.2815	0.6906	0.0191	98.0880
42	0.015	0.3	100	1.7160	98.2840	4.9142	0.3492	0.2345	0.6915	0.0172	98.2840
44	0.015	0.3	100	1.2900	98.7100	4.9355	0.2614	0.1106	0.6933	0.0129	98.7100
46	0.015	0.3	100	1.7170	98.2830	4.9142	0.3494	0.2348	0.6914	0.0172	98.2830
48	0.015	0.3	100	1.6570	98.3430	4.9172	0.3370	0.2193	0.6917	0.0166	98.3430
50	0.015	0.3	100	1.1950	98.8050	4.9403	0.2419	0.0774	0.6937	0.0120	98.8050
52	0.015	0.3	100	1.7150	98.2850	4.9143	0.3490	0.2343	0.6915	0.0172	98.2850
54	0.015	0.3	100	1.8410	98.1590	4.9080	0.3751	0.2651	0.6909	0.0184	98.1590
56	0.015	0.3	100	1.9410	98.0590	4.9030	0.3959	0.2880	0.6905	0.0194	98.0590
58	0.015	0.3	100	1.9230	98.0770	4.9039	0.3921	0.2840	0.6905	0.0192	98.0770
60	0.015	0.3	100	1.9130	98.0870	4.9044	0.3901	0.2817	0.6906	0.0191	98.0870
62	0.015	0.3	100	1.9940	98.0060	4.9003	0.4069	0.2997	0.6902	0.0199	98.0060
64	0.015	0.3	100	2.1500	97.8500	4.8925	0.4394	0.3324	0.6895	0.0215	97.8500
66	0.015	0.3	100	2.0910	97.9090	4.8955	0.4271	0.3204	0.6898	0.0209	97.9090
68	0.015	0.3	100	2.0150	97.9850	4.8993	0.4113	0.3043	0.6901	0.0202	97.9850
70	0.015	0.3	100	1.8420	98.1580	4.9079	0.3753	0.2653	0.6909	0.0184	98.1580
72	0.015	0.3	100	1.6180	98.3820	4.9191	0.3289	0.2090	0.6919	0.0162	98.3820
74	0.015	0.3	100	2.0370	97.9630	4.8982	0.4159	0.3090	0.6900	0.0204	97.9630
76	0.015	0.3	100	1.8840	98.1160	4.9058	0.3840	0.2751	0.6907	0.0188	98.1160
78	0.015	0.3	100	1.9120	98.0880	4.9044	0.3899	0.2815	0.6906	0.0191	98.0880
80	0.015	0.3	100	1.5960	98.4040	4.9202	0.3244	0.2030	0.6920	0.0160	98.4040
82	0.015	0.3	100	1.9250	98.0750	4.9038	0.3926	0.2844	0.6905	0.0193	98.0750
84	0.015	0.3	100	1.0060	98.9940	4.9497	0.2032	0.0026	0.6946	0.0101	98.9940
86	0.015	0.3	100	0.9780	99.0220	4.9511	0.1975	-0.0097	0.6947	0.0098	99.0220
88	0.015	0.3	100	0.9500	99.0500	4.9525	0.1918	-0.0223	0.6948	0.0095	99.0500
90	0.015	0.3	100	1.0480	98.9520	4.9476	0.2118	0.0204	0.6944	0.0105	98.9520
92	0.015	0.3	100	0.9630	99.0370	4.9519	0.1945	-0.0164	0.6948	0.0096	99.0370
94	0.015	0.3	100	0.9680	99.0320	4.9516	0.1955	-0.0141	0.6947	0.0097	99.0320
96	0.015	0.3	100	0.9190	99.0810	4.9541	0.1855	-0.0367	0.6950	0.0092	99.0810
98	0.015	0.3	100	0.9250	99.0750	4.9538	0.1867	-0.0339	0.6949	0.0093	99.0750
100	0.015	0.3	100	0.9220	99.0780	4.9539	0.1861	-0.0353	0.6949	0.0092	99.0780

Table C 2: BH Column data for Mn

Time (mins)	Volume (L)	Mass (g)	Ci (mg/L)	Ce (mg/L)	Ci-Ce	Qe (mg/g)	Ce/Qe	Log Ce	Log Qe	Ce/Ci	% Adsorbed
2	0.015	0.3	7.1	2.0939	10.4061	0.5203	4.0243	0.3209	-0.2837	83.2490	0.1675
4	0.015	0.3	7.1	7.0160	5.4841	0.2742	25.5867	0.8461	-0.5619	43.8724	0.5613
6	0.015	0.3	7.1	10.0146	2.4854	0.1243	80.5874	1.0006	-0.9056	19.8832	0.8012
8	0.015	0.3	7.1	11.6005	0.8995	0.0450	257.9322	1.0645	-1.3470	7.1960	0.9280
10	0.015	0.3	7.1	12.4172	0.0828	0.0041	2999.3237	1.0940	-2.3830	0.6624	0.9934
12	0.015	0.3	7.1	11.4291	1.0709	0.0535	213.4485	1.0580	-1.2713	8.5672	0.9143
14	0.015	0.3	7.1	10.6941	1.8059	0.0903	118.4351	1.0291	-1.0443	14.4472	0.8555
16	0.015	0.3	7.1	12.4239	0.0761	0.0038	3265.1511	1.0943	-2.4196	0.6088	0.9939
18	0.015	0.3	7.1	11.2837	1.2163	0.0608	185.5414	1.0525	-1.2160	9.7304	0.9027
20	0.015	0.3	7.1	11.4358	1.0642	0.0532	214.9182	1.0583	-1.2740	8.5136	0.9149
22	0.015	0.3	7.1	11.1663	1.3337	0.0667	167.4485	1.0479	-1.1760	10.6696	0.8933
24	0.015	0.3	7.1	11.1195	1.3805	0.0690	161.0938	1.0461	-1.1610	11.0440	0.8896
26	0.015	0.3	7.1	11.3106	1.1894	0.0595	190.1900	1.0535	-1.2257	9.5152	0.9048
28	0.015	0.3	7.1	11.1135	1.3865	0.0693	160.3101	1.0459	-1.1591	11.0920	0.8891
30	0.015	0.3	7.1	11.3935	1.1065	0.0553	205.9376	1.0567	-1.2571	8.8520	0.9115
32	0.015	0.3	7.1	10.4938	2.0062	0.1003	104.6137	1.0209	-0.9987	16.0496	0.8395
34	0.015	0.3	7.1	11.4955	1.0045	0.0502	228.8800	1.0605	-1.2991	8.0360	0.9196
36	0.015	0.3	7.1	11.4707	1.0293	0.0515	222.8835	1.0596	-1.2885	8.2344	0.9177
38	0.015	0.3	7.1	11.2145	1.2855	0.0643	174.4769	1.0498	-1.1920	10.2840	0.8972
40	0.015	0.3	7.1	10.5710	1.9290	0.0965	109.6008	1.0241	-1.0157	15.4320	0.8457
42	0.015	0.3	7.1	10.0568	2.4432	0.1222	82.3248	1.0025	-0.9131	19.5456	0.8045
44	0.015	0.3	7.1	10.7116	1.7884	0.0894	119.7898	1.0299	-1.0486	14.3072	0.8569
46	0.015	0.3	7.1	10.2241	2.2759	0.1138	89.8467	1.0096	-0.9439	18.2072	0.8179
48	0.015	0.3	7.1	9.6409	2.8591	0.1430	67.4401	0.9841	-0.8448	22.8728	0.7713
50	0.015	0.3	7.1	10.7246	1.7754	0.0888	120.8133	1.0304	-1.0517	14.2032	0.8580
52	0.015	0.3	7.1	10.4385	2.0615	0.1031	101.2709	1.0186	-0.9868	16.4920	0.8351
54	0.015	0.3	7.1	10.7737	1.7263	0.0863	124.8184	1.0324	-1.0639	13.8104	0.8619
56	0.015	0.3	7.1	12.1560	0.3440	0.0172	706.7442	1.0848	-1.7645	2.7520	0.9725
58	0.015	0.3	7.1	9.3930	3.1070	0.1554	60.4632	0.9728	-0.8087	24.8561	0.7514
60	0.015	0.3	7.1	11.0613	1.4387	0.0719	153.7680	1.0438	-1.1431	11.5096	0.8849
62	0.015	0.3	7.1	11.7465	0.7535	0.0377	311.7850	1.0699	-1.4239	6.0280	0.9397
64	0.015	0.3	7.1	12.5097	-0.0097	-0.0005	-25793.1959	1.0972	#NUM!	-0.0776	1.0008
66	0.015	0.3	7.1	11.2915	1.2085	0.0604	186.8680	1.0528	-1.2188	9.6680	0.9033
68	0.015	0.3	7.1	11.7324	0.7676	0.0384	305.6905	1.0694	-1.4159	6.1408	0.9386
70	0.015	0.3	7.1	10.7863	1.7137	0.0857	125.8832	1.0329	-1.0671	13.7096	0.8629
72	0.015	0.3	7.1	10.4907	2.0093	0.1005	104.4214	1.0208	-0.9980	16.0744	0.8393
74	0.015	0.3	7.1	11.9383	0.5617	0.0281	425.0774	1.0769	-1.5515	4.4936	0.9551
76	0.015	0.3	7.1	11.3800	1.1200	0.0560	203.2143	1.0561	-1.2518	8.9600	0.9104
78	0.015	0.3	7.1	10.7936	1.7064	0.0853	126.5073	1.0332	-1.0689	13.6512	0.8635
80	0.015	0.3	7.1	11.1186	1.3814	0.0691	160.9758	1.0461	-1.1607	11.0512	0.8895
82	0.015	0.3	7.1	7.4528	5.0473	0.2524	29.5319	0.8723	-0.5980	40.3780	0.5962
84	0.015	0.3	7.1	7.4678	5.0322	0.2516	29.6803	0.8732	-0.5993	40.2574	0.5974
86	0.015	0.3	7.1	7.4100	5.0900	0.2545	29.1157	0.8698	-0.5943	40.7202	0.5928
88	0.015	0.3	7.1	7.2971	5.2029	0.2601	28.0504	0.8632	-0.5848	41.6230	0.5838
90	0.015	0.3	7.1	7.3779	5.1221	0.2561	28.8083	0.8679	-0.5916	40.9766	0.5902
92	0.015	0.3	7.1	7.3901	5.1099	0.2555	28.9245	0.8686	-0.5926	40.8793	0.5912
94	0.015	0.3	7.1	7.3668	5.1332	0.2567	28.7026	0.8673	-0.5906	41.0656	0.5893
96	0.015	0.3	7.1	7.3278	5.1722	0.2586	28.3357	0.8650	-0.5874	41.3773	0.5862
98	0.015	0.3	7.1	7.4224	5.0776	0.2539	29.2358	0.8705	-0.5954	40.6209	0.5938
100	0.015	0.3	7.1	7.3358	5.1642	0.2582	28.4101	0.8654	-0.5880	41.3137	0.5869

Appendix D. Modelling data

Table D 1: Langmuir model parameters

Langmuir isotherm	**Intercept**	**Qmax**	**Slope**	**KL**	**RL**	**R 2**
Fe	3.7801	0.2645	-0.1959	-19.2961	0.0159	0.9944
Mn	0.0503	19.8807	0.1728	0.2911	0.0332	0.9964

Table D 2: Freundlich model parameters

Freundlich isotherm	**Intercept**	**Slope**	**n**	**KF**	**R 2**
Fe	-0.5440	-0.9960	-1.0040	0.2858	0.9641
Mn	0.3931	0.3133	3.1918	2.4723	0.9681

Table D 3: Model response factors

Biosorbent	**Experimental conditions**			**Response factors**					
Sample	**Ci (mg/L)**	**W (g)**	**Q (Ml/min)**	**tb (min)**	**ts (min)**	**Vs(Ml/g)**	**qb (mg/g)**	**qs (mg/g)**	**FBU**
0.2 g Mn	11.1	0.2	10	1	4	0.08	0.022	0.089	0.250
0.3 g Mn	11.1	0.3	10	2	10	0.30	0.067	0.333	0.200
1 g Mn	11.1	1	10	6	22	2.20	0.666	2.442	0.273
10ml/min Mn	11.1	0.3	10	2	22	0.66	0.067	0.733	0.091
15ml/min Mn	11.1	0.3	15	2	22	0.44	0.100	1.099	0.091
20ml/min Mn	11.1	0.3	20	2	22	0.33	0.133	1.465	0.091
Borehole water	7.1	0.3	10	2	10	0.30	0.075	0.375	0.200

Table D 4: Pseudo first order model data for Fe and Mn

			Fe			
Time	**Co (mg/L)**	**Ct (mg/L)**	**Qt**	**Qe**	**Qe-Qt**	**Ln (Qe-Qt)**
1	100	0.557	9.944	11.327	1.383	0.3240
3	100	0.517	9.948	11.327	1.379	0.3211
5	100	0.499	9.950	11.327	1.377	0.3198
10	100	0.428	9.957	11.327	1.370	0.3147
15	100	0.410	9.959	11.327	1.368	0.3133
20	100	0.412	9.959	11.327	1.368	0.3135
30	100	0.402	9.960	11.327	1.367	0.3128
45	100	0.215	9.978	11.327	1.349	0.2990
60	100	0.061	9.994	11.327	1.333	0.2875
90	100	0.051	9.995	11.327	1.332	0.2868

Mn						
Time	**Co (mg/L)**	**Ct (mg/L)**	**Qt**	**Qe**	**Qe-Qt**	**Ln (Qe-Qt)**
1	100	0.573	6.043	5.3	-0.743	#NUM!
3	100	0.402	6.060	5.3	-0.760	#NUM!
5	100	0.382	6.062	5.3	-0.762	#NUM!
10	100	6.034	5.497	5.3	-0.197	#NUM!
15	100	9.357	5.164	5.3	0.136	-1.997
20	100	10.230	5.077	5.3	0.223	-1.501
30	100	10.780	5.022	5.3	0.278	-1.280
45	100	11.360	4.964	5.3	0.336	-1.091
60	100	11.474	4.953	5.3	0.347	-1.057
90	100	11.481	4.952	5.3	0.348	-1.055

Table D 5: Pseudo second order model data for Fe and Mn

Fe				
Time	**Co (mg/L)**	**Ct (mg/L)**	**Qt**	**t/Qt**
1	100	0.557	9.944	0.1006
3	100	0.517	9.948	0.3016
5	100	0.499	9.950	0.5025
10	100	0.428	9.957	1.0043
15	100	0.410	9.959	1.5062
20	100	0.412	9.959	2.0083
30	100	0.402	9.960	3.0121
45	100	0.215	9.978	4.5097
60	100	0.061	9.994	6.0037
90	100	0.051	9.995	9.0046

Mn				
Time	Co (mg/L)	Ct (mg/L)	Qt	t/Qt
1	61	0.573	6.043	0.1655
3	61	0.402	6.060	0.4951
5	61	0.382	6.062	0.8248
10	61	6.034	5.497	1.8193
15	61	9.357	5.164	2.9046
20	61	10.230	5.077	3.9393
30	61	10.780	5.022	5.9737
45	61	11.360	4.964	9.0653
60	61	11.474	4.953	12.1148
90	61	11.481	4.952	18.1748

Table D 6: Intraparticle diffusion model data for Fe and Mn

Fe							
Time	**Co (mg/L)**	**Ct (mg/L)**	**Qt**	**t0.5**	**Slope/ k**	**Intercept**	**R 2**
1	100	0.557	9.944	1.000	0.0064	9.9353	0.9220
3	100	0.517	9.948	1.732			
5	100	0.499	9.950	2.236			
10	100	0.428	9.957	3.162			
15	100	0.410	9.959	3.873			
20	100	0.412	9.959	4.472			
30	100	0.402	9.960	5.477			
45	100	0.215	9.978	6.708			
60	100	0.061	9.994	7.746			
90	100	0.051	9.995	9.487			
Mn							
Time	**Co (mg/L)**	**Ct (mg/L)**	**Qt**	**t0.5**	**Slope/ k**	**Intercept**	**R 2**
1	61	0.573	6.043	1.000	-0.1542	6.0872	0.7445
3	61	0.402	6.060	1.732			
5	61	0.382	6.062	2.236			
10	61	6.034	5.497	3.162			
15	61	9.357	5.164	3.873			
20	61	10.230	5.077	4.472			
30	61	10.780	5.022	5.477			
45	61	11.360	4.964	6.708			
60	61	11.474	4.953	7.746			
90	61	11.481	4.952	9.487			

Table D 7: Fixed bed mathematical modelling parameters

Experimental conditions			Thomas model			Bohart-Adams model			Yoon Nelson model			Experimental
Ci	**W**	**Q**	**Kth**	**Qth**	**R^2**	**Kba**	**No**	**R^2**	**t50**	**Kyn**	**R^2**	**Qs**
(mg/L)	(g)	(ml/min)	(ml/mg/min)	(mg/g)		(ml/mg/min)	(mg/L)		(min)	L/mg		(mg/g)
11.1	0.2	10	0.0136	3.9971	0.8929	0.0210	51.2380	0.7412	7.202	0.1515	0.8929	0.178
11.1	0.3	10	0.0464	1.2656	0.9688	0.0128	12.5120	0.7806	3.421	0.5151	0.9688	0.333
11.1	1	10	0.0484	1.1662	0.9263	0.0234	5.7320	0.8430	10.086	0.4159	0.9482	2.442
11.1	0.3	10	0.0534	2.8830	0.9706	0.0318	31.0600	0.8946	7.792	0.5922	0.9484	0.733
11.1	0.3	15	0.0684	3.3625	0.9834	0.0277	40.5890	0.8342	6.059	0.7587	0.9386	1.099
11.1	0.3	20	0.0548	4.4091	0.8751	0.0311	60.8510	0.7297	5.446	0.6082	0.8504	1.465
7.1	0.3	10	0.0610	1.6334	0.9576	0.0074	8.1950	0.8892	4.218	0.7014	0.8929	0.375

Table D 8: Fixed bed model equations

	Bohart-Adams model		Thomas model		Yoon-Nelson model	
Mass (g)	**Bohart-Adams equation**	**R^2**	**Thomas equation**	**$R^2$2**	**Yoon-Nelson equation**	**$R^2$3**
0.2	y = 0.2326x-1.3352	0.7412	y = -0.1515x+1.0911	0.8929	y = 0.1515x-1.0911	0.8929
0.3	y = 0.142x-1.2674	0.7806	y = -0.5151x+1.7619	0.9688	y = 0.5151x-1.7619	0.9688
1	y = 0.2602x-3.8578	0.843	y = -0.5375x+5.6472	0.9263	y = 0.4159x-4.1947	0.9482
Flow rate (ml/min)						
10	y = 0.3525x-3.8360	0.8946	y = -0.5922x+4.6144	0.9706	y = 0.8708x-5.7266	0.9484
15	y = 0.3071x-3.1249	0.8342	y = -0.7587x+4.5966	0.9834	y = 0.2874x-3.1578	0.9386
20	y = 0.3453x-3.1732	0.7297	y = -0.6082x+3.6238	0.8751	y = 0.7749x-3.5968	0.8504
Borehole water	y = 0.093x-0.8710	0.8892	y = -0.7631x+2.9915	0.9576	y = 0.2373x-1.7082	0.8929